FORCED-CONVECTION DISPERSED-FLOW FILM BOILING

S.J. Hynek
W.M. Rohsenow
A.E. Bergles

Report No. DSR 70586-63

Contract No. NSF GK 1759

Department of Mechanical Engineering
Engineering Projects Laboratory
Massachusetts Institute of Technology

April 1969

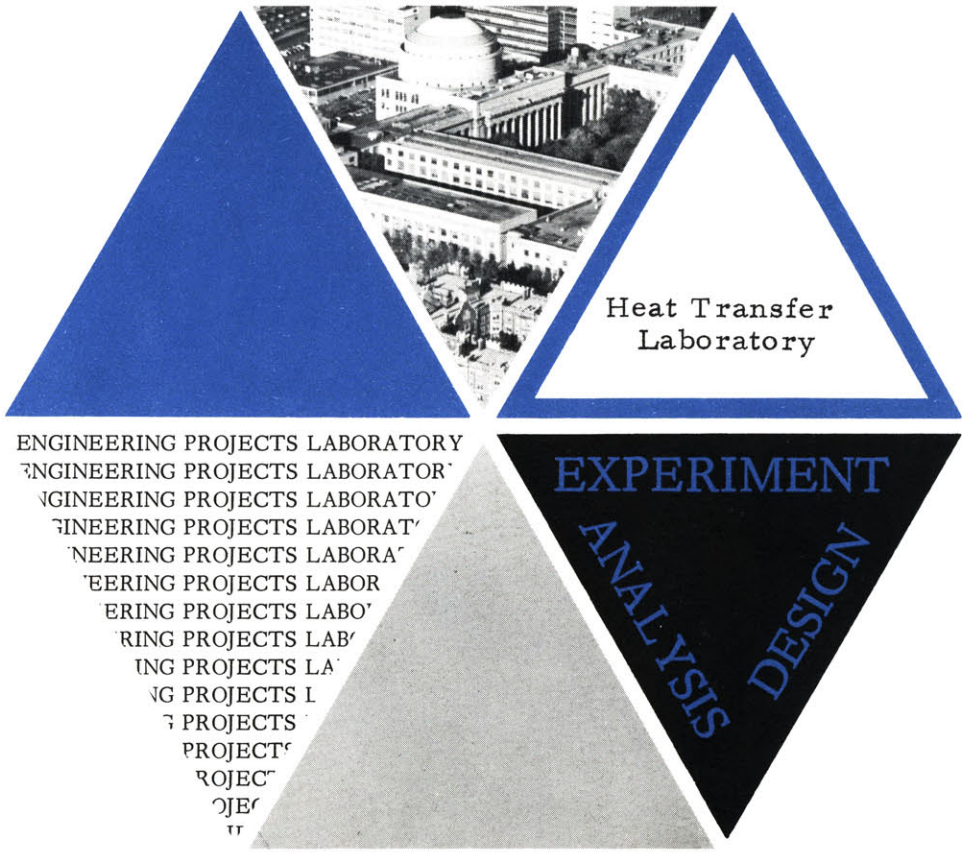

TECHNICAL REPORT NO. 70586-63

FORCED-CONVECTION, DISPERSED-FLOW FILM BOILING

by

S. J. Hynek
W. M. Rohsenow
A. E. Bergles

Sponsored by the
National Science Foundation
Contract No. NSF GK 1759
D.S.R. Project No. 7086

April 1969

Department of Mechanical Engineering
Massachusetts Institute of Technology
Cambridge, Massachusetts 02139

ABSTRACT

This report presents the latest results of an investigation of the characteristics of dispersed flow film boiling. Heat transfer data are presented for vertical upflow of nitrogen in an electrically heated tube, 0.4 in. I.D. and 8 ft long. Heat fluxes up to 18,000 Btu/ft^2-hr and mass fluxes up to 200,000 lb_m/ft^2-hr were investigated. By variation of the startup procedure, it was possible to operate in two distinct regimes of film boiling. By preheating the tube before introducing the flow, film boiling was observed throughout the test tube. If the flow was established before applying power, film boiling was initiated downstream of the inlet. For similar conditions, the local heat transfer coefficients were different in the two cases due to the different degrees of thermal nonequilibrium. The data for both regimes were satisfactorily predicted by a modified version of the non-equilibrium model presented in earlier reports. The model was also applied to available data for methane, propane, and water. By modification of the empirical constant governing the direct wall-to-droplet heat transfer, these data were generally predicted to within 10 percent.

The tests were repeated with tight-fitting, full-length twisted tapes installed in the test tube. Considerable augmentation of the heat transfer was achieved, with the heat transfer coefficient being increased by as much as a factor of 3 with the tightest tape twist. For the higher mass fluxes, it was observed that the tape promoted droplet deposition to such an extent that a continuous liquid film could be reestablished on the wall near the test section exit. The tape-generated swirl flow did not improve the "burnout" condition, primarily due to the fact that a liquid streamer forms on the twisted tape. The semi-empirical model gave a reasonable prediction of the heat transfer coefficient when the effects of the swirl flow were included.

ACKNOWLEDGMENTS

Financial support for this investigation was provided by the National Science Foundation under Grant GK 1759. Professor P. Griffith, Professor A. R. Rogowski, and Professor B. B. Mikic gave generously of their time to discuss various aspects of this work. Assistance in the experimental program was provided by Mr. W. D. Fuller and Mr. E. D. Fedorovitch. Mr. F. Johnson was project mechanic. Calculations were performed on the IBM 360 at the M.I.T. Computation Center and on the IBM 1130 at the Department of Mechanical Engineering Computation Center.

TABLE OF CONTENTS

LIST OF FIGURES

NOMENCLATURE

a	acceleration, ft/hr^2
a_c	centrifugal acceleration, ft/hr^2
A	current, amps
A	flow area, ft^2
A_f	cross-sectional area of liquid streamer, ft^2
A_v	flow area taken up by vapor, ft^2
C_D	coefficient of drag
C_o	constant in heat transfer coefficient correlation
C_{pv}	specific heat of vapor at constant pressure, $Btu/lb_m-°F$
D_T	diameter of tube, ft^2
f	Fanning friction factor
F	fraction of heat lost through outer wall of tube
g	acceleration of gravity = 4.17×10^8 ft/hr^2
G	mass flux or mass velocity, lb_m/ft^2-hr
Gr	Grashof number
h_{fg}	latent heat of evaporation, Btu/lb_m
h_{fg}'	latent heat of evaporation plus superheat, Btu/lb_m
h_{fg}^*	latent heat of evaporation, corrected (Baumeister et al.), Btu/lb_m
$h_{v,\delta}$	heat transfer coefficient from vapor to droplet, $Btu/ft^2-hr-°F$
$h_{w,\delta}$	heat transfer coefficient from wall to droplet, $Btu/ft^2-hr-°F$
$h_{w,v}$	heat transfer coefficient from wall to vapor, $Btu/ft^2-hr-°F$

K thermal conductivity, Btu/ft-hr-°F

$\mathcal{K}$ tape curvature, ft^{-1}

K_f thermal conductivity of vapor, evaluated at $\frac{T_v + T_w}{2}$, Btu/ft-hr-°F

K_1 empirical constant relating to gravity

K_2 empirical constant relating to packing

K_3 empirical constant relating to streamer width

K_4 empirical constant relating to friction factor

ℓ length of tube, ft

m exponent in heat transfer coefficient correlation

N_2 number of drops per unit surface area, ft^{-2}

N_3 number of drops per unit volume, ft^{-3}

Nu Nusselt number

p pressure, psia

P power, watts

Pr Prandtl number

(q/A) heat flux, Btu/ft^2-hr

r radius, ft

r_i inner radius of tube, ft

r_o outer radius of tube, ft

R half-width of liquid streamer, ft

Re Reynolds number

Re_δ Reynolds number for droplet

Re_H hydraulic Reynolds number

t	thickness of liquid streamer, ft
$\hat{t}$	average thickness of liquid streamer, ft
T_v	vapor temperature, °R or °F
T_{sat}	saturation temperature, °R or °F
T_w	wall temperature, °R or °F
V	emf across test section, volts
V_F	average axial velocity of liquid streamer, ft/hr
V_ℓ	average axial velocity of droplets, ft/hr
V_v	average axial velocity of vapor, ft/hr
V_z	axial velocity of liquid streamer, ft/hr
ΔV	difference in velocities, defined at each use, ft/hr
W	heat generation per unit volume, Btu/hr-ft^3
We	Weber number
We_c	critical Weber number
w_f	mass flow rate of liquid streamer, lb_m/hr
w_v	mass flow rate of vapor, lb_m/hr
X_A	actual quality
X_E	equilibrium quality
X_o	actual quality at point of last shattering
y	length of tape for 180° twist/tube diameter
z	axial position or dimension, ft
α	void fraction
γ	measure of tape twist = $\pi/2y$
δ	droplet diameter, ft

δ_o droplet diameter at point of last shattering

μ_f vapor viscosity evaluated at $\frac{T_v + T_w}{2}$, $lb_m/hr\text{-}ft$

μ_l liquid viscosity, $lb_m/hr\text{-}ft$

ρ_f vapor density, evaluated at $\frac{T_v + T_w}{2}$, lb_m/ft^3

ρ_l liquid density, lb_m/ft^3

ρ_v vapor density, lb_m/ft^3

σ surface tension, lb_m/hr^2

τ shear stress, lb_f/ft^2

ϕ phase angle in test section, radians

ω_l angular velocity of liquid streamer

ω_v angular velocity of vapor

INTRODUCTION

Forced convection dispersed flow film boiling is of more than academic interest. It occurs in once-through steam generators and in cryogenic transfer lines as well as in nuclear reactor cores and steam generators that have undergone loss-of-coolant flow accidents. It is important to be able to predict the tube wall temperatures involved in film boiling, since the temperatures are often close to or exceeding the melting point of the tube material.

Dispersed flow occurs under quality conditions and is characterized by liquid droplets entrained in a vapor flow. Dispersed flow film boiling generally involves thermodynamic non-equilibrium. Due to a lack of continuous direct contact between liquid and heated surface, the dominant path of heat transfer is from tube wall to vapor, thence from vapor to drop. Some heat is transferred directly from tube wall to droplet, but this is important only at low qualities. The fact that this process is not instantaneous means that the entrained drops (or droplets; the terms are used interchangeably) are carried past the point where they would have boiled under equilibrium conditions. This permits superheated vapor. A sizeable discrepancy often exists between equilibrium quality (as determined by the first law of thermodynamics) and actual quality (the flowing mass fraction of fluid that has evaporated); the actual quality may be as low as 60% of the equilibrium quality.

This report is one of a series of reports resulting from the Film Boiling Project at the MIT Heat Transfer Laboratory. The goal of this project is to better predict the behavior of forced convection film boiling by means of better understanding its mechanisms. Early work on this project by Kruger[1]* and by Dougall[2] used Freon - 113 as the experimental fluid. This work was limited to low qualities, partly because Freon - 113 was observed to decompose at the temperatures associated with film boiling. Laverty[3, 4] introduced the use of liquid nitrogen as the experimental fluid because it does not decompose and because it can film boil at temperatures below room temperature, and developed a procedure for calculating actual qualities and tube wall temperatures based on a model of heat transfer from wall to vapor and from vapor to drop. Forslund[5, 6] measured the extent of the non-equilibrium by measuring actual vapor qualities; he also introduced a term describing the heat transferred directly from wall to droplet into the calculation procedure. By the use of two empirical constants, he arranged to fit the theory to the nitrogen data that he took.

It was the purpose of this work to take data under a wider range of conditions than those of Forslund and to see if his model would fit the data without having to change the empirical constants, and to see if the model could predict the data of other experimenters using other fluids. A second goal was to investigate the effect of a twisted tape inserted into the test section, of which the purpose was to augment the heat transfer coefficient (particularly the wall to droplet portion) by

*Numbers in parentheses refer to references, found on p. 46.

centrifuging the drops against the heated wall. Finally, the model was to be adapted to this more complex geometry.

EXPERIMENTAL PROGRAM

2.1 Apparatus

The experimental apparatus was originally built by Laverty, modified by Forslund, and further modified by the author.

2.1.1. General Description of Apparatus:

A schematic diagram of the system is given in Figure 1. Liquid nitrogen at 106 psia is allowed to flow through two heat exchangers that cool it down sufficiently that it remains liquid as it passes through the flow control valve. The subcooling is achieved by bleeding part of the main flow into a vacuum line, which forms the outer part of the two concentric-tube heat exchangers. The nitrogen enters the test section at about 20 psia.

In the vertical test section, the pressure is monitored by five pressure taps in conjunction with a manometer board. Tube wall temperatures are measured at 24 points by copper-constantan thermocouples that are spot-welded to the outer tube wall. The tubular test section is direct resistance heated by a power supply described by Figure 2 and is insulated on its outer surface by a jacket containing 1-1/2 inches of Santocel, a finely powdered silica.

The nitrogen then passes through a visual test section consisting of a glass tube with an electrically conducting coating on the outside. Current is passed through the coating to heat the tube to keep it from frosting up. The nitrogen then passes through one or two concentric-tube heat exchangers which serve to heat up or cool down the nitrogen to roughly room temperature before it goes through the rotameters. The steam or water that flows through the outer part of these heat exchangers also flows through another heat exchanger that heats up the vacuum line so that the vacuum pump does not freeze up.

Further description of the apparatus can be found in references 5 and 7.

2.1.2. Modifications and Improvements:

2.1.2.1. Test Section

The test section for the majority of the tests was made of Inconel 600 supplied by Whitehead Metals Company instead of stainless steel as was used by previous investigators (however, Forslund's 0.228" stainless steel test section was used for the tests reported in section 2.3.1.1.).

The electrical resistivity of Inconel varies by about 4% over the range of 600°R to 1700°R; this change is small enough to permit the assumption that the heat generation is constant along the entire length of the tube, even in the presence of large temperature gradients. The dimensions of the test section were: length = 8 ft, I. D. = 0.400 in., O. D. = 0.500 in.

2.1.2.2. Nitrogen Supply

The 50 liter Dewar flask used by Laverty and Forslund was replaced by a 160 liter Dewar (Linde LS-160). Besides the obvious advantage of less frequent replacement, the 160 liter Dewar could withstand pressures up to 150 psi. To achieve high pressures, the standard 22 psig relief valve was replaced by a 100 psig valve. High pressures were deemed useful because it was felt that one type of flow oscillation could be avoided by severe throttling at the test section inlet, and a high pressure permits such throttling. During operation, flow oscillations were observed, particularly during start-up. They were described to other causes, as detailed in section 2.3.1.2. Higher pressures and larger nitrogen capacity also permitted operation at higher mass fluxes.

2.1.2.3. Power Supply

The use of two ganged,variable transformers and two stepdown transformers in parallel, as shown in Figure 2, permitted heat fluxes up to 18,000 Btu/ft^2-hr. Forslund achieved higher heat fluxes (up to 23,000 Btu/ft^2-hr, averaged along the length of the test section) but by using tubes of smaller diameters (0.228 in. and 0.323 in.).

The power factor was measured (see Appendix 1) and found to be 0.94. The increased current made it necessary to install a current transformer as shown in Figure 2. This transformer has more than one secondary tap;

the tap with the 80:1 ratio was used. This transformer, Weston Model 401, Type 2, has a nickel alloy core with a low phase angle for use with wattmeters; thus, it was suitable for measuring the power factor.

2.1.2.4. Guard Cooler

For some of the experiments it was necessary to prevent heat from leaking in through the power lead at the inlet of the test section. To effect this, the guard cooler shown in Figure 3 was bolted into the power line roughly six inches away from the test section inlet and the power line was well wrapped with fiber glass insulation. The two flare fittings permitted the cooler to be connected, in series, into the vacuum line between the transfer tube heat exchanger and the bleed back pressure control valve. In practice, it cooled down the line so well that heat conduction away from the test section became something of a problem. Unfortunately, it could not be controlled, as the vacuum line could not be throttled and still have the heat exchangers prevent flashing at the flow control valve.

2.1.2.5. Twisted Tape

A twisted strip of Inconel 600, 0.400 in. x 0.020 in. x 8 ft., was inserted in the test section and secured at the upstream end by silver soldering.

The purpose of the tape was to centrifuge the droplets onto the tube wall so as to hasten their evaporation and to cool the wall. After data were taken with the twist ratio y (defined as the number of tube diameters per 180° of twist) equal to 8.5, the tape was removed, twisted again to a twist ratio of 4.1, and reinserted. As the tape was designed to fit tightly inside the tube, insertion involved lubrication with oil and subsequent flushing with solvents.

The twist ratio was not perfectly uniform along the length of the tape. Indeed, for the twist ratio reported as 8.5, the local twist ratio varied from 7.0 to 10.0, with three maxima and four minima regularly spaced along the tape. This was thought to be due to the fact that the tape was made up of four 2' sections welded together; the three maxima in twist ratios (i.e., least twisted portions) occurred in the vicinity of these welds. These welds were necessary because the longest sheet of Inconel 600 available to us was two feet long.

2.1.2.6. Emergency Shutdown System

The emergency shutdown system was modified to include a normally-closed solenoid valve in the liquid delivery line connected across the primary of one of the variable transformers, as shown in Figure 2. Thus, one emergency switch could shut off the power and the flow. A small variable transformer was installed in the solenoid valve circuit, since the other 75% of the power would have been dissipated into the delivery line because the solenoid valve as well as the delivery line was wrapped

in fiber glass insulation. This heat generation would have prevented the attainment of reasonable inlet subcooling, or could have even caused boiling in the delivery line.

2.2. Data Reduction

The data were reduced by a computer program, a sample printout of which is shown in Figure 4. This program calculates heat flux from voltage and current readings, and mass flux from flowmeter (Rotameter) readings. As a check for error, the latter readings are also printed out. Note that the current readings are those in the secondary circuit of the current transformer; the test section current is 80 times this.

The five manometer readings are converted to five pressures at the pressure taps, from which a fourth-order curve fit to the pressure along the test section is made. This curve fit is evaluated at each of the 24 points along the test section at which there is a thermocouple. From the pressure are calculated the pressure gradient and the saturation temperature.

From the inlet temperature is calculated the inlet subcooling. This allows calculation of the equilibrium quality at the 24 points. The bulk temperature, which assumes equilibrium conditions, is set equal to the saturation temperature for equilibrium qualities between zero and one; for equilibrium qualities less than zero or greater than one, the bulk temperature is modified by the specific heat of the liquid and vapor,respectively.

The thermocouple readings are converted to outer wall temperatures by means of a subroutine which is a collection of eleven fourth-order curve fits to the thermocouple tables, each spanning a different portion of the tables. The inner wall temperatures are calculated by means of an equation derived in Appendix 2. The temperature drop across the tube wall was never more than 5°F, and was usually much less.

The equilibrium heat transfer coefficient is then calculated, based on the bulk temperature and the inside wall temperature and on the average (assumed uniform) heat flux. This heat flux was simply the heat generated divided by the inside tube area. It was not modified to account for end conduction, for with the exception of the tests described in section 2.3.1.3. (for which end conduction was treated in Appendix 3), the area of interest was not near either end. The formula for heat flux was not modified for the tests with the twisted tape, either. Although 10% of the heat was generated in the tape (based on the observed change of the test section resistance when the tape was installed), its area was sufficiently large that heat flux from the tape was quite small. The fin efficiency of the tape was calculated by Lopina[8] and found to be small enough that the tape could be ignored as a heated surface. This does admit some error; but the error is lessened by the fact that both the data reduction program and the analytical model program use the same assumption.

The reduced data for over 200 runs are on file in the MIT Heat Transfer Laboratory.

2.3. Experimental Results

2.3.1. Data Without the Twisted Tape:

2.3.1.1. Visual Observations

The increased mass flux possible with the large Dewar permitted the confirmation of a trend observed by Forslund. The existence of thermodynamic non-equilibrium is easily and demonstrably observed by the viewing of droplets in the visual test section at exit qualities greater than one. Forslund observed that the equilibrium quality at which droplets disappear is much greater at low mass fluxes than at high mass fluxes. This is an indication that non-equilibrium decreased with increasing mass flux.

To achieve high mass fluxes, Forslund's 0.228 in. diameter, 8 ft. long test section was used. These were the only tests for which this test section was used. The method of looking for drops was to aim a strobe light into the visual test section and to try to "stop" their motion. It was often observed, generally near the point of marginal visibility of drops, that they seemed to appear in bursts, or clusters. The existence of drops was only one of several factors entering into their visibility. Others were the angle of the incident light and even the amount of time spent looking for drops. Liquid nitrogen drops are colorless, fast-moving, and easily overlooked when present and imagined when not under conditions of poor visibility. It is difficult to estimate the size of the smallest drops observed, for drops of almost any

size will scatter light. Our data (the filled-in circles of Figure 5) confirm the trend of Forslund's data.

2.3.1.2. Flow Oscillations

Despite the severe throttling at the test section inlet, flow oscillations of several types were encountered. The first, and most easily explained, was that which occurred during startup. As the inlet plumbing was cooled down by the nitrogen flowing through it, liquid began to replace the vapor flowing through the flow control valve. As a slug of liquid passed through, the pressure drop across the valve decreased markedly, causing a sudden flow increase until the liquid slug had passed entirely through. Once the flow through the valve became entirely liquid, the valve could be closed down some and the flow would become constant.

Under all running conditions, small pressure fluctuations typical of two phase flow were present. As they affected the manometers just enough to render readings difficult, throttling orifices were put in the manometer lines which slowed the response time of the manometers from the order of a tenth of a second to the order of a second. Flow oscillations with a period larger than about a second were still observable.

One type of flow oscillation that was not so easily explained was the sort that occurred in the early runs whenever the ratio of mass

flux to heat flux fell below 4.0 (lb_m/Btu). This was not observed with the stainless steel test section, nor with the twisted tape installed. Flow oscillations of perhaps another type were preceded by considerable pressure changes in the bleed flow line. These were thought to be due to flashing in the delivery line or freezing in the bleed line, as conditions in the bleed line were near the triple point.

A complete explanation of the observed flow oscillations is not the goal of this thesis; these observations are reported merely for their value as observations. It should be noted that no flow oscillations (except, of course, the small fluctuations that were masked by the throttling orifices) were present in any of the data runs reported in this thesis.

2.3.1.3. Existence of Two Distinct Types of Film Boiling Behavior

Two distinctly different regimes of film boiling were observed. The first, shown qualitatively in Figure 6 (an actual example is shown in Figure 22), was the same kind observed by Laverty and Forslund. The entire test section is in film boiling, the burnout point being essentially at the entrance to the test section. The second, shown qualitatively in Figure 7 (an actual example is shown in Figure 23), has nucleate boiling and an annular dispersed region before the burnout point. The wall temperature in the annular region was noticeably lower than that in the nucleate boiling region.

The term "burnout" is not used here in its usual sense, as the phonomenon it describes occurs at low enough temperatures with nitrogen that the tube is in no danger of melting. Indeed, this is why nitrogen was chosen as the experimental fluid.

Both regimes can occur at a given heat flux and mass flux, as evidenced by Figure 8. Which regime will occur is determined by the manner in which the test conditions are achieved. If the tube is allowed to heat up before flow is begun and if the entrance of the test section is always kept at a temperature above the Leidenfrost temperature, then a Type I regime will occur. Figure 9, a sketch of the boiling curve, provides a good definition of the Leidenfrost point. If the temperature of the test section entrance is cooled below the Leidenfrost temperature, such as by letting liquid nitrogen flow through it before the power is turned on, then a Type II regime will occur. Both regimes were also observed to occur with the twisted tape installed.

The two regimes have different degrees of thermodynamic non-equilibrium, even at the same heat and mass flux, which results in different tube wall temperatures. Type I regimes, with burnout at the entrance, build up non-equilibrium from the entrance, whereas Type II regimes are in equilibrium upstream of the burnout point (superheated vapor cannot exist inside a liquid film at saturation temperature). The greater the discrepancy between actual and equilibrium qualities, the greater the vapor superheat, according to the first

law of thermodynamics.

$$X_E h_{fg} = X_A \left[h_{fg} + c_{pv} (T_v - T_{sat}) \right] \quad (2\text{-}1)$$

Thus, at a given equilibrium quality, a Type I run will have a lower actual quality, thus a higher vapor temperature and a higher wall temperature than will a Type II run with the same heat and mass fluxes. Figure 10 shows this for a collection of early runs.

Transition from Type I to Type II, but not from Type II to Type I, is possible by changing the heat flux. Once the heat flux is dropped below that value corresponding to the Leidenfrost point, a liquid film will appear at the beginning of the test section and will in some cases move up the test section, asymptotically approaching some equilibrium point. When operating in the Type II regime, however, increasing the heat flux past the Leidenfrost point merely causes the liquid film to recede; no doubt there is some heat flux at which the Type II to Type I transition will occur, but it is beyond the capability of our apparatus.

The heat flux at which the Type I to Type II transition occurred was measured for several different mass fluxes in an effort to determine what effect mass flux had on the Leidenfrost point. As Figure 11 will attest, the change is small and vague. On the theory that conduction into the test section through the power line could be present in sufficient degree to mask the observation of such a trend, the

guard cooler of Figure 3 was installed to halt (or, as it turned out, to reverse) this conduction. Measurement of the heat flux below which transition occurred (or minimum heat flux) was made difficult because sufficient heat was conducted from the test section to the cooler so that the full capacity of electrical power was needed to maintain a Type I regime. Measurement of this minimum heat flux was impossible at more than one mass flux; increasing the mass flux caused transition (this did indicate that the minimum heat flux does increase with increasing mass flux), and decreasing the mass flux would have resulted in dangerously high temperatures at the downstream end of the test section. As it was, at the one mass flux at which the minimum heat flux was determined, the last six inches (which had become uncovered by the insulation) was glowing red and estimated to be at 1400°F and all the thermocouples except those in the first two inches of the test section were off the scale of the recorder, which corresponded to temperatures greater than 700°F.

In Appendix 3, the heat flux at the Leidenfrost point was determined to be 2,200 Btu/ft^2-hr at a mass flux of 40,000 lb$_m$/ft^2-hr under conditions of conduction into the test section inlet through the power line and 18,700 Btu/ft^2-hr at the same mass flux under conditions of conduction away from the test section. This conduction at the test section ends can explain the discrepancy between the data and the predictions of the model developed in the next chapter that occurred at the thermocouple nearest each end of the test section, because the model didn't take into account axial conduction.

Type I film boiling is the regime that occurs in a cryogenic transfer line when flow of a cryogenic liquid is first introduced into a warm line. Transition from Type I to Type II occurs after the first portion of the tube has cooled below the Leidenfrost point. Type II film boiling is the regime that exists after burnout in a boiler tube.

The equilibrium quality at burnout for the Type II runs was observed to decrease with increasing heat flux and to increase with increasing mass flux, as indicated by Figure 12.

2.3.2. Results with Twisted Tape:

2.3.2.1. Effect on Heat Transfer Coefficient

The twisted tape was effective in raising the heat transfer coefficient at all values of heat flux and mass flux, as shown in Figures 13, 14, and 15. The tighter tape twist was more effective. The next section will explain why the dashed lines of Figure 15 go off scale. It is interesting to note that in Figure 13, some of the lines are observed to cross, indicating that at low qualities and low mass fluxes, the heat transfer coefficient decreases with increasing mass flux; the opposite is generally the case, as evidenced by Figures 14 and 15 and the high quality portion of Figure 13. This phenomenon is due to the direct heat transfer from wall to droplet, which becomes most noticeable under the conditions of low quality and mass flux. At low quality, droplets are numerous, whereas at high

quality, droplets are scarce. As will be pointed out in the next chapter, the heat transfer coefficient for the wall to droplet term is relatively insensitive to mass flux, whereas the wall to vapor term is proportional to mass flux. The heat transfer coefficient at the wall, defined by

$$h_w = \frac{(q/A)}{T_w - T_{sat}} \tag{2-2}$$

is the sum of a convective (wall to vapor) term and a direct (wall to droplet) term.

$$h_w = h_{w,v} + h_{w,\delta} \tag{2-3}$$

For the reasons given above, the direct term is dominant under these circumstances. As will be shown more exactly in the next chapter,

$$h_{w,\delta} \sim (T_w - T_{sat})^{-\frac{1}{3}} \tag{2-4}$$

The exponent is not exactly - 1/3, nor is it constant, but this is a good rough idea. Thus, neglecting the convective term of equation (2-3)

$$(q/A) = h_w (T_w - T_{sat}) \sim (T_w - T_{sat})^{2/3} \tag{2-5}$$

Comparing equations (2-4) and (2-5) , it is seen that

$$h_{w,\delta} \approx h_w \sim (q/A)^{-1/2} \tag{2-6}$$

Thus, at low mass flux and low quality (as is the case for the left-hand portion of Figure 13), the heat transfer coefficient should increase with decreasing heat flux, as is evidenced by the crossing of the lines on Figure 13.

The pressure drop across the test section was also observed to increase as well; this effect and its significance in view of the increased heat transfer coefficient are dealt with in detail by Fuller,[7] who concluded that for a tube-temperature-limited system, the increased heat transfer coefficient allows considerably shorter tubes with no increase in pressure drop.

Figures 16 and 17 show the effect of mass flux and illustrate the fact that both regimes can exist with the twisted tape. The similarity of curves of each family would indicate the possibility of a correlation; however, this was not the purpose of this work.

2.3.2.2. Re-wetting of Tube Wall

For high values of mass flux the act of decreasing the heat flux below a fairly definite point resulted in the establishment of a liquid film after a section of film boiling. The heat transfer coefficient increases to values typical of nucleate boiling, as indicated by the dashed lines of Figure 15. A typical temperature profile is shown in Figure 18. This was observed only with Type I regimes; however, no particular effort was made to observe this phenomenon with Type II regimes. Raising the heat flux again above this point results in the disappearance of the film. Once the film does form on the wall, no further decrease in power is necessary to allow it to spread in both directions. This is because axial conduction along the test section

toward the portion with the liquid film cools the adjacent portion, thus decreasing the force repelling the drops from the wall until they too contact and wet it. The film was not allowed to expand until it stabilized, if indeed it ever would have. The expansion was slow, the phenomenon occurred only at high mass fluxes, and it appeared that we would run out of nitrogen before expansion ceased.

Listed below are the pertinent operating conditions and resulting temperatures at a heat flux barely above that which made the re-wetting occur.

Run No.	Mass Flux lb_m/ft^2-hr	Heat Flux Btu/ft^2-hr	T_{wall} °R	T_{sat} °R	Quality	y
221	100,000	9,400	312	146	.909	4.14
158	84,000	4,300	265	144	.549	8.50
160	85,000	4,500	259	144	.545	8.50
166	133,000	10,100	288	146	.806	8.50
168	132,000	10,000	293	145	.840	8.50
173	185,000	15,600	305	147	.895	8.50

These data represent conditions under which the centrifugal force on the droplet is just enough to overcome the Leidenfrost force (that force, due to rapid vapor generation between the drop and the heated surface, which repels the drop from the surface) and to allow the drops to touch (and presumably to wet) the wall. The very high heat transfer coefficient that results indicates that the wall is completely re-wetted. These data, particularly when coupled with calculations of the droplet's diameter made possible

by the procedure outlined in the next chapter, form a basis for evaluation of any theoretical calculation of the Leidenfrost force.

It is worth noting that while the term 're-wetting' is used, this phonomenon was observed only with Type I runs, where no liquid film existed on the wall upstream of the point described by the above Table. Two Type II runs with the twisted tape were taken with mass fluxes comparable to those listed above. These are tabulated below.

Run No.	Mass Flux lb_m/ft^2-hr	Heat Flux Btu/ft^2-hr	Quality at Burnout	y
241	104,000	8,500	0.768	4.14
242	101,000	12,200	0.740	4.14

Of these, only Run 241 had a heat flux comparable to the 're-wetting' runs. The quality at burnout of Run 241 was almost as high as the quality at which re-wetting occurred for Run 221, which suggests that were the heat flux decreased further, the centrifuged droplets would merely extend the existing film, rather than establish a new one. This hypothesis is borne out both by Figure 12, which shows that burnout quality increases as heat flux decreases; and by the fact that the most easily wetted portion of the dry wall is the relatively cool portion bordering the liquid film, as evidenced by the tendency of a re-wetted film to expand, once formed, with no further decrease in power.

2.3.2.3. Effect on Burnout Quality

When a Type II run with the twisted tape is compared with a Type II run with the same heat and mass fluxes but without the twisted tape, the former is seen to burn out upstream of the point at which the latter burns out, and often at a lower equilibrium quality. See Figure 19 for an example of two Type II runs with roughly the same heat and mass fluxes. The apparent anomaly in the above statement is due to the reduction in flow area caused by the presence of the twisted tape.

Moeck et al.[32] observed a similar phenomenon with 1000 psig water, namely that burnout heat flux was increased by the presence of a twisted tape provided that the mass flux was greater than 500,000 $lb_m ft^2$-hr. The opposite effect was observed for mass fluxes smaller than 500,000 lb_m/ft^2-hr. Figure 20 shows the effect of heat and mass fluxes on the equilibrium quality at burnout, for the nitrogen data of the present study, both with and without the twisted tape. It is to be noted that the difference in burnout qualities due to the tape is most pronounced in the high quality, low heat flux portion of Figure 20. Two conflicting phenomena enter into this result, and their relative intensities determine its extent.

The first effect of the twisted tape is to set up a centrifugal force field that tends to centrifuge the droplets toward the wall and into the liquid film that covers the wall upstream of the burnout point. This effect alone would cause the presence of the twisted tape to bring about a higher burnout quality; for with more liquid on the wall, more

evaporation must take place before the film is thin enough to permit burnout. Were this the only effect of the twisted tape, the result would be as described in this paragraph and not as observed.

Another effect of the twisted tape, and an important one, is that it provides an area on which a portion of the liquid can cling. In the center of the tube, centrifugal force (assuming that the tape produces essentially a solid body rotation) is zero. Near the center, surface tension can hold together a streamer of liquid against the small centrifugal force near the center. An attempt to calculate the amount of liquid that could be contained on the tape by this force balance is made in Appendix 4; the conclusion is that surface tension can account for large amounts of liquid and that surface tension is not the limiting factor.

The theory of a streamer running up the middle of the tape is strengthened by the observation of droplets in the visual test section at exit qualities greater than one with the tape installed. The main function of the tape was originally to decrease the non-equilibrium.

2.3.2.4. Pure Vapor Correlation

In an effort to determine the validity of the conventional correlation for single phase forced convection heat transfer to a tube containing a twisted tape under conditions of a high ratio between the wall temperature and the fluid temperature, some pure vapor runs were taken. Once the liquid in the Dewar was expended, the pressurizing nitrogen flowed through the cold Dewar and delivery

line and reached the test section at a temperature only slightly above saturation. Data runs had to be taken quickly, as the inlet temperature of the vapor rose steadily as the temperatures of the Dewar and delivery line rose. The vapor temperature was calculated at each point in the test section using the first law of thermodynamics, based on the exit temperature. The use of the inlet temperature gave very scattered results; this was assumed to be due to the fact that the fluid was not quite pure vapor at the inlet, but that it had some drops entrained in it, causing the inlet thermocouple to read various temperatures between saturation temperature and the vapor temperature. Neither heat flux nor mass flux was varied more than 10% as the object was to observe the effect of different temperature ratios. The inlet vapor temperature increased from about 160°R to about 250°R during the course of these four runs. After these four runs were taken, the inlet temperature began rising too fast for all 24 wall temperatures to be read at essentially the same time as the fluid temperature.

A conventional correlation for single-phase flow with a twisted tape is given by Thorsen and Landis.[9]

$$Nu = C_o\,(1 + 0.07\,K)\,Re_H^{0.8}\,Pr^{0.4}\,(T_v/T_w)^m\left(1 + \frac{\sqrt{Gr}}{4\,Re_H}\right) \qquad (2\text{-}7)$$

where

$$K = \frac{2\,\gamma^2}{(1+\gamma^2)\,D_T} \qquad (2\text{-}8)$$

where, in turn,

$$\gamma = \frac{\pi}{2y} \tag{2-9}$$

Thorsen and Landis found that their data were correlated by the values $C_o = 0.021$ and $m = 0.32$. Different exponents for the temperature corrector term were tried when this correlation was compared to the data mentioned above; it was observed that the scatter of this data was affected little by the choice of exponent. Thus, it was decided to use $m = 0.5$ to conform to general practice.[10, 11]

Figure 21 shows the measured Nusselt number, divided by all parts of the Thorsen-Landis correlation except Re_H, plotted versus the hydraulic Reynolds number. A straight line drawn by inspection through the points representing fully developed flow (i.e., excluding the points in the upper righthand portion where entrance effects and perhaps some entrained droplets serve to raise the heat transfer coefficient) describes the equation

$$\frac{Nu_{MEASURED}}{(1+0.07\mathcal{K})\left(\frac{T_v}{T_w}\right)^{0.5} Pr^{0.4}\left(1+\frac{\sqrt{Gr}}{4\,Re_H}\right)} = 0.0265\, Re_H^{0.8} \tag{2-10}$$

where $\mathcal{K} = 1.98\ ft^{-1}$ for $y = 8.5$, $D_T = 0.4"$

This corresponds to a correlation described by equation (2.7) with $C_o = 0.023$ and $m = 0.5$. This is the correlation used in the analytical program described in the next chapter.

THEORETICAL PROGRAM

3.1 Description of Calculation Procedure

The analytical program referred to earlier is similar to one used by Forslund[5, 6] who extended the basic analysis proposed by Laverty[3, 4]. A fairly detailed description of the calculation procedure is followed by a discussion of the assumptions made and of the differences between this computer program and its predecessors.

The method of calculation is to determine vapor velocity, droplet velocity and droplet size, at a point in the tube where equilibrium conditions are assumed to exist, by iterating equations (A5-16) and (A5-11) of Appendix 5. The first of these equations is one form of the continuity equation; the second is an expression of the force balance between drag, gravity, and acceleration of the drop, constrained by the critical Weber number criterion for determination of maximum drop size. These equations are solved by iteration, as described in Appendix 5. The tube wall temperature is calculated next by evaluating the wall-to-vapor heat transfer and the wall-to-drop heat transfer, where it is assumed (for this initial point only) that the vapor temperature is equal to the saturation temperature (because equilibrium was assumed).

The wall-to-vapor heat transfer coefficient is based on a Nusselt number determined by Forslund,[5] modified to include the measured power factor of 0.94 (see Appendix 1)

$$h_{w,v} = \frac{K_v}{D_T} Nu = \frac{K_v}{D_T} 0.94\ Re^{0.743}\ Pr^{0.4}\ 0.035 \qquad (3\text{-}1)$$

where the Reynolds number is based on the vapor velocity and all properties are evaluated at the vapor temperature (which, again, is equal to the saturation temperature for this first step only). Results obtained using equation (3-1) did not differ significantly from those obtained using the more widely accepted Dittus-Boelter[12] equation

$$h_{w,v} = \frac{K_v}{D_T} Nu = \frac{K_v}{D_T}\ 0.023\ Re^{0.8}\ Pr^{0.4} \qquad (3\text{-}2)$$

Perhaps a correlation for $h_{w,v}$ that included a temperature correction factor like that of equation (2-7) would be more appropriate; however, the data from which equation (3-1) was made contained only a 10% spread in $\left(\frac{T_v}{T_w}\right)$, which is too small to evaluate accurately the exponent m.

The wall-to-droplet heat transfer coefficient was derived by Forslund[5] on the basis of the heat transfer coefficient for a single drop resting on a horizontal flat surface reported by Baumeister et al.[13]

$$h = K_1 \left[\frac{K_f^3\ h_{fg}^*\ g\ \rho_f\ \rho_l}{(T_w - T_{sat})\ \mu_f \sqrt[3]{\frac{\pi}{6}}\ \delta} \right]^{1/4} \qquad (3\text{-}3)$$

where

$$h_{fg}^* = \frac{1}{\left[h_{fg} + \frac{7}{20} \frac{C_{pv}(T_w - T_{sat})}{h_{fg}} \right]^3}, \qquad (3\text{-}4)$$

K_1 = 1.1 for single drops,

and K_f, ρ_f, and μ_f are vapor properties evaluated at the film temperature $\frac{T_v + T_w}{2}$.

Forslund[6] modified the above to include the number of droplets present per unit volume

$$N_3 = \frac{6\,G\,(1 - X_A)}{\rho_l\, V_l\, \pi\, \delta^3} \tag{3-5}$$

by assuming that the number of droplets per unit surface area was given by

$$N_2 = K_2\,(N_3)^{2/3} \tag{3-6}$$

where K_2 is a "packing factor" representing the packing geometry and the possibility that the spatial distribution of drops may not be uniform. Since the gravity factor in equation (3-3) represents a condition which is not present in a vertical tube, another constant, K_1, the "gravity factor", is introduced in place of the coefficient in equation (3-3). These constants are seen to group together in the expression for the heat transfer coefficient to all droplets present

$$h_{w,\delta} = K_1 K_2 \left(\frac{\pi}{4}\right)\left(\frac{6G}{\pi \rho_l}\right)^{2/3}\left(\frac{1 - X_A}{V_l}\right)^{2/3}\left[\frac{K_f^3\, h_{fg}^*\, g\, \rho_f\, \rho_l}{(T_w - T_{sat})\,\mu_f\, \sqrt[3]{\frac{\pi}{C}}\,\delta}\right]^{1/4} \tag{3-7}$$

Forslund suggested that K_1K_2 should be set equal to 0.2 on the basis of his nitrogen data. As mentioned later in this report, $K_1K_2 = 0.2$ works well for nitrogen data but should be set to higher values for successful prediction of data taken with other fluids.

Equations (3-1) and (3-7) must be combined to calculate the wall temperature*

$$\left(q/A\right) = h_{w,v}\left(T_w - \overline{T}_v\right) + h_{w,\delta}\left(\overline{T}_w - \overline{T}_{sat}\right) \qquad (3\text{-}8)$$

or

$$\overline{T}_w = \frac{\left(q/A\right) + h_{w,v}\,\overline{T}_v + h_{w,\delta}\,\overline{T}_{sat}}{h_{w,v} + h_{w,\delta}} \qquad (3\text{-}9)$$

Since equation (3-7) is dependent upon T_w both directly and through the properties evaluated at the film temperature, it must be evaluated at this value of T_w. Standard practice was to initially set T_w to T_{sat} + 100 and to iterate equations (3-7) and (3-9) four times. All iterations were checked for convergence.

For the next and all successive steps the calculation moves an increment downstream. During this interval, the drops are accelerated by drag forces

$$\frac{dV_\ell}{dz} = \frac{3\,C_D\,\rho_v\left(V_v - V_\ell\right)^2}{4\,V_\ell\,\rho_\ell\,\delta} - \frac{g}{V_\ell} \qquad (3\text{-}10)$$

---

* This formulation presumes that the droplets cover a negligibly small fraction of the tube surface, an assumption which is valid except at very low quality.

(except for the first interval, where an assumption of initial drop acceleration, equation (A5-6) requires that

$$\left.\frac{dV_\ell}{dz}\right|_{\substack{first\\interval}} = \frac{4\,(q/A)\,X_A}{h_{fg}\,D_T\,\rho_g} \qquad (3\text{-}11)$$

The drag coefficient is evaluated as follows:

$$C_D = \frac{24}{Re}\left(1.0 + 0.142\,Re^{0.698}\right) \qquad Re < 2000 \qquad (3\text{-}12)$$

$$C_D = 0.45 \qquad Re > 2000 \qquad (3\text{-}13)$$

This equation is a curve fit[14] to the drag coefficient of a solid sphere[15] which is good for Reynolds numbers up to 2000. For Reynolds numbers between 2,000 and 20,000 the data[15] indicate that the drag coefficient is fairly constant at 0.45.

The droplets are partially evaporated in this interval both by heat transferred from the wall and by heat transferred by the vapor (once the vapor superheat builds up). The heat transfer coefficient from vapor to drop is given by

$$h_{v,\delta} = \frac{K_v}{\delta}\left(2.0 + 0.55\,Re_\delta^{0.5}\,Pr^{0.33}\right) \qquad (3\text{-}14)$$

Once the total heat transfer to a droplet is established by means of equations (3-5), (3-6), (3-7), and (3-14), the change in drop size is calculated to be

$$\frac{d\delta}{dz} = -\frac{2\,(q/A)_\delta}{h_{fg}\,\rho_\ell\,V_\ell} \tag{3-15}$$

where $(q/A)_\delta$ = total heat flux to a droplet.

The change in actual quality is then

$$\frac{dX_A}{dz} = -\frac{(1-X_0)\,3\delta^2}{\delta_0^3}\,\frac{d\delta}{dz} \tag{3-16}$$

where X_0 and δ_0 are the quality and drop diameter, respectively, at the beginning or after the most recent shattering.

The first law of thermodynamics gives the change in equilibrium quality

$$\frac{dX_E}{dz} = \frac{4\,(q/A)}{G\,h_{fg}\,D_T} \tag{3-17}$$

Differentiation of equation (2-1) yields the change in vapor temperature

$$\frac{d T_v}{dz} = \frac{h_{fg} \frac{dX_E}{dz} - h_{fg}' \frac{dX_A}{dz}}{X_A C_{pv}} \qquad (3\text{-}18)$$

where

$$h_{fg}' = h_{fg} + C_{pv} \left(T_v - T_{sat} \right) \qquad (3\text{-}19)$$

By means of equations (3-11), (3-15), (3-16), (3-17), and (3-18) and the values of V_v, V_ℓ, δ, X_A, X_E, and T_v after the last increment, the new values of V_ℓ, δ, X_A, X_E, and T_v are calculated. The new value of V_v is calculated from the continuity equation, equation (A5-16).

The tube wall temperature is again calculated by means of equation (3-9). Iteration for the proper value of T_w for use in equation (3-7) is still necessary.

After each increment, the Weber number

$$We = \frac{\rho_v (V_v - V_\ell)^2 \delta}{\sigma} \qquad (3\text{-}20)$$

is calculated and compared against the critical Weber number. Should the critical Weber number be exceeded, the drop is assumed to have shattered during the interval; the number of drops is doubled, the diameter reduced by $\frac{1}{\sqrt[3]{2}}$, and X_o and δ_o are set equal to new values.

The model makes many assumptions. These follow, together with their justification.

The model assumes that at one point in the tube, thermodynamic equilibrium exists. This is necessary for setting the initial conditions for calculation. Once the initial vapor velocity, drop velocity, and drop size are determined (see Appendix 5), vapor superheat can be accounted for. For a Type II regime, this is taken to be at the burnout point (more precisely, at the first thermocouple location past the burnout point), for as noted before, vapor inside a liquid film cannot be superheated. For a Type I regime, Forslund suggested initiating the calculation at a quality of about 10%. This point is not very critical to the calculation, as the non-equilibrium is small at low quality (see Figure 24). Initiating the calculation at qualities much below 5% leads to instability in the calculation of the drop velocity, so one is restricted to larger qualities, around 8% and above. This presents no serious difficulty, as it is difficult to imagine that dispersed flow exists at such low qualities anyway.

The model assumes that all drops are of the same diameter and that this diameter is determined by a critical Weber number criterion. This is obviously a simplification; Cumo, Farello, and Ferrari[16] show that the drops follow a normal distribution with a definite maximum diameter determined by the critical Weber number. However, it is the larger drops that contain most of the mass and, due to

their higher slip velocity, do most of the evaporating. The critical Weber number has been chosen as 7.5, based on data taken by Isshiki[17]. Varying this critical Weber number in the calculation produces little effect, and that only at low qualities.

When a droplet shatters, it is assumed to shatter into two drops, each containing half the mass (and $1/\sqrt[3]{2}$ of the diameter) of the original droplet. According to pictures of drop shattering taken by Lane[18], the number of resulting drops is closer to 8 or 10. This is accompanied by a more substantial change in diameter. However, by keeping the number down to two, we account, to some degree, for neglecting the distribution of drop sizes; the drop that doesn't change its diameter drastically becomes, in effect, the drop that was not quite big enough to shatter. Isshiki[17] reasons that if the Weber number of the droplet far exceeds the critical Weber number (as in the case of a shock wave), the number of droplets resulting from shattering is large; but if the critical Weber number is exceeded by only a small fraction, as is the case in dispersed flow, the number of resultant droplets should only be two. However, Lane's pictures include drops shattered into many (at least 12) droplets under free fall conditions.

The coefficient of drag on a liquid drop is assumed to be that of a solid sphere, as represented by equations (3-12) and (3-13). This is a departure from Forslund, who used an average of the above

and of that reported by Ingebo[19] for liquid drops. However, Buzzard & Nedderman[20] make a convincing case that while the drag coefficient for liquid drops is a function of such things as liquid viscosity and surface tension, it does not differ from that of a solid sphere nearly as much as Ingebo would suggest.

The model assumes that the heat flux is uniform along the test section. Except for the effects of axial conduction within three inches or so of the burnout point (see Appendix 6) and within four inches or so of either end, this is a good assumption for an Inconel test section. It may not be such a good assumption with the test sections of other experimenters, generally made of stainless steel; Forslund allowed for this in his analysis by including in his original data reduction a correction for the change in electrical resistivity with temperature. Inasmuch as the other experimenters, whose data is compared with the model later in this chapter, report a uniform heat flux, it may be assumed that they did not make this correction.

The model neglects the pressure gradient along the test section and the concomitant change in saturation temperature and fluid properties. The pressure drop is generally quite small and the effects of the property changes are second order. This is not the case, however, for the changes of vapor properties with vapor temperature. The program allows for a linear change with temperature of the vapor's thermal conductivity, viscosity, and specific heat capacity;

changes in density are calculated by means of the perfect gas relation. Over the range of temperature that the vapor reaches, the changes are small enough so that no large error is introduced by restricting the change to a linear representation.

The model also assumes that the heat transferred directly from wall to drop can be calculated from a correlation of data of droplets film boiling on a flat plate by Baumeister et al.[13] with an empirically determined constant accounting for the facts that:

(1) not all droplets are in contact with the surface, and

(2) gravity has considerably less effect in a vertical tube than it has on a horizontal plate.

This constant, herein called K_1K_2, was found by Forslund to fit his data reasonably well when set at 0.2.

3.2. Calculations Performed

3.2.1. Prediction of Two Regimes:

One change must be made in Forslund's procedure to predict wall temperatures of Type II regimes. The assumption that

$$\frac{d V_\ell}{d z} = 0 \tag{3-21}$$

which is valid at low qualities and necessary to calculate initial conditions, is no longer valid. The calculation requires not that

this derivative equal zero but that it be known. The method outlined in Appendix 5 is to calculate $\frac{dV_v}{dz}$ and to set

$$\frac{dV_\ell}{dz} = X_A \frac{dV_v}{dz} \tag{3-22}$$

This assumption satisfies both extremes of $X_A = 0$ and $X_A = 1$. Any positive power of X_A would satisfy these extremes, though, and the choice of one as the exponent is somewhat arbitrary.

The program predicts, for a pair of runs with equal heat and mass flux and at a given equilibrium quality, that Type I run (#195) will have a higher wall temperature than the Type II run (#28). Figures 22 and 23 show this; they also show that the data shows the same trend. Figures 24 and 25 show that this is because the Type I run has greater non-equilibrium than the Type II run, which in turn is because the Type II run was in thermodynamic equilibrium upstream of the burnout point.

Figures 22 and 23 show also that any change in K_1K_2 has much more effect at low quality than at high quality. This, of course, is to be expected because at high quality there is less liquid. The calculation is made here with more than one value of K_1K_2 partly to demonstrate this point and partly to show that 0.2 is a reasonable choice for K_1K_2 in the case of nitrogen data. Figures 26 and 27 show the same effect for high mass flux and low heat flux conditions.

The significance of the existence of two regimes and of the choice between them afforded by startup procedure is that the Type II regime has lower wall temperatures than the Type I regime, given equal heat and mass fluxes. Upstream of the burnout point, this is due to liquid film on the wall; downstream, lower wall temperatures are due to lesser thermodynamic non-equilibrium. This fact is of interest to designers of systems which are temperature-limited. The lower non-equilibrium of Type II runs also yields a higher actual quality at the exit; this feature is of interest to designers of boilers that are meant to connect directly to turbines; liquid droplets have an adverse effect on the life of turbine blades.

3.2.2. Fluids Other than Nitrogen:

The program was set up to handle any fluid for which both data and properties were available, as long as the temperatures stayed below those at which radiation becomes important (Appendix 7 calculates that the temperature above which radiation cannot be neglected is in the neighborhood of 1400°F). Attempts were made to predict film boiling data for methane, propane, and water.

3.2.2.1. Methane

Figure 28 shows that $K_1K_2 = 0.2$ is not acceptable for the methane data,[23] but that $K_1K_2 = 2.0$ may be. Figure 29 shows the results of using $K_1K_2 = 2.0$ for three other methane runs. Twelve inches or

so after the calculation is begun, the agreement is quite good for these randomly selected runs.

No good reason immediately presents itself to explain why K_1K_2 should be ten times the value that works for nitrogen. This test section, like ours, was oriented vertically. The test section dimensions are not greatly different. Their test section was 0.35" I.D. and 3 feet long, whereas ours was 0.4" I.D. and 8 feet long. Forslund, who used more than one tube diameter and length, reported that neither had much effect.

3.2.2.2 Propane

Propane runs tended to group themselves into two categories: those which, after a foot or so, tended to agree with $K_1K_2 = 2.0$, and those which tended to agree with $K_1K_2 = 1.0$.

Examples of the former, shown in Figures 30 and 31, are characterized by relatively high mass flux and by a relatively low degree of non-equilibrium (see Figure 32). That the two should go together is not surprising in view of Figure 5, which shows that the degree of non-equilibrium decreases as the mass flux increases.

Examples of the latter, shown in Figures 33 and 34, are characterized by lower mass flux and more non-equilibrium, as shown by Figure 35. Again, consider Figure 5, which shows that the degree of non-equilibrium increases as the mass flux decreases.

3.2.2.3. Water

Agreement between theory and the data of Mueller[21] for 1000 psi water is poor. However, agreement between the data of one run and the next seems poor, too.

Except for run #5 (Figure 37), the agreement between theory and experiment is generally within 150°R, or about 25% of $T_w - T_{sat}$ for this data of water at 1000 psi (Figures 36 through 39). The program indicates very little rise in actual quality as the calculation progresses up the test section. This is due primarily to the high heat of vaporization of water, as Appendix 8 will attest.

It is strange that while run #5 has less than 10% more heat flux than run #6, it has roughly 45% higher difference between the measured wall and saturation temperatures, although mass flux and quality are the same. This would suggest that one of these runs (probably #5) is in error.

Figures 40 through 43 show that agreement between the theory and the data of Bennett et. al.[22] is much better. The effects of end conduction, discussed earlier, are evident in these figures, as the experimental wall temperatures drop at the right-hand end of the graphs. In the theoretical calculations, K_1K_2 was arbitrarily set equal to one. Since the theory gave consistently higher wall temperatures than were observed experimentally, more so at lower

qualities, the choice of a higher value of K_1K_2 is indicated.

The proper value of K_1K_2 seems to be a function of the fluid. One value of K_1K_2 can satisfactorily account for most data for a particular fluid, whereas a different value will satisfactorily account for another fluid.

The data for both methane and propane were provided by M. R. Glickstein [23]. Properties for nitrogen were obtained from references 24 and 25; properties of methane were obtained primarily from reference 24; properties of propane were obtained primarily from reference 26; properties of water were obtained primarily from reference 27. These properties are listed in Appendix 8.

3.3. Twisted Tape

Modification of the program so that it can predict data taken with the twisted tape installed requires changing the wall-to-vapor heat transfer coefficient to allow for the swirling vapor by replacing equation (3-1) with equation (2-13), the equation best describing the single phase twisted tape data of section 2.3.2.4.

The wall-to-drop heat transfer coefficient, equation (3-7), requires two changes. First the gravity factor g must be replaced by the centrifugal acceleration

$$a_c = r\omega_v^2 = \frac{D_T}{2}\left(\frac{\pi V_v}{y D_T}\right)^2 \qquad (3\text{-}23)$$

Second, the empirical constant K_1K_2 must be changed to reflect the new physical situation. Since the model is no longer dealing with the hypothetical fraction of gravity referred to in section 3.1 and represented by K_1, but with the entire centrifugal acceleration, K_1 should now be set equal to 1.1. The model for the physical situation existing with the twisted tape no longer assumes that droplets exist everywhere within the tube, but that the droplets are all near the tube wall, at a distance from the wall where centrifugal force is balanced by the Leidenfrost force. As the Leidenfrost force is very localized, having an inverse fourth power dependence on distance between the drop and the wall,[28] this distance is quite small and all droplets can be considered to be essentially at the tube wall for purposes of calculating the centrifugal acceleration. The packing factor referred to in section 3.1 and referred to by K_2, should now be greater than for the tube without the twisted tape. This is not to imply that the wall is covered with drops; at any but the lowest qualities, the void fraction is too high to permit this. At the low qualities near the inlet, an exception is made, as explained below. The product K_1K_2, which essentially replaced the coefficient of equation (3-3), should again be determined by the data and equation (3-7) is replaced by

$$h_{w,\delta} = K_1 K_2 \left(\frac{\pi}{4}\right)\left(\frac{6G}{\pi \rho_g}\right)^{2/3}\left(\frac{1-x_a}{v_f}\right)^{2/3}\left[\frac{K_f^{\,3} h_{fg}^{\,*} \pi^2 V_r^{\,2} \rho_f \rho_g}{(T_w - T_{sat})\mu_f \sqrt[3]{\frac{\pi}{6}}\delta 2 y^2 D_T}\right]^{1/4} \qquad (3\text{-}24)$$

Figures 44 through 47 show results of calculations using the twisted tape model for both regimes and for both degrees of tape twist. Here calculations were made for K_1K_2 equal to 0, 1, and 2. K_1K_2 = 1.5 appears to be the best choice, but the data seems to be bounded roughly by K_1K_2 = 0.5 and K_1K_2 = 2.5. This deviation from the predicted temperatures seems to indicate that two changes to the model are necessary.

First of all, at the beginning of the test section the swirl flow of the vapor is not established immediately but the centrifuging effect takes a finite length to become developed. This means that near the test section entrance the drops are not all near the wall, and the packing factor must reflect this. K_1K_2 cannot be as high as it would be downstream. This idea is strengthened by the observation that in Figure 45, with y = 4.1, the experimental and theoretical temperature profiles cross in one half the length that is required for those of Figure 46, with y = 8.5, to cross; the tape with y = 4.1 has roughly half the pitch of the tape with y = 8.5, so it takes one half the length to rotate the flow the required number of turns to put the drops on the wall.

Second, it appears that the empirically determined value of K_1K_2 is roughly 1.5.

CONCLUSIONS AND RECOMMENDATIONS

4.1 Conclusions

To be concluded are the following:

1) There are two distinct regimes of forced convection dispersed flow film boiling. Which occurs depends on the manner in which the operating point is reached; their dissimilarity in heat transfer coefficient is due to different degrees of non-equilibrium; and transition from one regime to the other is greatly affected by conduction at the test section entrance.

2) Installation of a twisted tape increases the heat transfer coefficient by a factor of 2 or 3 and can, for high mass fluxes, cause re-establishment of a liquid film on the wall near the test section exit.

3) There is definite evidence that a liquid streamer forms on the twisted tape:

   a) Droplets are observed at exit qualities greater than one, indicating more non-equilibrium than should be expected with the tape.

   b) The quality at burnout is decreased by the presence of the twisted tape.

4) The modified calculation procedure of Laverty and Forslund, based on thermodynamic non-equilibrium, is capable of predicting the data of other experimenters within 10% in regions unaffected by axial conduction using fluids other than nitrogen; however, an unexplained change in the empirical constant governing the direct wall-to-droplet heat transfer is necessary.

4.2 Recommendations

1) Visual evidence of the streamer should be gathered, perhaps most easily by extending the twisted tape into the visual test section and photographing the streamer.

2) Experiments with film boiling of water at high temperatures should be made, and the analysis thereof should include the effects of radiation from wall to drop.

3) For purposes of augmentation, the plain twisted tape should be replaced by a tape with an occasional hole in the center or by twisted internal fins; this would eliminate the streamer.

REFERENCES

1. Kruger, R. A., "Film Boiling on the Inside of Horizontal Tubes in Forced Convection", Ph.D. Thisis, MIT Dept. of Mech. Eng., June, 1961.

2. Dougall, R. S., and W. M. Rohsenow, "Film Boiling on the Inside of Vertical Tubes with Upward Flow of the Fluid at Low Qualities", MIT, Dept. of Mech. Eng., EPL Report No. 9079-26, Sept., 1963.

3. Laverty, W. F., and W. M. Rohsenow, "Film Boiling of Saturated Liquid Flowing Upward Through a Heated Tube: High Vapor Quality Range", MIT, Dept. of Mech. Eng., EPL Report No. 9857-32, Sept., 1964.

4. Laverty, W. F., and W. M. Rohsenow, "Film Boiling of Saturated Nitrogen Flowing in a Vertical Tube", ASME Paper 65-WA/HT-26, 1965.

5. Forslund, R. P., and W. M. Rohsenow, "Thermal Non-Equilibrium in Dispersed Flow Film Boiling in a Vertical Tube", MIT, Dept. of Mech. Eng., EPL Report No. 75312-44, November, 1966.

6. Forslund, R. P., and W. M. Rohsenow, "Dispersed Flow Film Boiling", ASME Journal of Heat Transfer, 90 (1968), 4, pp. 399-407.

7. Fuller, W. D., "Swirl Flow in Dispersed Flow Film Boiling", MIT, Dept. of Mech. Eng., S. M. Thesis, September, 1968.

8. Lopina, R. F., and A. E. Bergles, "Heat Transfer and Pressure Drop in Tape Generated Swirl Flow", MIT, Dept. of Mech. Eng., EPL Report No. 70281-47, June, 1967.

9. Thorsen, R., and F. Landis, "Friction and Heat Transfer Characteristics in Turbulent Swirl Flow Subjected to Large Transverse Temperature Gradients", ASME Journal of Heat Transfer, 90 (1968), 4, pp. 87-97.

10. Petukhov, B. S., V. V. Kirillov, and V. N. Mardanik, "Heat Transfer Experimental Research for Turbulent Gas Flow in Pipes at High Temperature Difference Between Wall and Bulk Fluid Temperature", Proceedings of the Third International Heat Transfer Conference, Vol. 1, August, 1966.

11. Taylor, M. F., "Experimental Local Heat Transfer Data for Precooled Hydrogen and Helium at Surface Temperatures up to 5300 Deg. R", NASA TND-2595, January 1965.

12. McAdams, W. H., Heat Transmission, 3rd Ed., McGraw-Hill, New York, 1954.

13. Baumeister, K. J., T. D. Hamill, and G. J. Schoessow, "A Generalized Correlation of Vaporization Times of Drops in Film Boiling on a Flat Plate", US-A.I.Ch.E.-No. 120, Third International Heat Transfer Conference and Exhibit, August 7-12, 1966.

14. Kent, J. C., General Motors Research Laboratory, personal communication, 1966.

15. Eisner, F., 3rd Int. Cong. App. Mech., Stockholm, 1930.

16. Cumo, M., G. E. Farello, and G. Ferrari, "Notes on Droplet Heat Transfer", Comitato Nazionale Energia Nucleare, Rome, Italy.

17. Isshiki, N., "Theoretical and Experimental Study on Atomization of Liquid Drop in High Speed Gas Stream", Report No. 35, Transportation Technical Research Institute, Tokyo, Japan.

18. Lane, W. R., "Shatter of Drops in Streams of Air", Ind. and Eng. Chem., 43 (1951), pp. 1312-1317.

19. Ingebo, R. D., "Drag Coefficients for Droplets and Solid Spheres in Clouds Accelerating in Airstreams", NACA TN 3762, September, 1956.

20. Buzzard, J. L., and R. M. Nedderman, "The Drag Coefficients of Liquid Droplets Accelerating Through Air", Chem. Eng. Sci., Vol. 22 (1967), pp. 1577-1586.

21. Mueller, R. E., "Film Boiling Heat Transfer Measurements in a Tubular Test Section", GEAP-5423 (1967).

22. Bennett, A. W., G. F. Hewitt, H. A. Kearsey, and R. F. F. Keeys, "Heat Transfer to Steam-Water Mixtures Flowing in Uniformly Heated Tubes in which the Critical Heat Flux Has Been Exceeded", AERE-R5373, 1967.

23. Glickstein, M. R., Pratt & Whitney Aircraft Co., personal communication, 1967.

24. Thermophysical Properties Research Center Data Book, Vol. 2.

25. Strobridge, T. R., "The Thermodynamic Properties of Nitrogen from 114 to 540 °R between 1.0 and 3000 psia, Supplement A (British Units)", NBS Tech. Note 129A, February, 1963.

26. A Compendium of the Properties of Materials at Low Temperatures, WADD TR 60-56, July, 1960.

27. Keenan, J. H. and F. G. Keyes, Thermodynamic Properties of Steam, Wiley, New York, 1936.

28. Hynek, S. J., "The Effect of Duct Curvature on Dispersed Flow", MIT 2.57 Term Paper, May, 1967.

29. Rohsenow, W. M., and H. Y. Choi, Heat, Mass, and Momentum Transfer, Prentice-Hall, 1963.

30. Chemical Rubber Co. Standard Mathematical Tables, 12th edition.

31. Sparrow, E. M., and R. D. Cess, Radiation Heat Transfer, Brooks/Cole, 1966.

32. Moeck, E. O., G. A. Wikhammer, I. P. L. MacDonald, and J. G. Collier, "Two Methods of Improving the Dryout Heat Flux for High Pressure Steam/Water Flow", AECL-2109, December 1964.

APPENDIX 1

MEASUREMENT OF THE POWER FACTOR

The power dissipated by an electric heater is given by

$$P = V A \cos \phi \qquad \text{(A1-1)}$$

where ϕ is the phase angle between the voltage and current. This phase angle comes about because a hollow tube is not a purely resistive load but has some inductance.

To measure the power factor, the voltmeter was connected to the X axis of an oscilliscope and the ammeter to the Y axis, thus generating a Lissajous figure which indicated the phase lag. The results are shown in Figure 48 . The average value of the power factor was measured to be 0.94. The fact that there is no apparent dependence of power factor on power level may be interpreted to mean that the power factor is due only to constant factors, such as the tube inductance, and not to factors that vary with power level, such as saturation of transformers.

Note: An independent power factor evaluation was made after this report was completed. It was found that the actual power factor was 0.99; hence, there is a small error in some of the data reported for nitrogen.

APPENDIX 2

DERIVATION OF TEMPERATURE DIFFERENCE ACROSS TUBE WALL

Let $\left(q/A\right)$ be the heat flux on the inside wall if no heat were lost through the outisde wall. Let F be the fraction of the heat generated in the tube that is lost through the outer wall. Let W be the heat generated per unit volume of tube. Let ℓ, K, r_i, and r_o be the length, conductivity, inside and outside radii , respectively, of the tube. Since neither the resistivity, conductivity, nor density of Inconel 600 change rapidly with temperature and since temperature differences calculated by this method never exceed 5 °F, constant properties can be assumed.

W is calculated from q/A

$$W = \frac{(q/A)\,2\pi\ell\, r_i}{\pi\ell\,(r_o^2 - r_i^2)} \qquad \text{(A2-1)}$$

Heat loss through the outside wall is taken to be the fraction F of the heat generated, yielding the boundary condition

$$(q/A)_{out} = -K\left.\frac{dT}{dr}\right|_{out} = -F\,\frac{W\pi\ell\,(r_o^2 - r_i^2)}{2\pi\ell\, r_o} = -F\,(q/A)\,\frac{r_i}{r_o} \qquad \text{(A2-2)}$$

or

$$\frac{dT}{dr} = -\frac{F}{K}\,(q/A)\,\frac{r_i}{r_o} \qquad \text{(A2-3)}$$

Given a uniform W and K, we can make use of the standard solution to the conduction equation in cylindrical coordinates.[29]

$$T = -\frac{W}{4K} r^2 + C_1 \ln r + C_2 \tag{A2-4}$$

This must also apply at $r = r_o$

$$T = -\frac{W}{4K} r_o^2 + C_1 \ln r_o + C_2 \tag{A2-5}$$

Equation (A2-5) can be differentiated to make use of the boundary condition implied by equation (A2-3)

$$\left.\frac{dT}{dr}\right|_o = -\frac{W}{2K} r_o + \frac{C_1}{r_o} = -\frac{F}{K} (q/A) \frac{r_i}{r_o} \tag{A2-6}$$

Solving equation (A2-6) for C_1, we get

$$C_1 = -\frac{F}{K} (q/A) r_i + \frac{W}{2K} r_i^2 \tag{A2-7}$$

Equation (A2-7) is now inserted into equation (A2-5) and the result is solved for C_2

$$C_2 = T_o + \frac{W}{4K} r_o^2 - \ln(r_o) \left(\frac{W}{2K} r_o^2 - \frac{F}{K} (q/A) r_i \right) \tag{A2-8}$$

Equation (A2-4) is evaluated at $r = r_i$; equations (A2-7) and (A2-8) are inserted into it.

$$T_i = T_o + \frac{W}{4K}(r_o^2 - r_i^2) - \ln\left(\frac{r_o}{r_i}\right)\left(\frac{W}{2K} r_o^2 - \frac{F}{K}(q/A) r_i\right) \quad \text{(A2-9)}$$

APPENDIX 3

MEASUREMENT OF THE MINIMUM HEAT FLUX

The minimum heat flux that could support a Type I regime (film boiling beginning at the test section entrance) was measured under both sets of conditions shown in Figure 49; that is, for the cases of thermal conduction into and out of the inlet flange via the power line. The minimum heat flux was determined by establishing a Type I regime with a mass flux of 40,000 lb_m/ft^2-hr, and by decreasing the power incrementally until the vapor film at the entrance collapsed, as indicated by a sharp decrease in the temperature monitored by the flange thermocouple. After each power change, the system was allowed to reach steady state.

Figure 49A shows the case of conduction into the test section. For this case, the heat transmitted to the fluid is the sum of the heat generated in the tube and that conducted in through the power connection. The minimum heat flux was observed to be 2,200 Btu/ft^2-hr; the flange thermocouple read 220°R at this point. Data were taken at other mass fluxes, and the results were very nearly the same (see Reference 7).

Figure 49B shows the case of conduction away from the test section. This was brought about by the guard cooler mentioned in section 2.1.2.4. For this case, the heat transmitted to the fluid is the difference between the heat generated in the tube and that conducted away by the power connection. The minimum heat flux was observed to be 18,700 Btu/ft^2-hr; the flange thermocouple read 452°R at this point.

From the difference in the measured heat fluxes it is apparent that the heat conducted into or away from the test section inlet is considerable.

APPENDIX 4

DERIVATION OF LIQUID FILM THICKNESS, VELOCITY AND FLOW RATE ON THE TWISTED TAPE

To determine the maximum amount of liquid that can exist on the wall, it is necessary to balance centrifugal force against surface tension. Centrifugal force is related to rotational velocity which in turn is related to the axial velocity of the film. This axial velocity is determined by the shear stress of the vapor phase flowing by.

First, the average film thickness (see Figure 50) is solved for as a function of rotational velocity. There exists pressure gradients due to centrifugal force fields in both the vapor and the liquid.

$$\left.\frac{dp}{dr}\right|_{\ell} = \rho_{\ell}\, r\, \omega_{\ell}^{2} \tag{A4-1}$$

and

$$\left.\frac{dp}{dr}\right|_{v} = \rho_{v}\, r\, \omega_{v}^{2} \tag{A4-2}$$

Integrating each derivative from the center, where pressures in the liquid and vapor are equal, and taking the difference yields

$$\Delta p(r) = p_{\ell}(r) - p_{v}(r) = \frac{r^2}{2}\left(\rho_{\ell}\,\omega_{\ell}^{2} - \rho_{v}\,\omega_{v}^{2}\right) \tag{A4-3}$$

The thickness t of the film is a function of r and is related to the pressure difference across the liquid-vapor interface by

$$\frac{d^2 t}{dr^2} = -\frac{\Delta p}{2\sigma} = -\frac{r^2}{2\sigma}\left(\rho_{\ell}\,\omega_{\ell}^{2} - \rho_{v}\,\omega_{v}^{2}\right) \tag{A4-4}$$

Integrating,

$$\frac{dT}{dr} = -\frac{r^3}{6\sigma}\left(\rho_\ell \omega_\ell^2 - \rho_v \omega_v^2\right) + C_1 \qquad \text{(A4-5)}$$

Since $\frac{dT}{dr} = 0$ at r = 0, $C_1 = 0$.

Integrating again,

$$t(r) = -\frac{r^4}{24\sigma}\left(\rho_\ell \omega_\ell^2 - \rho_v \omega_v^2\right) + C_2 \qquad \text{(A4-6)}$$

Since t(r) = 0 at r = R,

$$C_2 = \frac{R^4}{24\sigma}\left(\rho_\ell \omega_\ell^2 - \rho_v \omega_v^2\right) \qquad \text{(A4-7)}$$

Thus,

$$t(r) = \frac{R^4}{24\sigma}\left(\rho_\ell \omega_\ell^2 - \rho_v \omega_v^2\right)\left(1 - \left(\frac{r}{R}\right)^4\right) \qquad \text{(A4-8)}$$

The average film thickness is given by

$$\hat{t} = \frac{1}{R}\int_0^R t(r)\, dr \qquad \text{(A4-9)}$$

or

$$\hat{t} = \frac{R^4}{30\sigma}\left(\rho_\ell \omega_\ell^2 - \rho_v \omega_v^2\right) \qquad \text{(A4-10)}$$

It is assumed now that the film covers a fraction K_3 of the tape's surface. Thus,

$$R = \frac{K_3 D_T}{2} \qquad \text{(A4-11)}$$

and $$\hat{t} = \frac{(K_3 D_r)^4}{480\sigma} \left(\rho_\ell \omega_\ell^2 - \rho_v \omega_v^2 \right) \tag{A4-12}$$

Since ω_v is close to ω_ℓ and ρ_v is much less than ρ_ℓ, $\rho_v \omega_v^2$ can be neglected compared with $\rho_\ell \omega_\ell^2$.

Thus,

$$\hat{t} = \frac{(K_3 D_r)^4}{480\sigma} \rho_\ell \omega_\ell^2 \tag{A4-13}$$

Perhaps one of the boundary conditions should specify that dt/dr at r = R should equal the tangent of the contact angle; however, another boundary condition would over-specify the problem. Differentiating equation (A4-8), using a value for ω_ℓ calculated from equations (A4-16) and (A4-26) using actual running conditions, yields a contact angle on the order of one degree. As liquid nitrogen wets Inconel quite well, this calculated contact angle indicates that although a highly wetting condition is not specified in the problem, it is in good agreement with the answer.

In the liquid film, the velocity is related to the shear stress

$$\tau = -\mu_\ell \frac{d V_z}{d t} \tag{A4-14}$$

This assumes laminar flow in the film, which doesn't exist at the Reynolds numbers calculated for the film. However, values of calculated by equation (A4-19), which is derived from equation (A4-14), are in reasonable agreement with those values of wall shear stress calculated from the observed axial pressure gradient. Thus, in the interest of solution, and with no great sacrifice of reality, equation (A4-14) is assumed valid.

Neglecting gravity (which is possible only at high quality, where velocities and shear forces are high), the average film velocity V_F can be related to the shear stress and the average film thickness by

$$V_F = \frac{\hat{t}\,\tau}{2\mu_\ell} \tag{A4-15}$$

Geometrical considerations allow calculation of the rotational velocity

$$\omega_\ell = \frac{\pi V_F}{y D_T} = \frac{\pi \hat{t}\,\tau}{2\mu_\ell\, y D_T} \tag{A4-16}$$

The shear stress is calculated from the friction factor, which in turn is taken from a curve fit to the appropriate portion of the Moody diagram[29]

$$\tau = f \frac{\rho_v \Delta V^2}{2} = \left(\frac{0.046}{Re_H^{0.2}}\right) \frac{\rho_v}{2} \left(V_v - 2V_F\right)^2 \tag{A4-17}$$

It could be assumed that the ripples that form on the film have the same effect on the friction factor as does tube roughness; therefore, the variable constant K_4 is introduced into τ

$$\tau = K_4 \left(\frac{0.046}{Re_H^{0.2}}\right) \frac{\rho_v}{2} \left(V_v - 2V_F\right)^2 \tag{A4-18}$$

Solving equation (A4-15) for τ in terms of V_F yields another expression for τ

$$\tau = \frac{2\mu_\ell}{\hat{t}}\, V_F \tag{A4-19}$$

Inserting ω_l from equation (A4-16) into equation (A4-13), solving the resultant equation for $\hat{t}$, inserting this into equation (A4-19), and equating this value for τ with that given by equation (A4-18) yields

$$\left(V_V - 2V_F\right)^2 V_F = 4V_F^3 - 4V_V V_F^2 + V_V^2 V_F = \left(\frac{y}{\pi D_T}\right)^2 \frac{480\sigma 64 \mu_L Re_H^{0.2}}{\rho_l \rho_v K_3^4 K_4 0.046} \quad \text{(A4-20)}$$

The problem now is to find the appropriate root of equation (A4-20). By inspection it is apparent that the $\left(V_V - 2V_F\right)^2$ factor yields a repeated root. Page 328 of reference 30 indicates that this means (using the nomenclature of reference 30 for the next ten equations

$$\frac{b^2}{4} + \frac{a^3}{27} = 0 \quad \text{(A4-21)}$$

This means that

$$A = B = \sqrt[3]{\frac{-b}{2}} \quad \text{(A4-22)}$$

For A and B not to be imaginary (which would yield an imaginary answer which is impossible given our two equal real roots), must be positive and A and B must be negative.

Of the three choices for X

$$X = A + B \quad ; \quad X = -\frac{A+B}{2} + \frac{A-B}{2}\sqrt{-3} \quad ; \quad X = -\frac{A+B}{2} - \frac{A-B}{2}\sqrt{-3}$$

(A4-23,24,25)

the condition that A and B be equal and negative makes equation (A4-23) negative and equations (A4-24) and (A4-25) equal and positive.

Then

$$V_F = y = X - \frac{\rho}{3} = -\sqrt[3]{\frac{b}{2}} - \frac{\rho}{3} \tag{A4-26}$$

where

$$b = \frac{1}{27}\left(2\rho^3 - 9\rho q + 27 r\right) \tag{A4-27}$$

$$\rho = -V_v \tag{A4-28}$$

$$q = \frac{V_v^4}{4} \tag{A4-29}$$

and

$$r = \frac{-120\,\sigma\,64\,\mu_l\,Re_H^{0.2}}{\rho_l\,\rho_v\,K_3^4\,K_4\,0.046} \tag{A4-30}$$

Inserting equation (A4-16) into equation (A4-13) yields

$$\hat{t} = \frac{K_3^4\,D_T^2\,\pi^2\,\rho_l\,V_F^2}{480\,\sigma\,y^2} \tag{A4-31}$$

The mass flow rate of the streamer is given by

$$w = \rho_l\,A_F\,V_F = \rho_l\,4\hat{t}\,K_3\,D_T\,V_F \tag{A4-32}$$

Inserting equation (A4-31) (A4-32) into equation (A4-32) yields the streamer flow rate in terms of the streamer velocity.

$$w = \frac{K_3^5\,D_T^3\,\pi^2\,\rho_l^2\,V_F^3}{120\,\sigma\,y^2} \tag{A4-33}$$

Evaluation of equation (A4-33) under actual running conditions using reasonable values ($K_3 = 0.6$, $K_4 = 4$) for the flexible constants indicates that large fractions of the liquid flow can be contained in the streamer, even more liquid than is present in the flow. This indicates that the force balance between centrifugal force and surface tension is not the limiting factor in determining the amount of liquid in the streamer. Rather, the amount of liquid present near the tape at the point where the streamer is formed and the rate of evaporation of the streamer (due primarily to heat generation within the tape) are more likely to be the factors that limit the streamer flow rate. In view of the uncertainty in this analysis, the liquid on the tape was not considered in the analytical prediction of the swirl flow data (3.3).

APPENDIX 5

DERIVATION OF INITIAL VELOCITIES AND DROP DIAMETER

Initial velocities for vapor and droplets are calculated by a method similar to Forslund's but with two differences. First, the initial acceleration of the droplet is not assumed to be zero, for this method must apply to conditions where the calculation is initiated at high qualities. Second, the form of the equations and the method of iteration is different, for Forslund's iteration scheme was seen to be unstable at high qualities. Droplet size is achieved by means of the critical Weber number and is eliminated from the early equations by the same means.

A force balance on the drop yields

$$a = \frac{dV_f}{dt} = V_f \frac{dV_f}{dz} = \frac{\frac{1}{2}\rho_v (V_f - V_v)^2 C_D \frac{\pi}{4}\delta^2}{\pi/6\ \rho_f \delta^3} - g = \frac{.75\rho_v C_D \Delta V^2}{\rho_f \delta} - g \qquad \text{(A5-1)}$$

Intuitively one can see that while the droplet acceleration is zero at zero quality, it must equal the vapor acceleration at an actual quality of unity. Thus one could expect the drop acceleration to be equal to the vapor acceleration multiplied by the quality to some power. This power was somewhat arbitrarily set to be one.

Vapor acceleration can be found under isothermal conditions to be proportional to the rate of vapor generation, as no heat is lost to superheat the vapor.

$$\frac{d w_v}{dz} = \frac{(q/A)\pi D_T}{h_{fg}} \qquad \text{(A5-2)}$$

Since

$$w_v = \rho_v A_v V_v \qquad \text{(A5-3)}$$

and since ρ_v is constant under isothermal conditions when pressure drop in the test section is small, and since A_v is almost constant and equal to A with length at any but the lowest quality (see Figure 51),

$$\frac{d w_v}{dz} = \rho_v A_v \frac{d V_v}{dz} \tag{A5-4}$$

or

$$\frac{d V_v}{dz} = \frac{1}{\rho_v A_v} \frac{d w_v}{dz} = \frac{(q/A)\pi D_T}{h_{fg} \rho_v \frac{\pi}{4} D_T^2} \tag{A5-5}$$

or

$$\frac{d V_\ell}{dz} = X_A \frac{d V_v}{dz} = \frac{4 X_A (q/A)}{\rho_v h_{fg} D_T} \tag{A5-6}$$

Inserting equation (A5-6) into equation (A5-1) yields

$$g + \frac{4 X_A (q/A) V_\ell}{\rho_v h_{fg} D_T} = \frac{.75 \rho_v C_D \Delta V^2}{\rho_\ell \delta} \tag{A5-7}$$

The maximum drop size is determined by the Weber number criterion

$$\frac{\rho_v (\Delta V)^2 \delta}{\sigma} \geq We_c \tag{A5-8}$$

where We_c is in the neighborhood of 7.5 or, inverting

$$\delta = \frac{We_c \sigma}{\rho_v (\Delta V)^2} \tag{A5-9}$$

Inserting equation (A5-9) into equation (A5-7) and solving for ΔV yields

$$\Delta V = \sqrt[4]{\left(g + \frac{4(q/A) X_A V_\ell}{\rho_v h_{fg} D_T} \right) \frac{\rho_\ell We_c \sigma}{.75 C_D \rho_v^2}} \tag{A5-10}$$

Thus,

$$V_v = V_\ell + \Delta V = V_\ell + \sqrt[4]{\left(g + \frac{4(\rho/A)\, X_A V_\ell}{\rho_v h_{fg} D_T}\right) \frac{\rho_\ell We_c \sigma}{.75 C_D \rho_v^2}} \qquad \text{(A5-11)}$$

In addition to equation (A5-11), V_v and V_ℓ must satisfy the continuity equation.

From the definition of flowing quality

$$X_A = \frac{\rho_v A_v V_v}{\rho_v A_v V_v + \rho_\ell A_\ell V_\ell} = \frac{\rho_v A_v V_v}{G A} \qquad \text{(A5-12)}$$

we see that

$$1 - X_A = \frac{\rho_\ell A_\ell V_\ell}{G A} = \frac{\rho_\ell V_\ell}{G}\left(1 - \frac{A_v}{A}\right) \qquad \text{(A5-13)}$$

since

$$A_v + A_\ell = A \qquad \text{(A5-14)}$$

Solve equation (A5-13) for A_v/A

$$\frac{A_v}{A} = 1 - \frac{G(1 - X_A)}{\rho_\ell V_\ell} \qquad \text{(A5-15)}$$

and insert it into equation (A5-12) solving equation (A5-12) for V_v

$$V_v = \frac{G X_A}{\rho_v}\left(\frac{A}{A_v}\right) = \frac{G X_A}{\rho_v}\left[1 - \frac{G(1 - X_A)}{\rho_\ell V_\ell}\right]^{-1} \qquad \text{(A5-16)}$$

Both velocities are now determined by equation (A5-11) and equation (A5-16). Neither equation is linear, but iterative techniques

can be used to find a value for V_ℓ that satisfies both equations. However, there are in general two values for V_ℓ that satisfy both equations, as is indicated by Figure 52. It is possible, particularly at low qualities, to converge at the wrong point; therefore V_ℓ is set initially to a value just above that which makes equation (A5-16) blow up,

$$V_\ell\Big|_{initial} = \frac{G(1-X_a)}{\rho_\ell} + 10 \qquad \text{(A5-17)}$$

to insure that the iteration proceeds to the meaningful (positive) root. The existence of more than one root is shown by Figure 52, which graphs equations (A5-11) and (A5-16).

Using equation (A5-17) as the initial guess, the iteration scheme evaluates equations (A5-11) and (A5-16) at successively larger values of V_ℓ until equation (A5-11) is greater than (A5-16). The increment in V_ℓ is decreased by a factor of 10, and the iteration proceeds toward lower values of V_ℓ until the intersection point of Figure 52 is again crossed. The increment is again decreased by a factor of 10, and the iteration proceeds toward larger values of until the intersection point is again crossed. Now that both calculated values for V_v agree to within one percent, the iteration ceases and V_v is taken to be the average of the two calculated values. Knowing V_v and V_ℓ, δ is now calculated from equation (A5-9)

$$\delta = \frac{We_c\,\sigma}{\rho_v (V_v - V_\ell)^2} \qquad \text{(A5-9)}$$

In evaluating equation (A5-11), the value of C_D is taken to be 0.45. After the iteration is finished, the Reynolds number of the drop is calculated. If it is less than 2000, a new value of C_D is calculated from equation (3-12); the iteration is begun anew and repeated four times to converge on an acceptable value for C_D .

APPENDIX 6

EFFECTS OF AXIAL CONDUCTION NEAR THE BURNOUT POINT

At the burnout point the change of temperature with test section length is so great that axial conduction occurs. To determine the degree and extent along the test section of this conduction, the following sample calculation was made.

We assume cylindrical symmetry, reducing the problem to two dimensions. Noting that the tube thickness (0.050") is small compared to the radius (0.250"), we use Cartesian coordinates. The boundary conditions, shown in Figure [53], are as follows: one side, representing the outer wall of the tube, is adiabatic; two other sides, at a distance from the burnout point that is large compared with the extent of the observed effect, are assumed adiabatic; and the side representing the inner wall has an assumed heat transfer coefficient that is discontinuous at the burnout point. On the liquid-film side of the burnout point, we assume that h = 500; on the burnedout side, we assume that h = 50. The actual heat transfer coefficients observed experimentally differ more. We have chosen a value of 20,000 Btu/ft^2-hr for the heat flux, which is slightly higher than our apparatus would allow.

The method of solution is to set up a matrix whereby the steady-state conduction equation

$$\frac{\partial^2 T}{\partial x^2} + \frac{\partial^2 T}{\partial y^2} = -\frac{W}{K} \qquad \text{(A6-1)}$$

where W = volumetric rate of heat generation

is satisfied at the 176 nodes shown in Figure 53 . Once we have the temperatures, we use the two rows of nodes nearest the inner wall to give us the temperature gradient, thus heat flux, across the inner wall. Both the inner wall temperature and the heat flux are shown in Figure 54 .

As can be seen, the effect of axial conduction, the disruption of uniformity of the heat flux, extends only an inch or so to either side of the burnout point.

APPENDIX 7

EFFECT OF RADIATION

It is rather obvious that the effect of radiation is negligible for film boiling of cryogenic fluids, but is not so readily apparent that it can be neglected for film boiling of water. The temperatures reported by Mueller (21) are as high as 1400°F. The following are sample calculations for radiation from wall to vapor and from wall to drop.

Radiation from Wall to Vapor:

We shall evaluate the worst possible case. Let the tube wall temperature be 1400°F, as in Run 5 for Mueller's (21) water data. It is difficult to use the Hottel Mean Beam Length (29) method, for the pressure is too high to allow calculation of the correction factor for converting the emissivity at 1 atm. to that at our 1000 psi pressure by means of the published graph; however, the absorptivity of the vapor cannot be any greater than one, so we will use this value for our worst-case calculation. The emissivity of stainless steel can be as high as 0.97 (when oxidized); however, a long tube can look like a cavity to the gas, so we can set the wall emissivity equal to one, especially for our worst case. When the vapor is not superheated at all, corresponding to the worst case, its temperature is 1005°R. Thus, the heat flux is given by

$$q/A\Big|_{radiation} = \sigma \left(T_w^{\,4} - T_v^{\,4} \right) = 18{,}800 \ \frac{Btu}{ft^2\text{-}hr} \qquad \text{(A7-1)}$$

where σ = Stefan-Boltzmann constant = $0.171 \times 10^{-8} \ \frac{Btu}{ft^2\text{-}hr\text{-}°R^4}$

This value is pretty small compared to the 292,000 Btu/ft^2-hr heat flux leaving the tube wall.

Radiation from Wall to Drop:

Here again we can set the wall emissivity, for the worst case, equal to one. The absorptivity of a water drop can be calculated given its temperature and size; the calculation is long, as one must determine an effective wavelength above which water absorbs essentially all radiation. This wavelength appears to be about 2 microns. According to Planck's black body energy distribution (31), roughly 90% of the energy emitted by a black surface at 1860°R is above 2 microns in wavelength and is thus absorbed. However, since this is a rough idea of the absorptivity and since this is a worst-case calculation, we shall set the absorptivity equal to one.

Equation (1) yields the same value as before. This must be compared with the heat flux entering the drop, as calculated by the analytical program. The calculated heat flux to the droplet depends strongly on K_1K_2 = 0 and 72,400 for K_1K_2 = 2.

This should mean that the addition of radiation to the analytical program for this run would be roughly equivalent to increasing K_1K_2 by 0.5, which in turn would result in decreasing the calculated wall temperature by 50°R. All this is based on the reported wall temperature of 1800°R. Were the radiation calculations based on the highest calculated wall temperature (remember, Run 5 was the least trusted of

the reported data), with $K_1K_2 = 0$, of 1780°R, we would have calculated a radiation heat flux of 15,700. Were the calculation based on the highest calculated wall temperature, with $K_1K_2 = 2$, of 1700°R, the radiation heat flux would be 13,100, or 18% of the heat flux calculated without radiation.

Radiation should account for a larger portion of the wall-to-drop heat transfer for drops smaller than the maximum size considered here. The radiation heat flux is independent of drop size, whereas the convective heat flux decreases with drop size, for the slip velocity decreases with decreasing drop size.

The conclusion is that radiation can be ignored if the wall temperatures are low, say below 1300°R, or if any significant measure of wall to drop heat transfer already exists.

APPENDIX 8

LIST OF FLUID PROPERTIES

Fluid		Nitrogen	Methane	Propane	Water
P	psia	20	150	150	1,000
T_{sat}	°R	144	187	542	1,005
h_{fg}	Btu/lb_m	84.2	269.8	142.3	649.4
σ	lb_m/hr^2	2.44×10^5	1.95×10^5	1.95×10^5	5.15×10^5
u_L	lb_m/hr ft	0.344	--	--	--
ρ_L	lb_m/ft^3	50.0	22.6	30.75	45.9
ρ_g	$lb_m ft^3$	0.39	1.0	1.45	2.24
k_g	Btu/hr ft°F	.0044	.008	.0108	0.0316
u_g	lb_m/hr ft	.0143	.0141	.0196	0.00695
c_{pg}	Btu/lb_m°F	.2481	.4955	.4023	1.25
$\frac{dk_g}{dT}$	Btu/hr ft $(°F)^2$	3×10^{-5}	4×10^{-5}	7.2×10^{-5}	0
$\frac{du_g}{dT}$	lb_m/hr ft°F	7.42×10^{-5}	5.08×10^{-5}	2.56×10^{-5}	1.85×10^{-6}
$\frac{dc_{pg}}{dT}$	Btu/$lb_m(°F)^2$	0	7.5×10^{-5}	4.81×10^{-4}	-2.4×10^{-3}

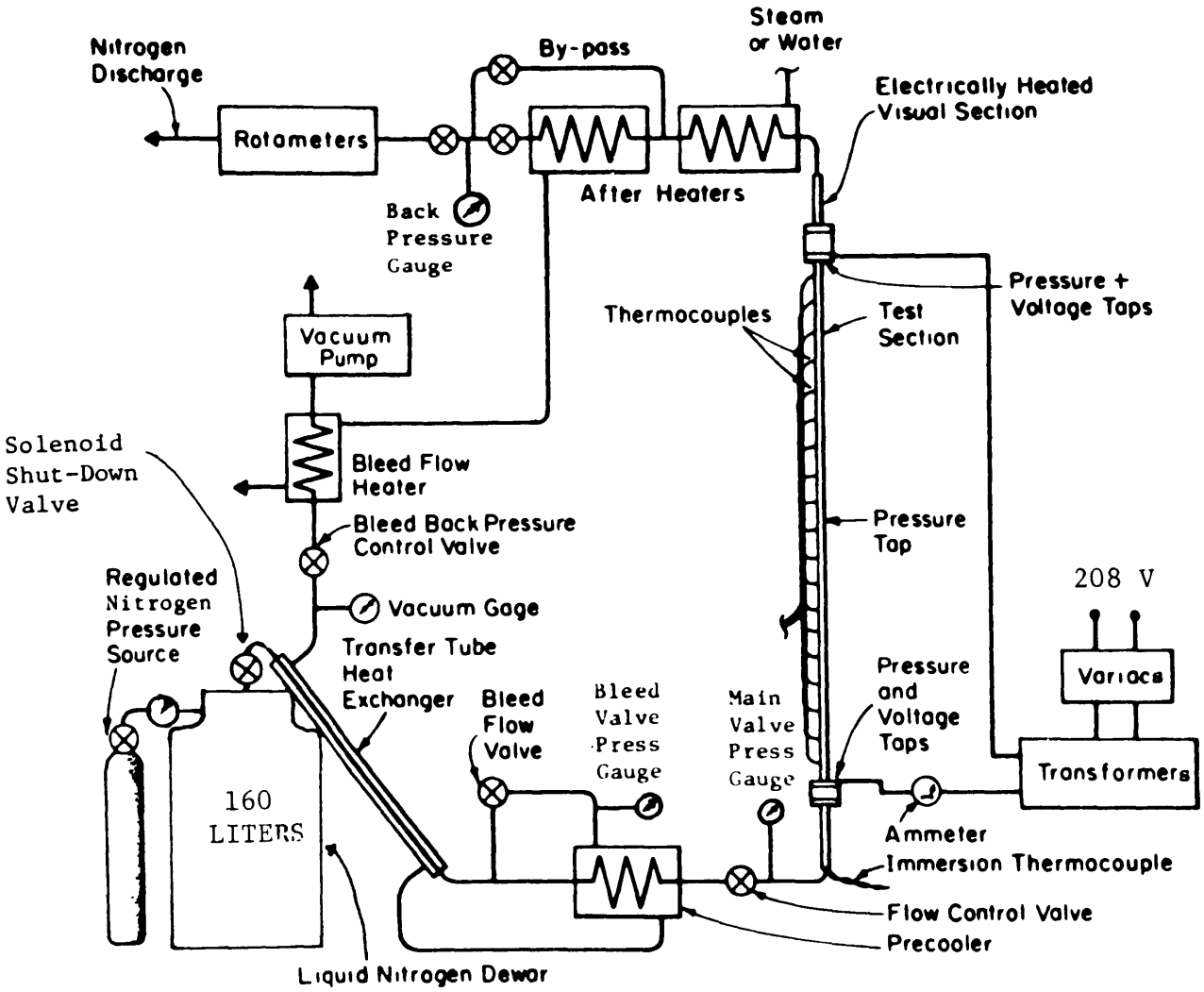

Fig. 1 Schematic Diagram of the Test Apparatus

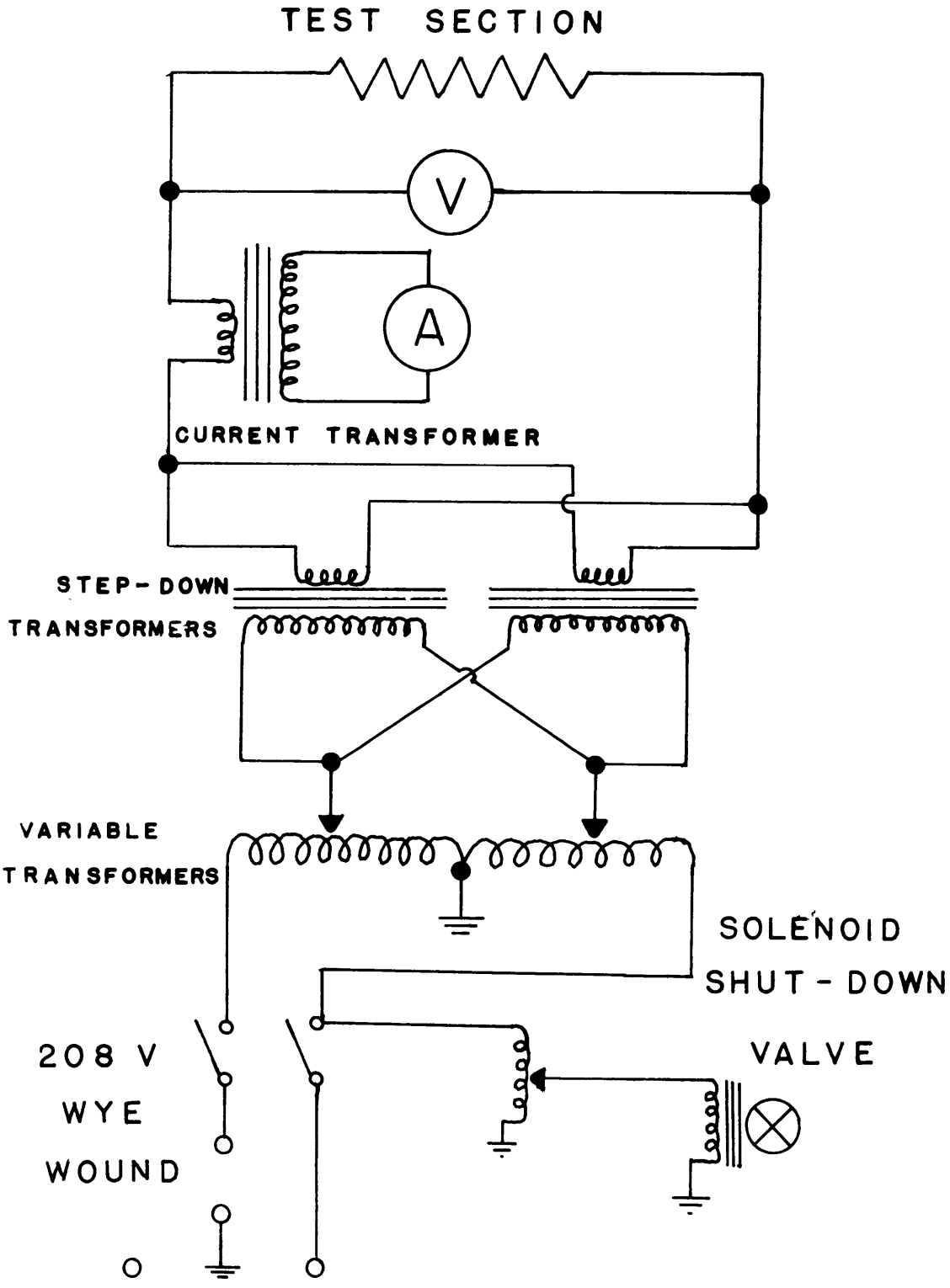

FIGURE 2. ELECTRICAL DIAGRAM OF THE TEST APPARATUS

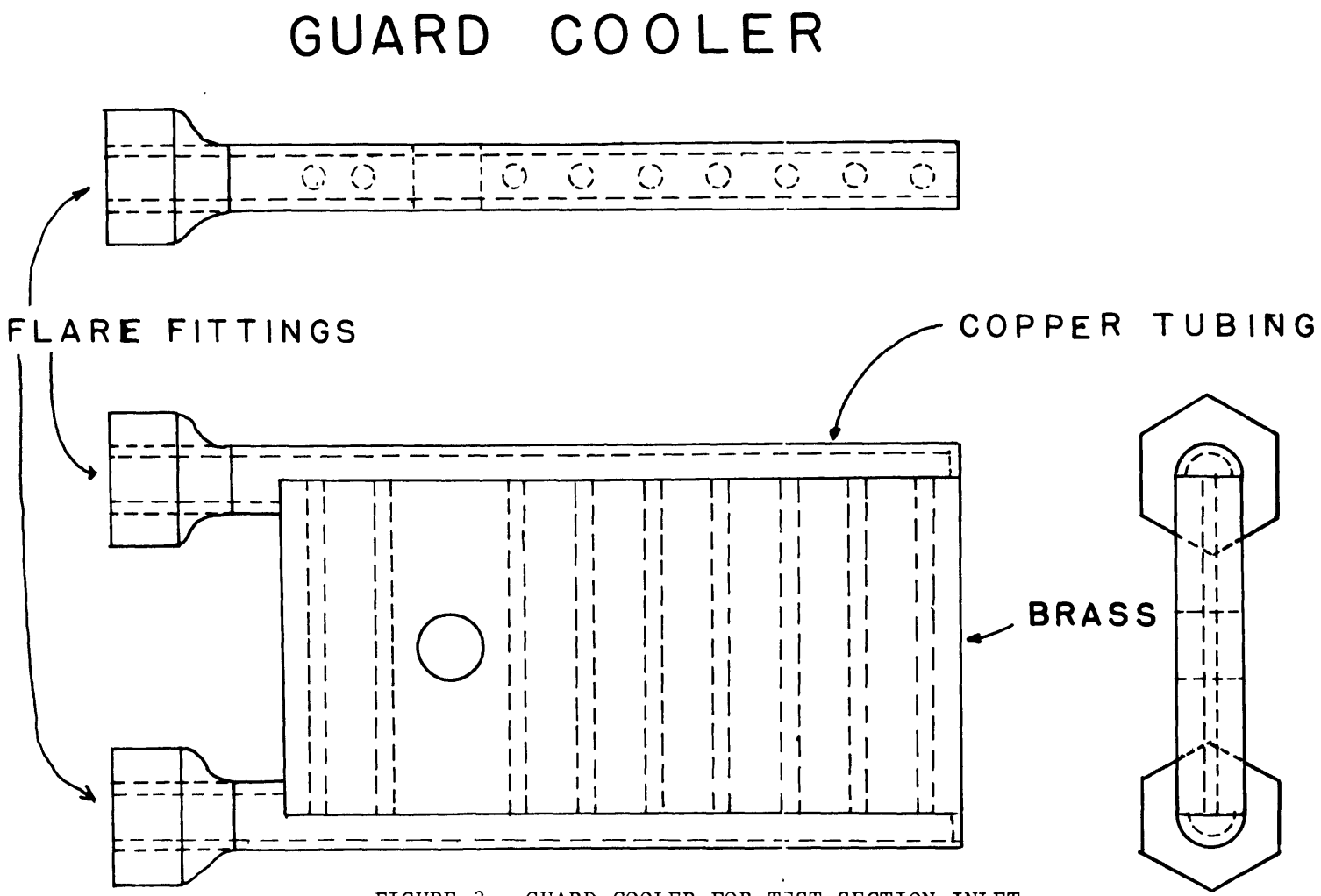

FIGURE 3. GUARD COOLER FOR TEST SECTION INLET

RUN NUMBER 232 DATE 9/14/68 TIME 1225

INCONEL, TAPE, T2=4.1

* HEAT FLUX = 13,243 BTU/HR-SQFT		VOLTS = 12.79		AMPS = 3.39	*
* MASS FLUX = 36,826 LBM/HR-SQFT		FLOWI = 129.0		FLOWR = 94.0	*
* BACK PRESSURE = 3.2 PSIG		MANH 735 561 604 647 766			*
* INLET SUBCOOLING = 10.0 DEGREES RANKINE		MANI 293 464 302 336 281			*
* INLET TEMPERATURE = 135.3 DEGREES RANKINE		BLEED VALVE PRESSURE = 18.30 PSIA			*
* OUTLET TEMPERATURE = 436.3 DEGREES RANKINE		BLEED LINE PRESSURE = 9.35 PSIA			*
* TEST SECTION RESISTANCE = 0.047 OHMS		CURRENT RATIO = 9.77			*
* INLET VELOCITY = 2.54 FT/SEC		DEWAR TEMPERATURE = 145.8 DEGREES RANKINE			*
* PRESSURE DROP IN SUBCOOLER = 8.95 PSI		BLEED LINE TEMPERATURE = 126.4 DEGREES R			*

TC NO	HEIGHT INCHES	ABS PRESS PSIA	PR GRAD PSI/IN	OUTER TEMP DEGREES R	INNER TEMP DEGREES R	SAT TEMP DEGREES R	BULK TEMP DEGREES R	HT COEFF BTU/HR-DEGF-FT2	EQUIL QUAL
1	2	23.20	-0.0050	624.22	621.22	146.75	141.36	27.60	-0.031
2	6	23.17	-0.0106	563.66	560.51	146.73	146.73	32.00	0.034
3	10	23.12	-0.0156	513.30	510.12	146.69	146.69	36.44	0.100
4	14	23.05	-0.0208	475.62	472.25	146.64	146.64	40.67	0.165
5	18	22.96	-0.0257	461.15	457.74	146.57	146.57	42.56	0.231
6	22	22.86	-0.0271	436.26	432.78	146.50	146.50	46.26	0.296
7	26	22.74	-0.0303	396.38	390.77	146.42	146.42	54.27	0.362
8	30	22.62	-0.0331	375.61	371.96	146.32	146.32	58.70	0.427
9	34	22.48	-0.0353	354.38	350.64	146.22	146.22	64.78	0.493
10	38	22.33	-0.0384	353.21	349.46	146.11	146.11	65.12	0.558
11	42	22.17	-0.0409	343.73	339.95	145.99	145.99	68.28	0.624
12	46	22.00	-0.0435	342.53	338.75	145.86	145.86	68.46	0.689
13	50	21.82	-0.0461	343.13	339.35	145.72	145.72	68.40	0.755
14	54	21.63	-0.0489	342.53	338.75	145.58	145.58	68.56	0.821
15	58	21.43	-0.0521	362.57	358.81	145.42	145.42	62.06	0.886
16	62	21.22	-0.0555	375.05	371.37	145.25	145.25	58.57	0.952
17	66	20.99	-0.0593	403.37	396.72	145.07	150.84	53.84	1.017
18	70	20.74	-0.0634	425.54	422.02	144.87	172.69	53.11	1.083
19	74	20.48	-0.0684	450.31	446.86	144.66	194.52	52.48	1.148
20	78	20.19	-0.0733	475.14	471.77	144.43	214.33	51.84	1.214
21	82	19.88	-0.0801	493.56	490.24	144.17	238.11	52.53	1.279
22	86	19.55	-0.0873	543.33	540.14	143.89	259.87	47.25	1.345
23	90	19.19	-0.0967	573.96	570.74	143.58	281.60	45.89	1.410
24	94	18.79	-0.1034	596.49	593.42	143.23	303.30	45.65	1.476

OUTLET TEMPERATURE= 436.26 DEGREES RANKINE
TOTAL PRESS DROP= 4.63 PSI
PRESS DROP(XE=0 TO 0.5)= 2.724 PSI
PRESS DROP(XE=0 TO 1.0)= 2.140 PSI

Figure Sample Printout from Data Reduction Program.

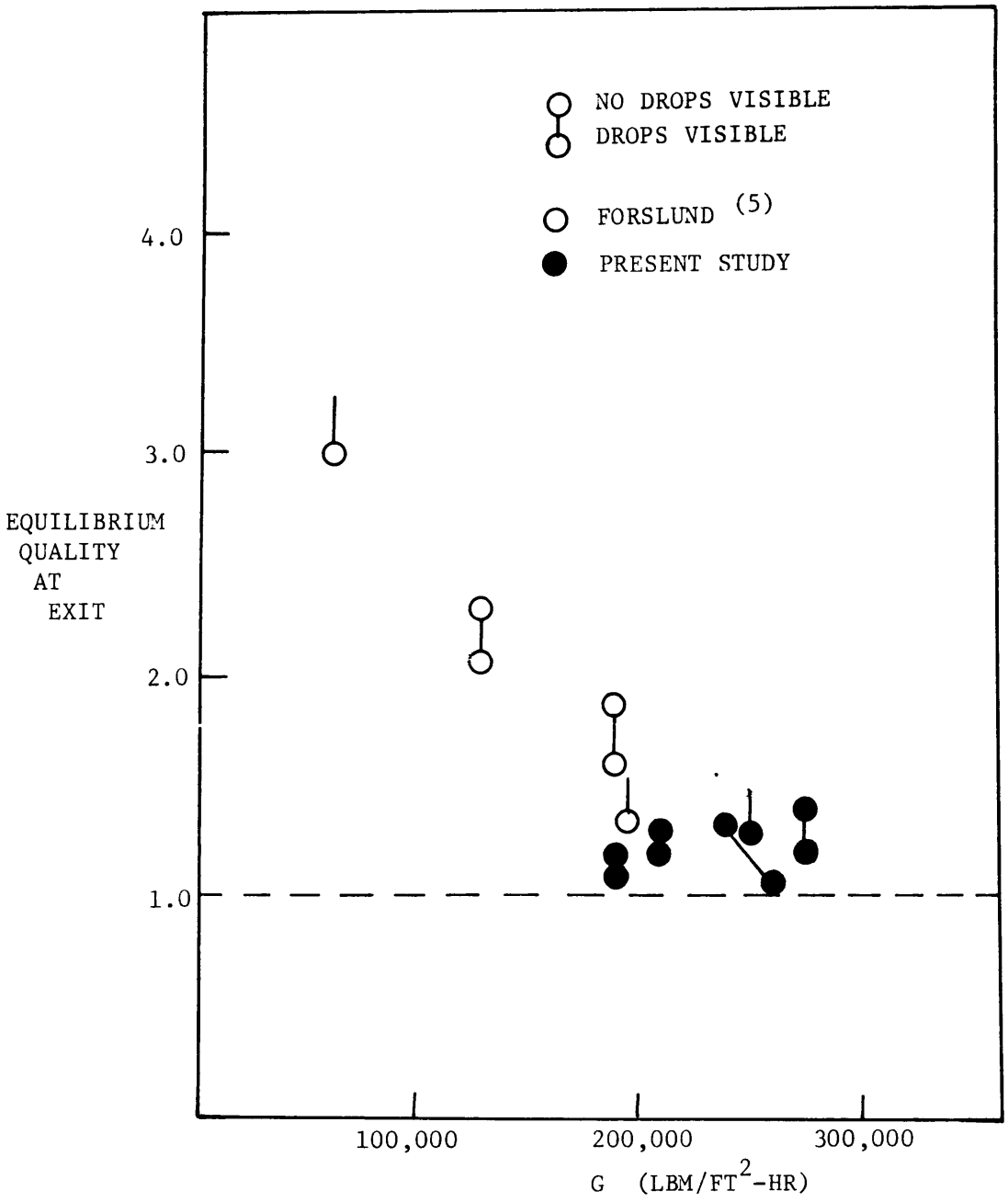

FIGURE 5. EQUILIBRIUM QUALITY CORRESPONDING TO COMPLETE EVAPORATION

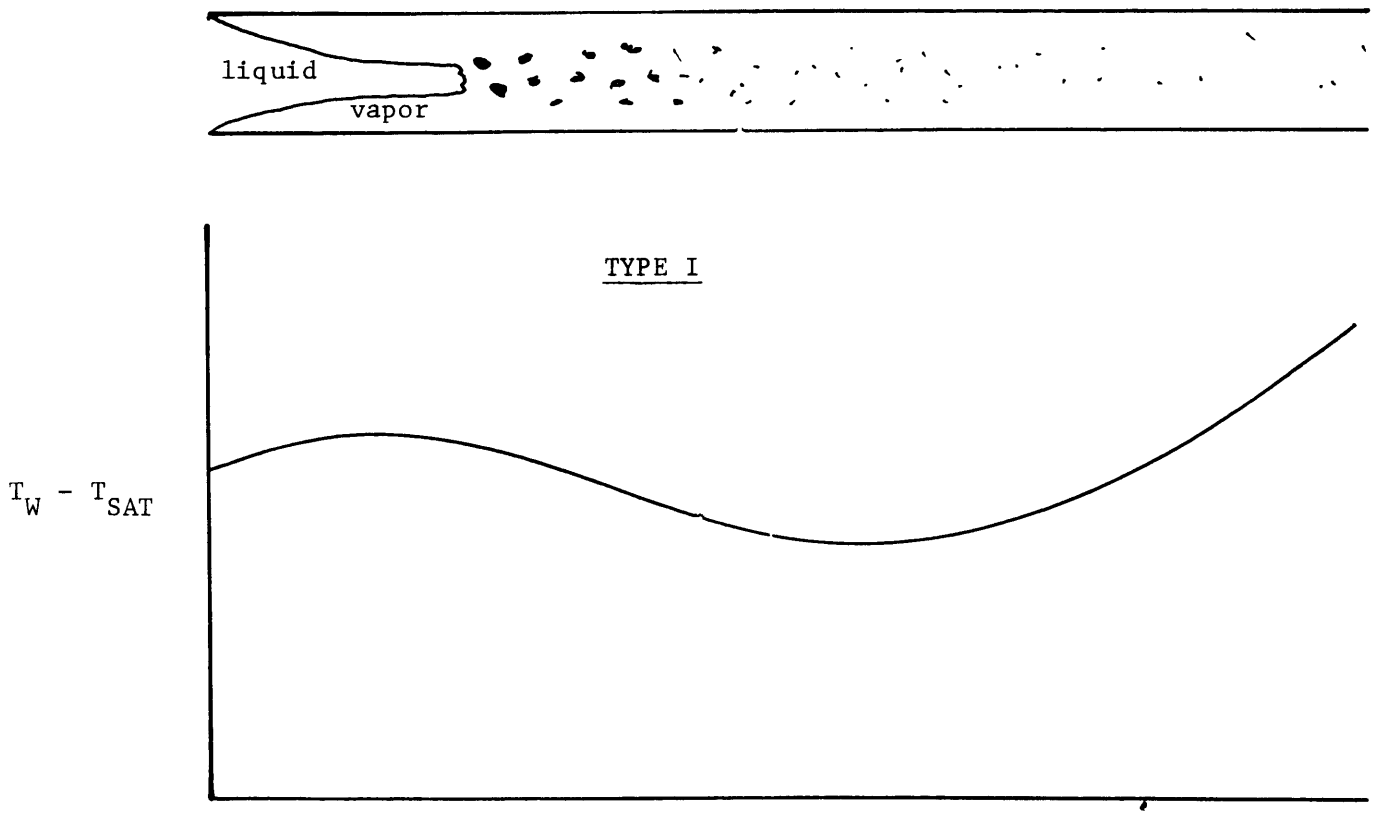

FIGURE 6. TYPE I REGIME

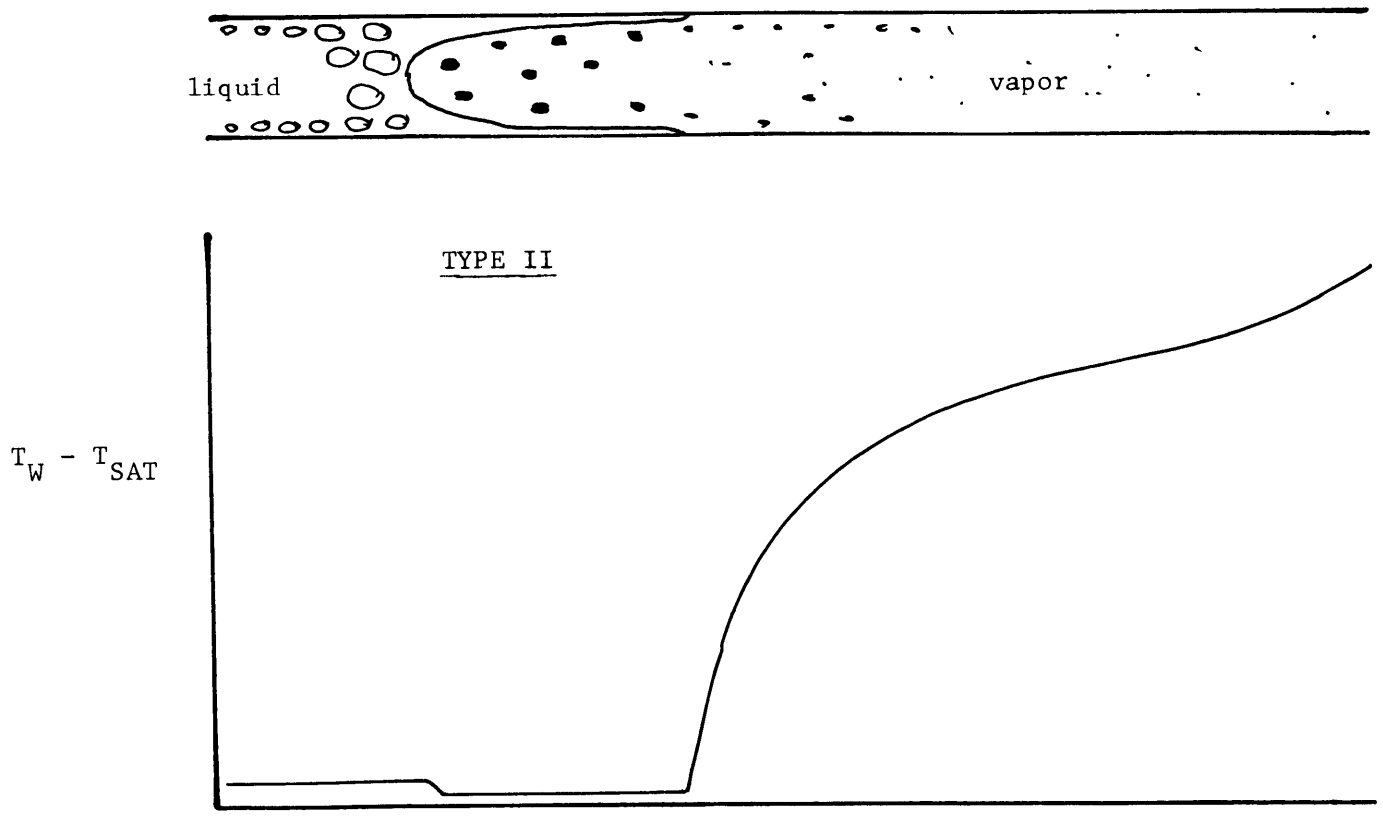

FIGURE 7. TYPE II REGIME

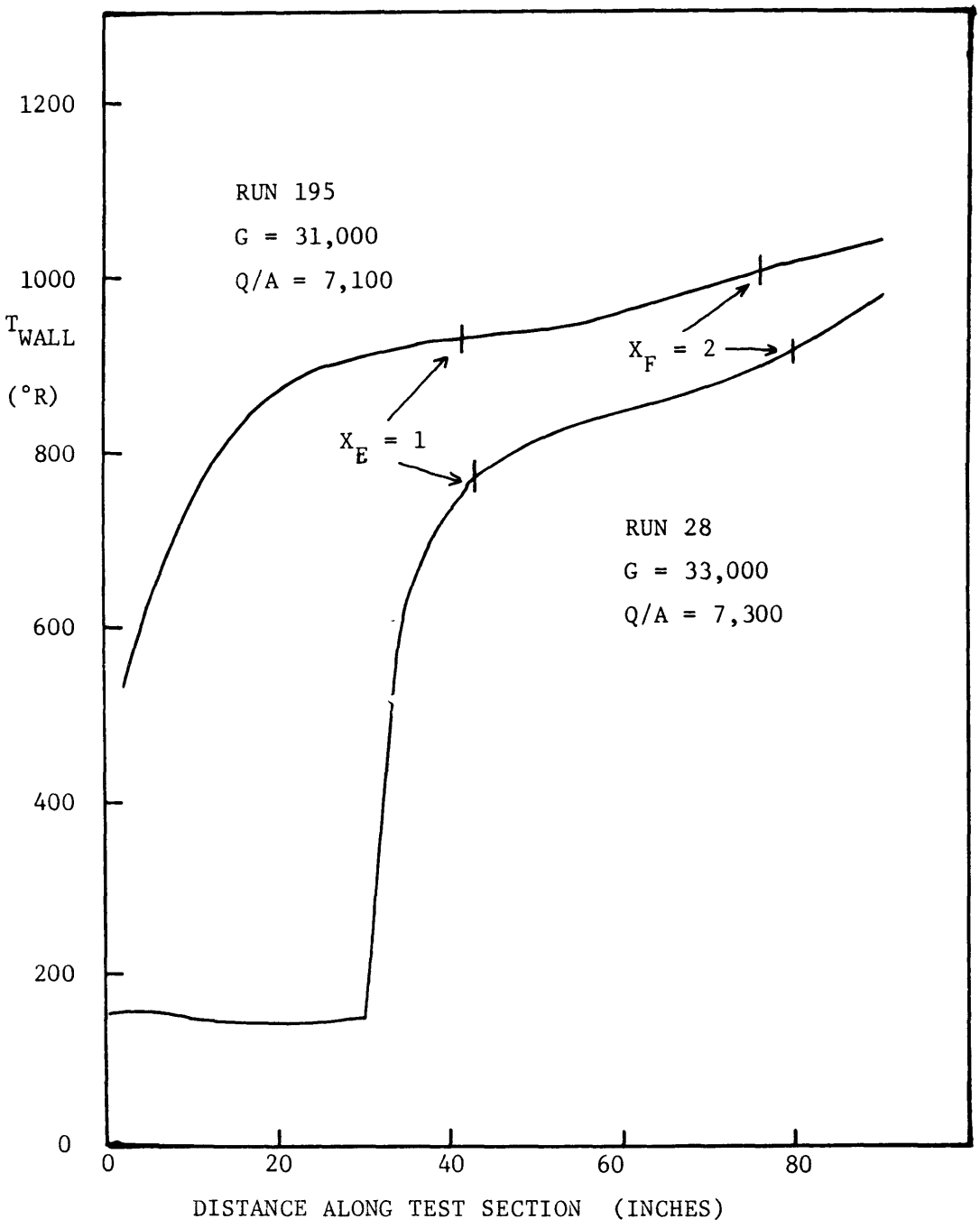

FIGURE 8. TYPES I & II AT THE SAME HEAT AND MASS FLUXES

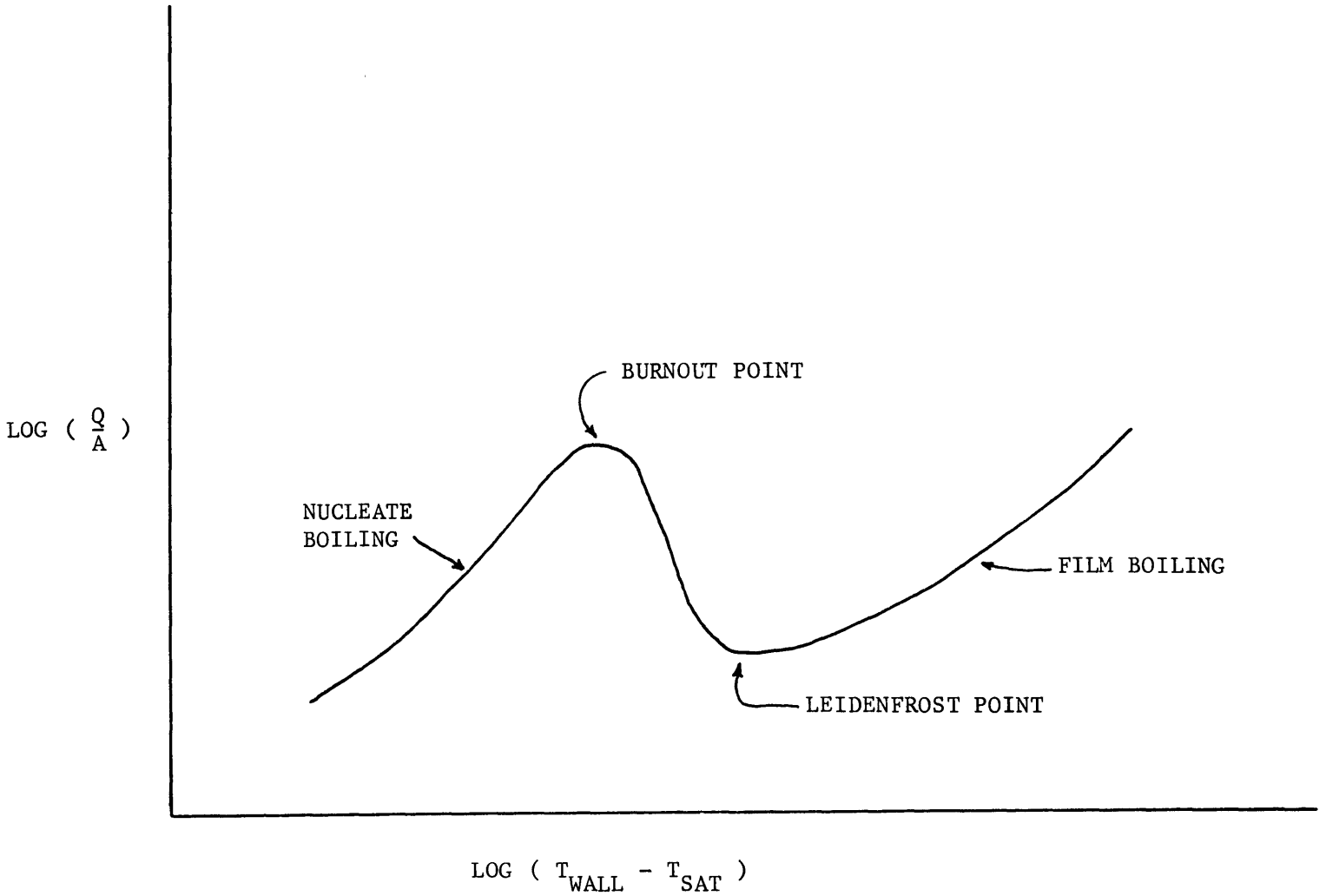

FIGURE 9. TYPICAL BOILING CURVE

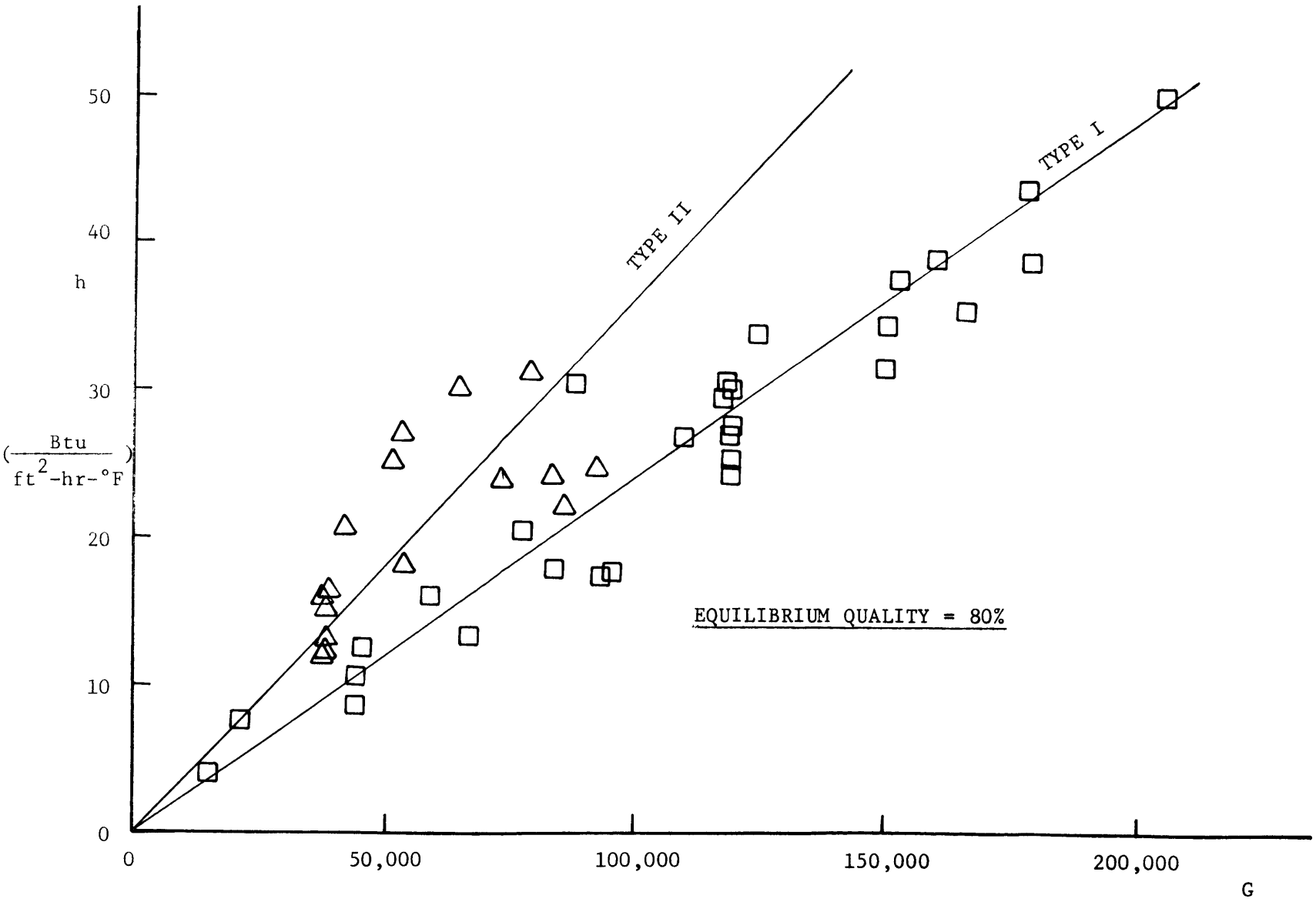

FIGURE 10. EFFECT OF REGIME ON HEAT TRANSFER COEFFICIENT

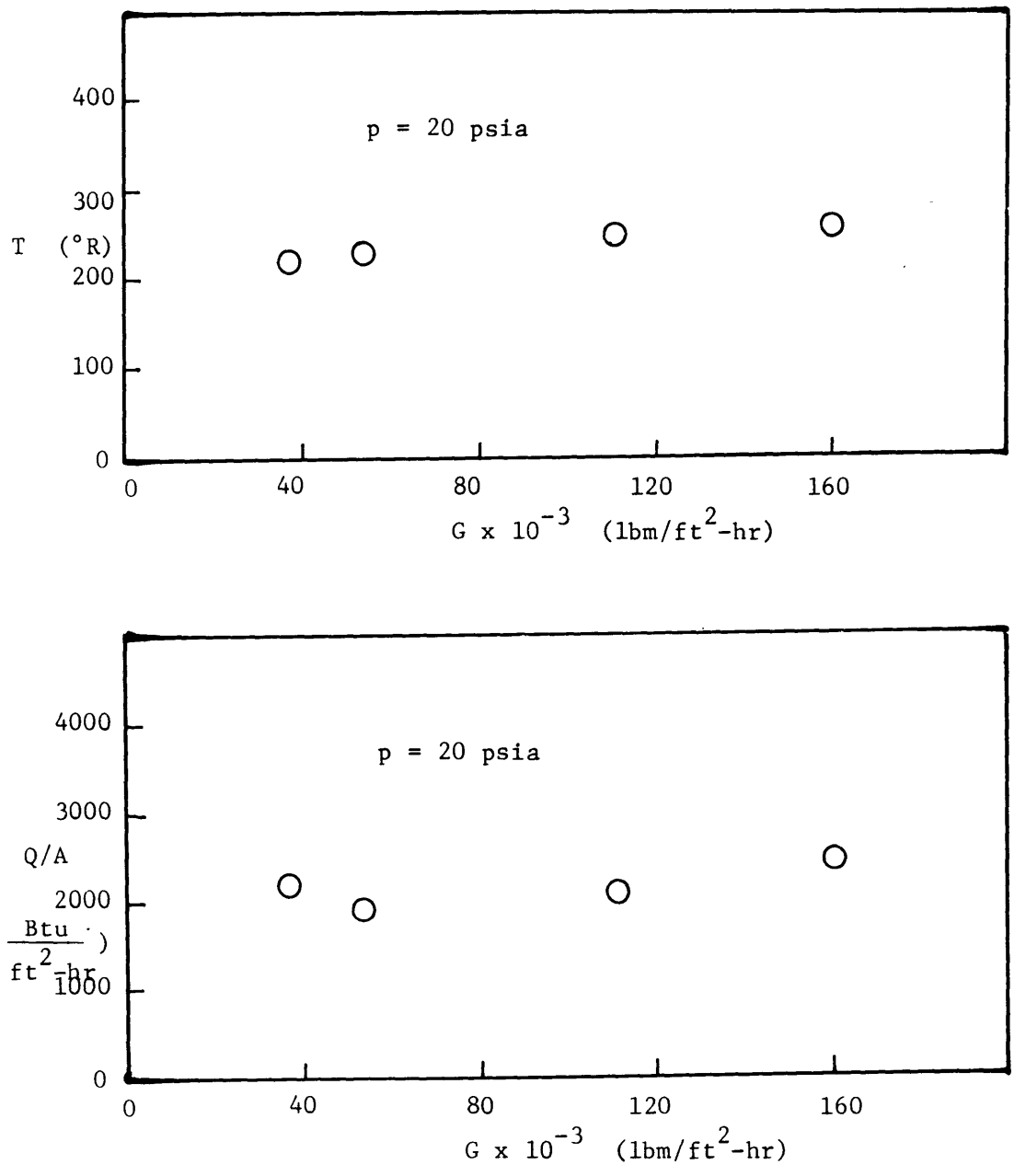

FIGURE 11. EFFECT OF G ON LEIDENFROST POINT, WITHOUT COOLER

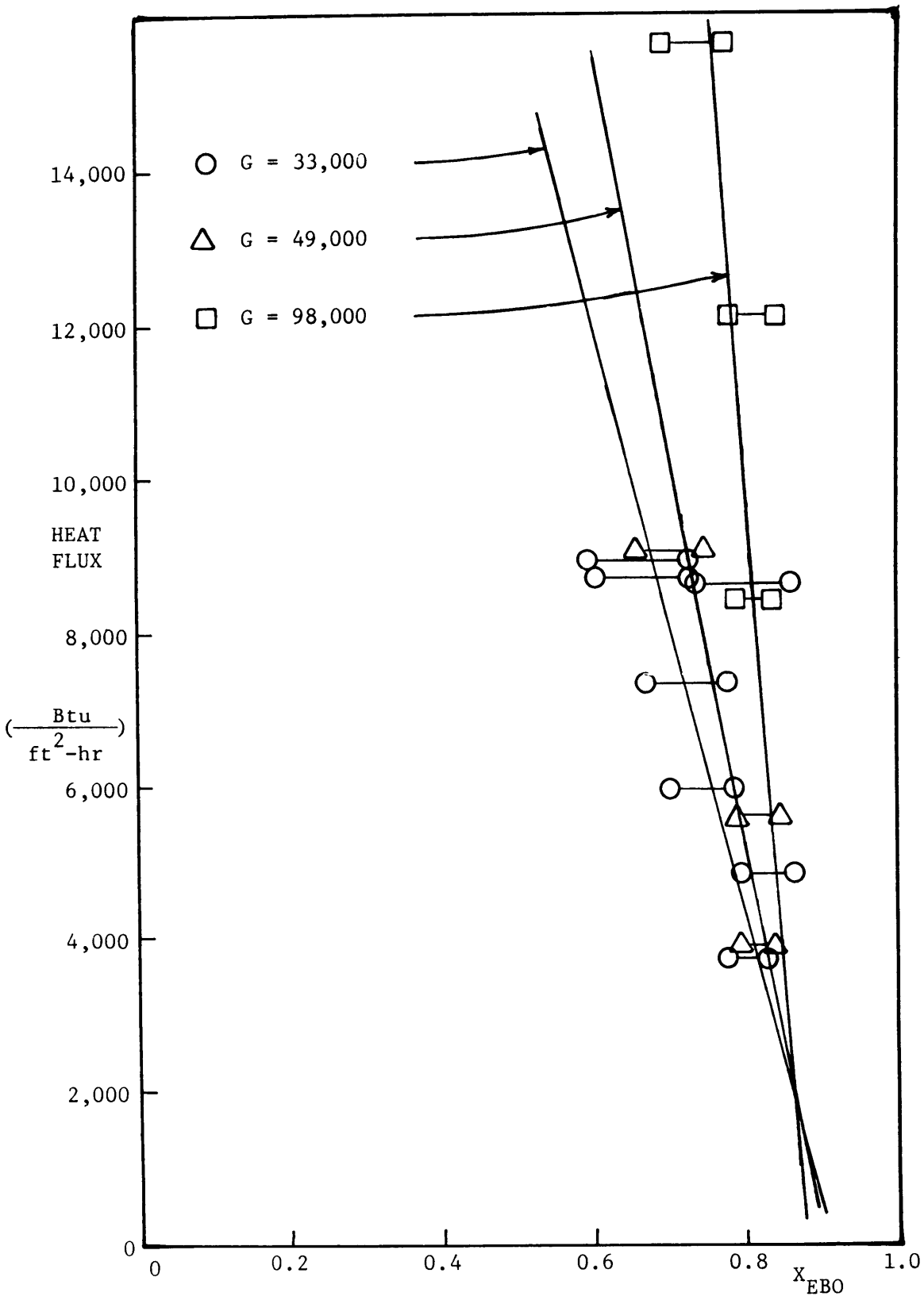

FIGURE 12. EFFECT OF HEAT AND MASS FLUXES ON BURNOUT QUALITY

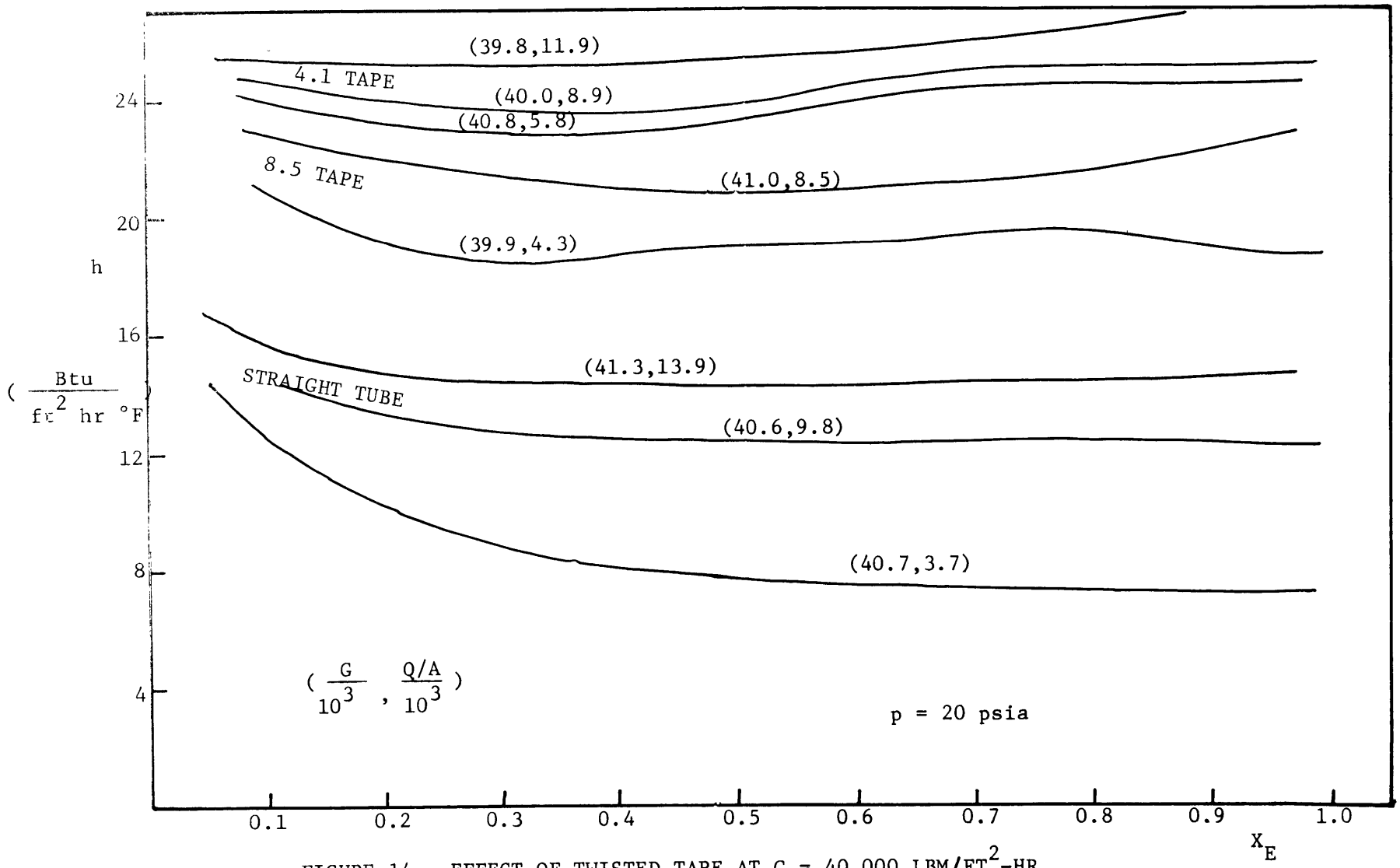

FIGURE 14. EFFECT OF TWISTED TAPE AT G = 40,000 LBM/FT^2-HR

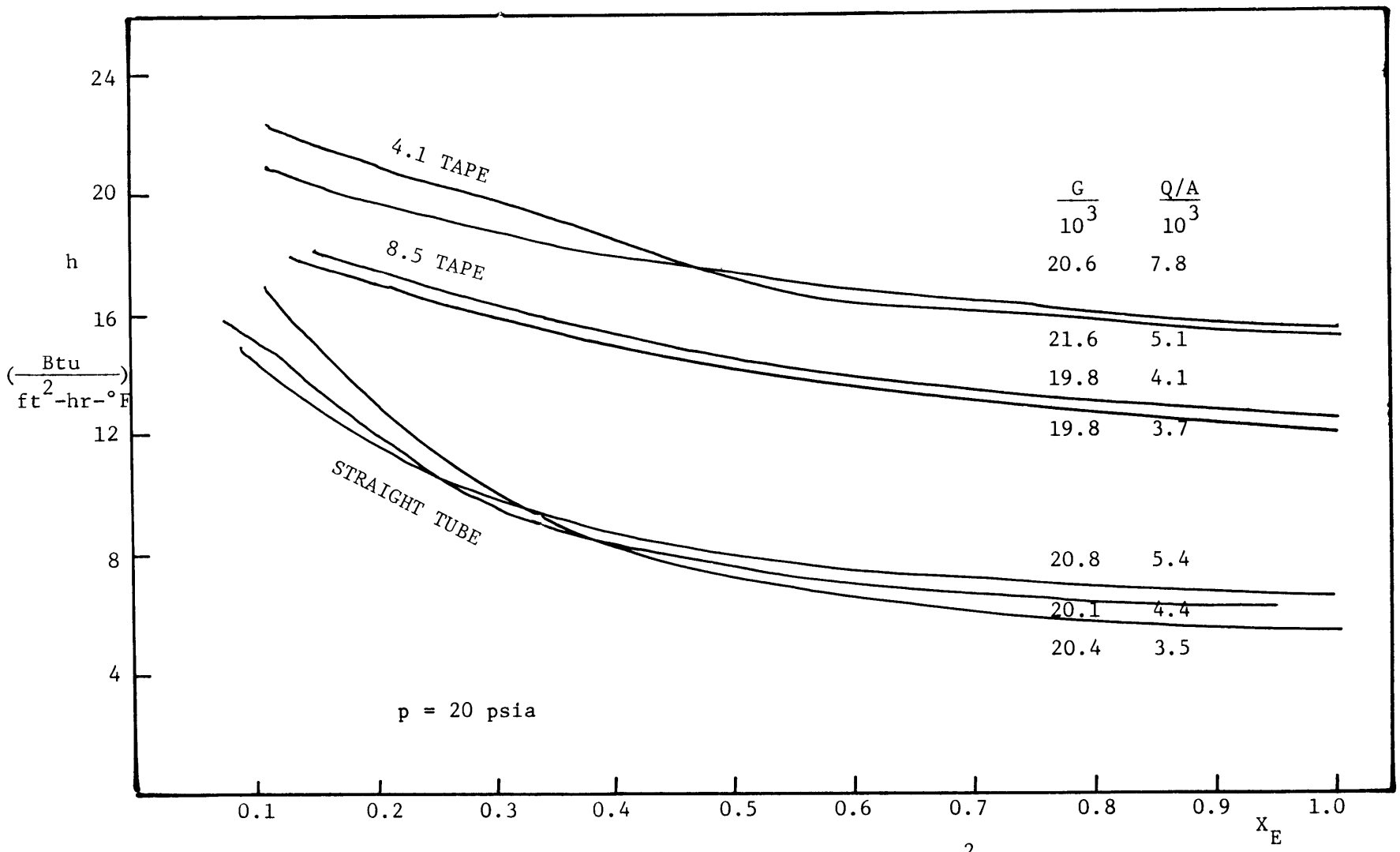

FIGURE 13. EFFECT OF TWISTED TAPE AT G = 20,000 LBM/FT^2-HR

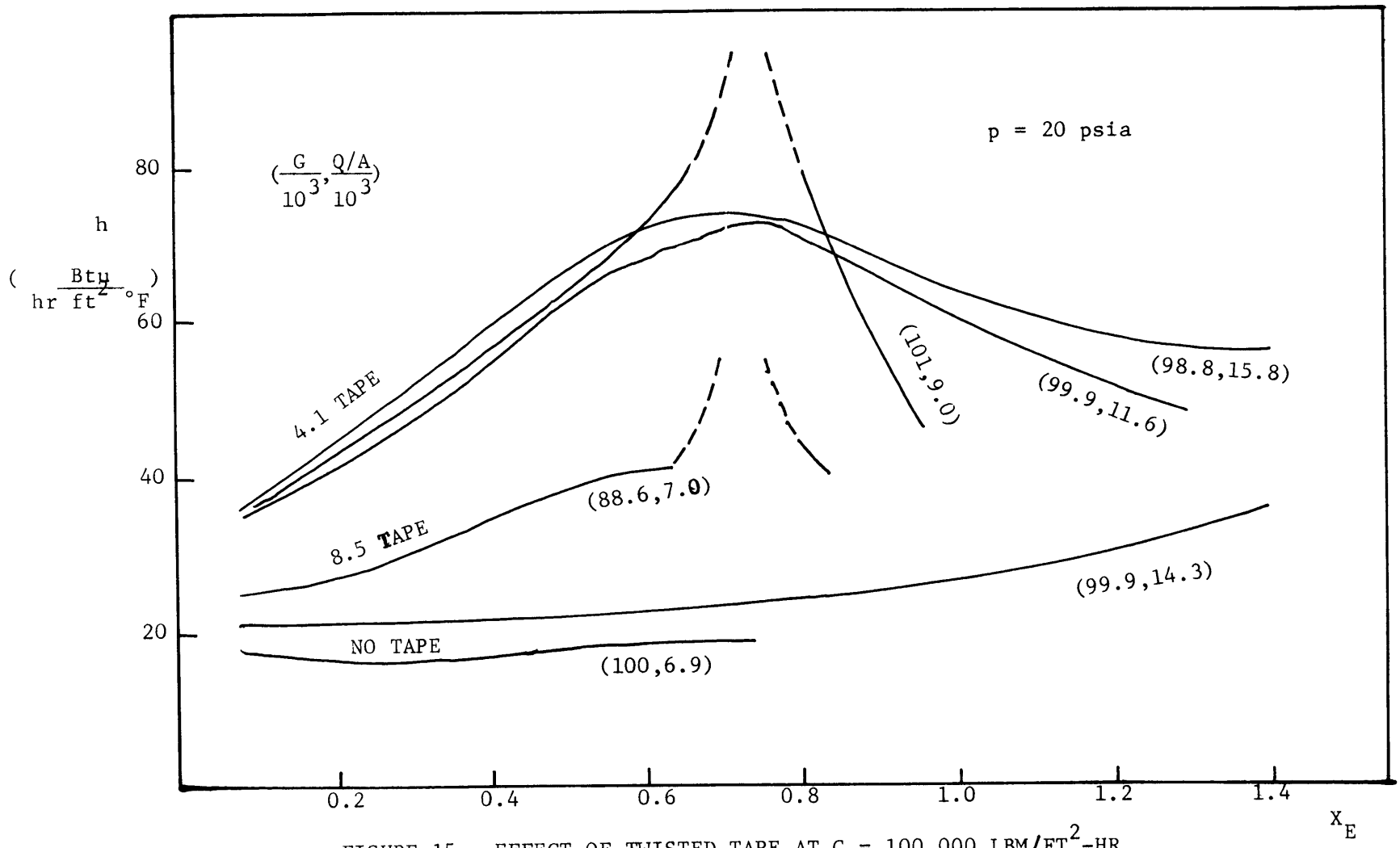

FIGURE 15. EFFECT OF TWISTED TAPE AT G = 100,000 LBM/FT^2-HR

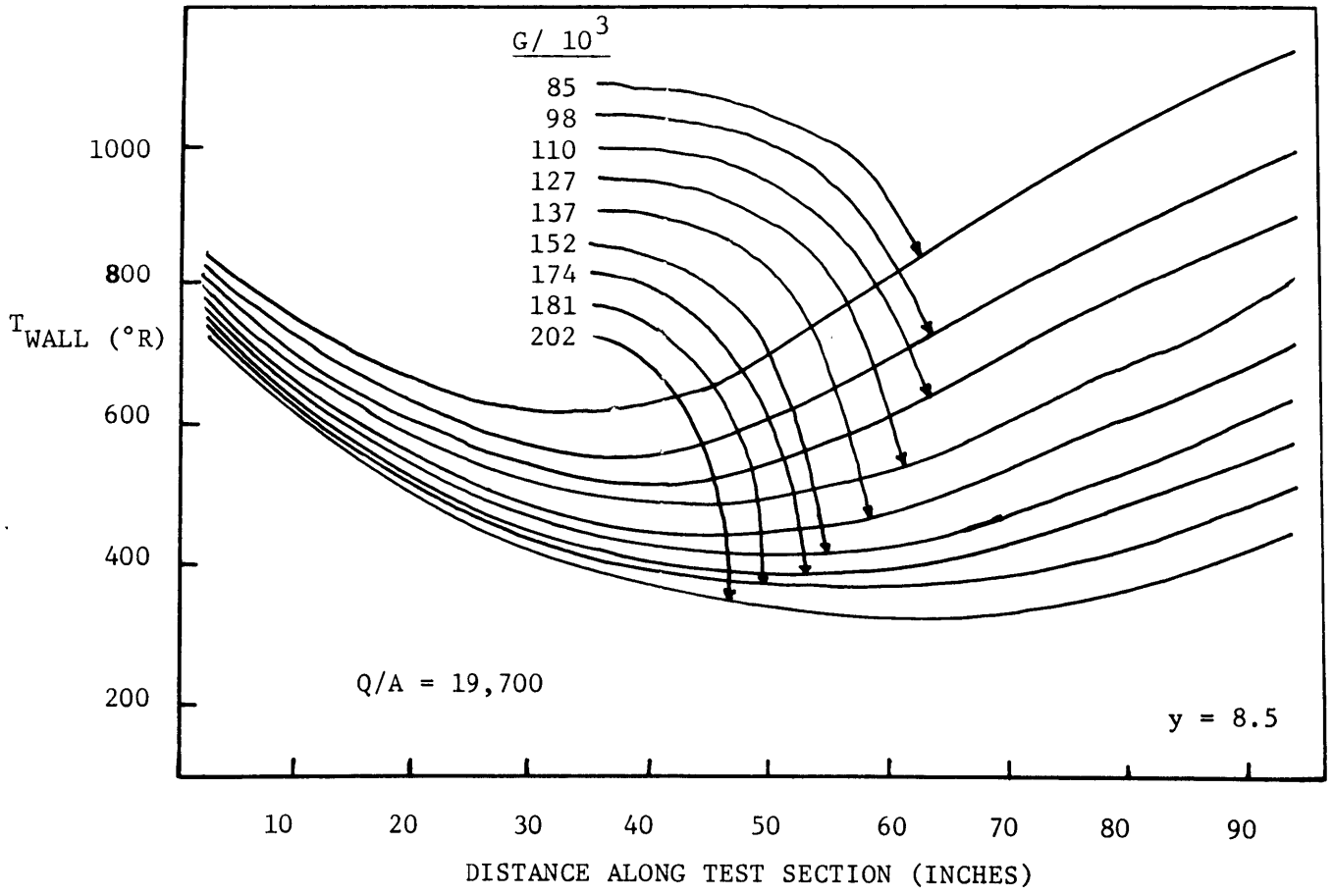

FIGURE 16. EFFECT OF MASS FLUX ON TYPE I RUNS

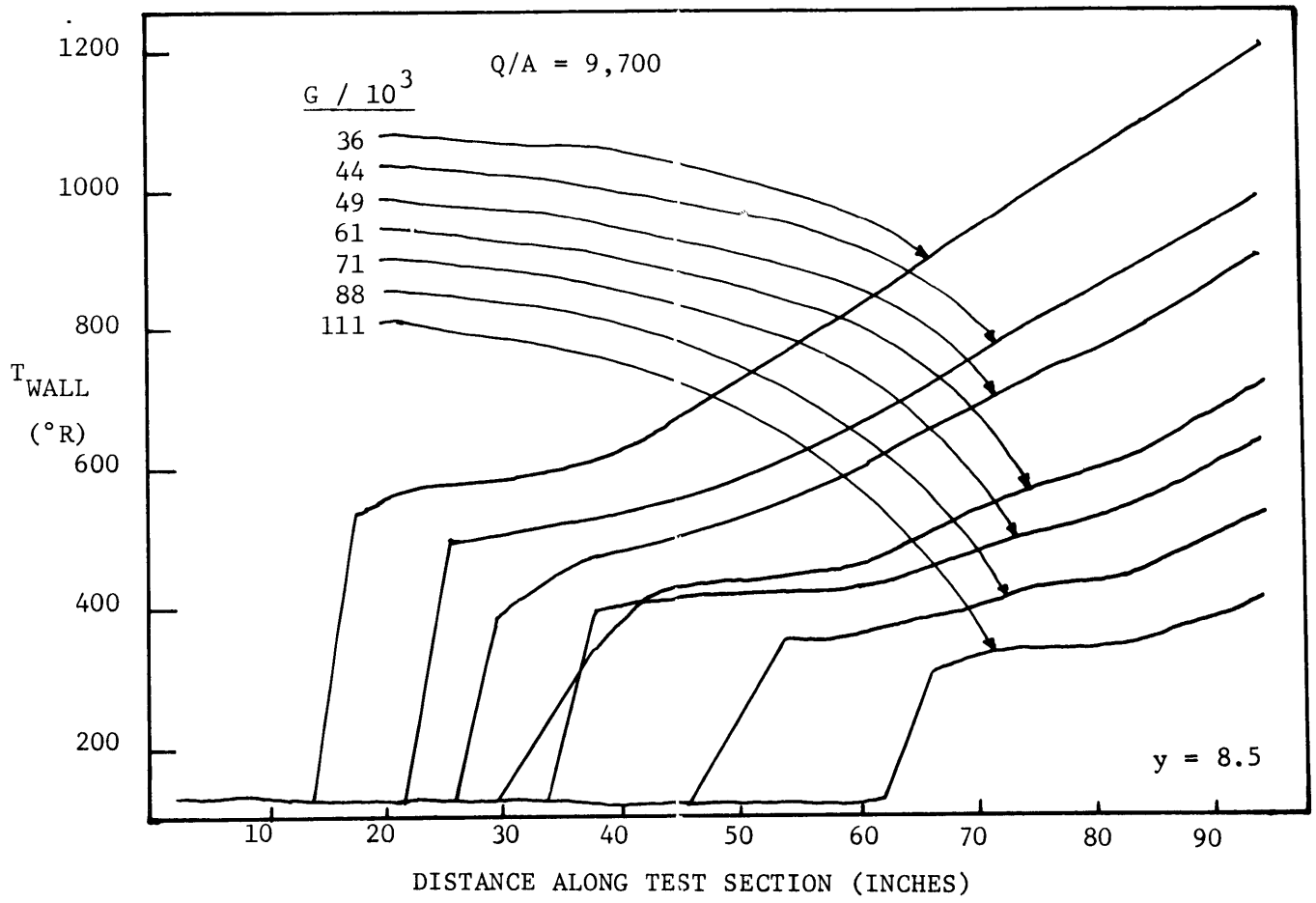

FIGURE 17. EFFECT OF MASS FLUX ON TYPE II RUNS

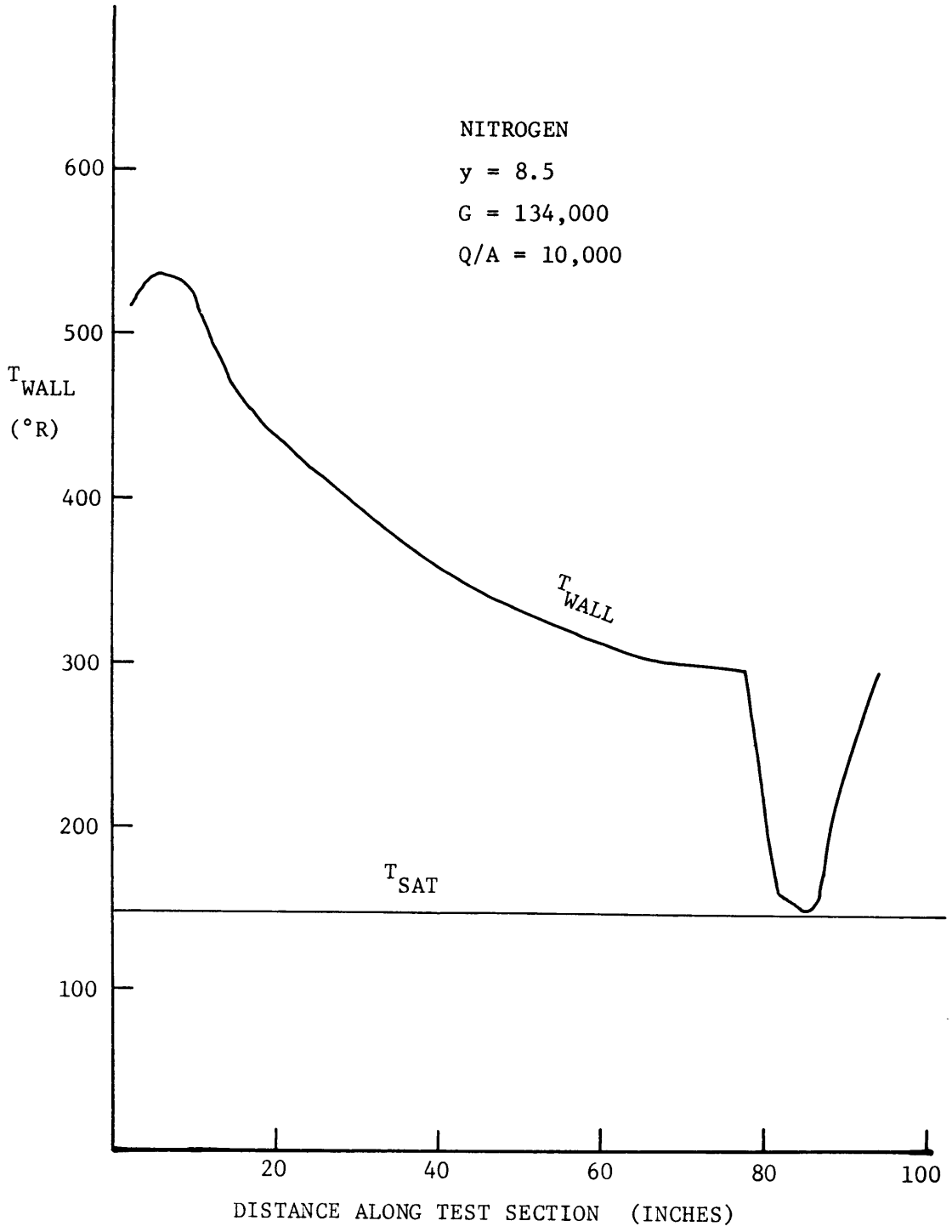

FIGURE 18. TEMPERATURE PROFILE FOR RE-WETTING TUBE WALL

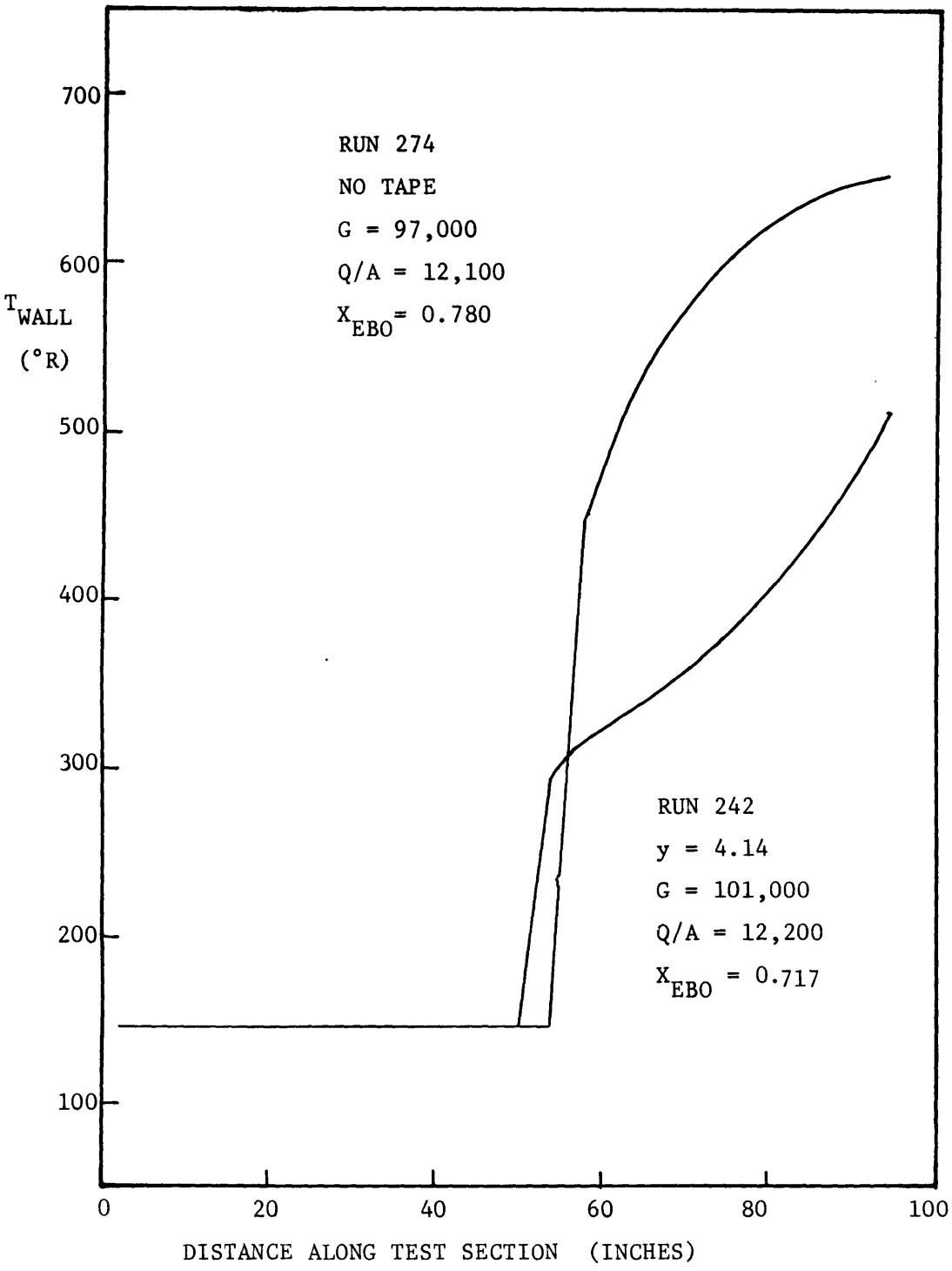

FIGURE 19. TEMPERATURE PROFILES SHOWING EFFECT OF TWISTED TAPE ON BURNOUT QUALITY

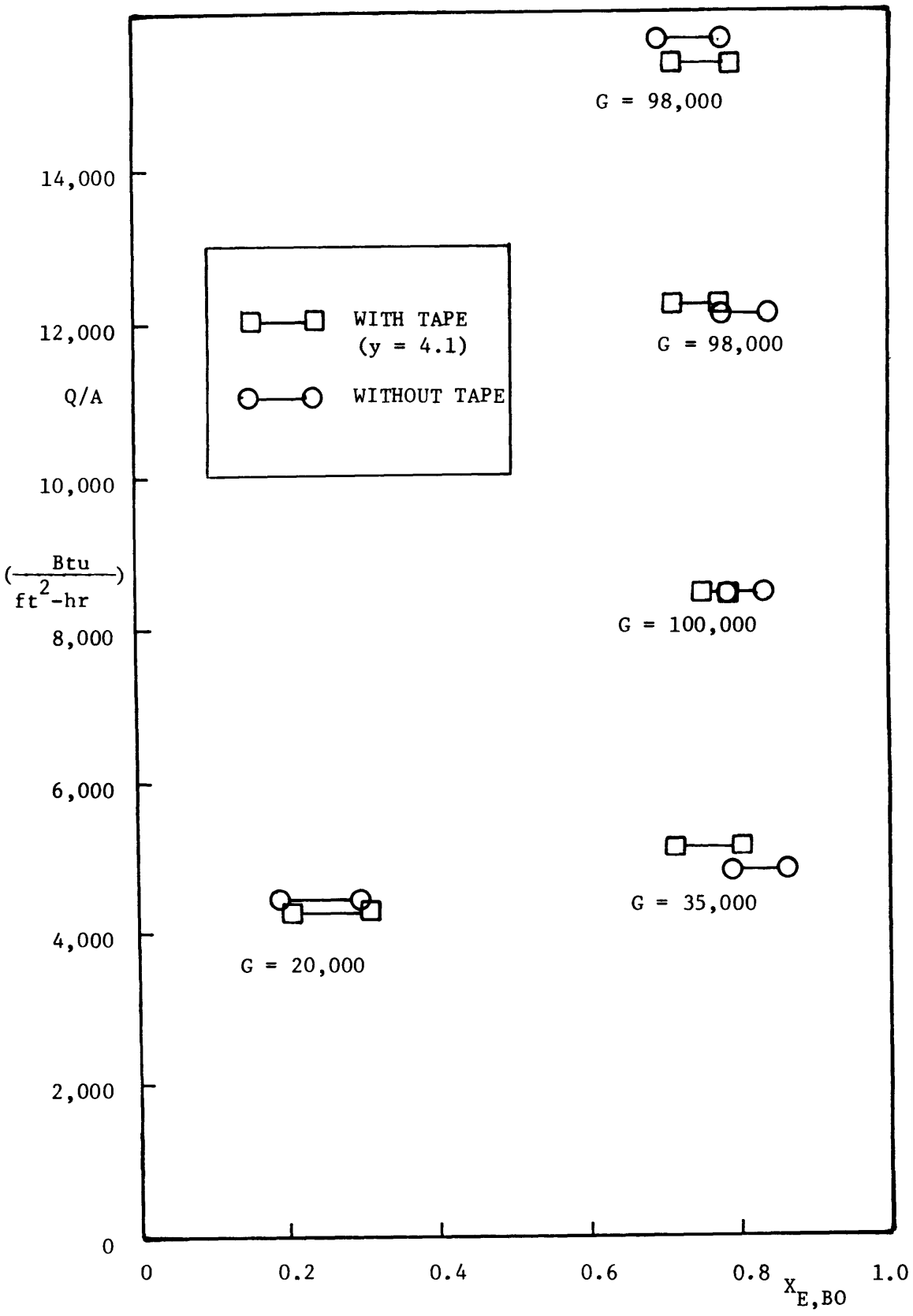

FIGURE 20. EFFECT OF TWISTED TAPE ON BURNOUT QUALITY

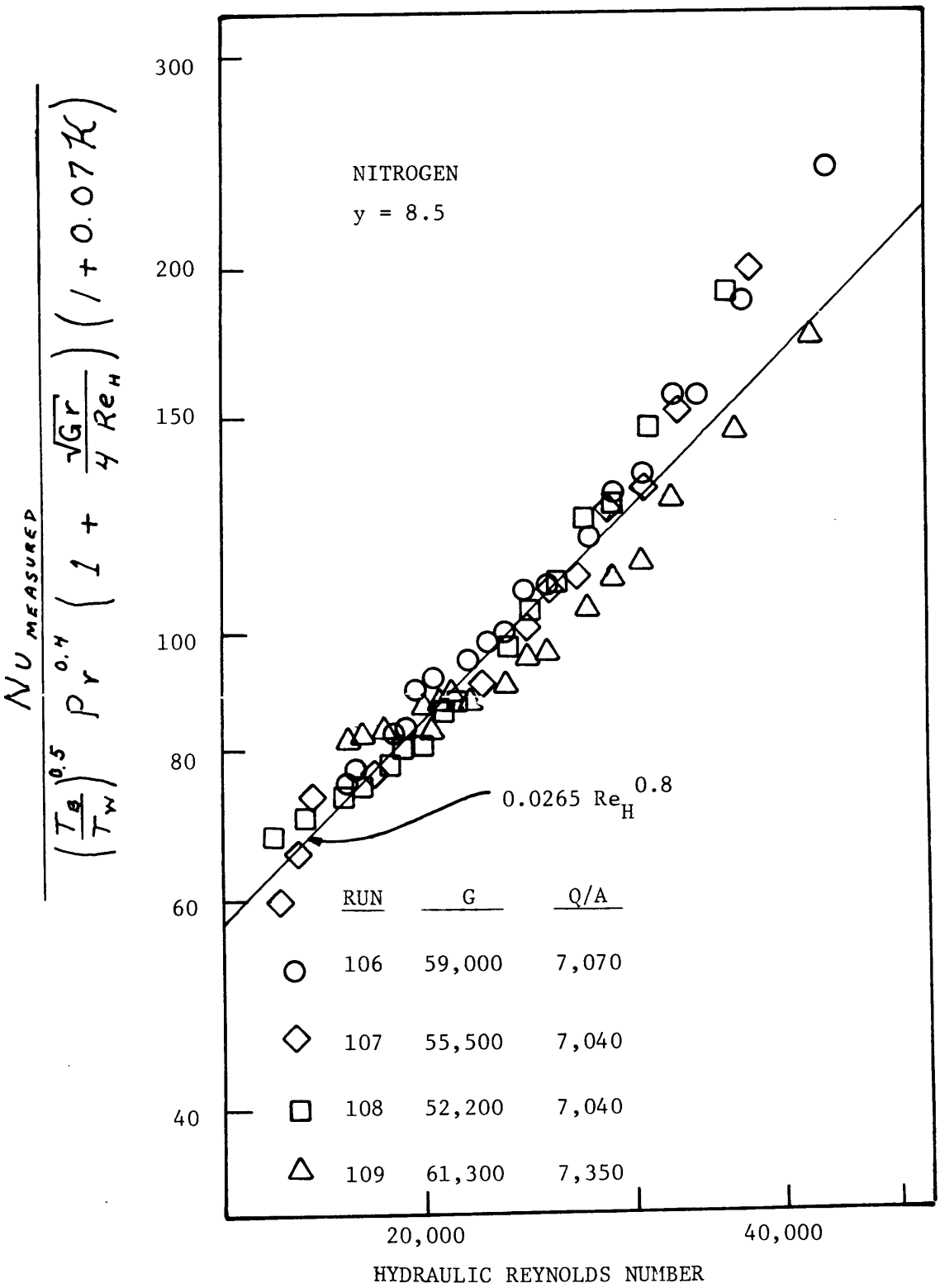

FIGURE 21. CORRELATION OF PURE VAPOR RUNS

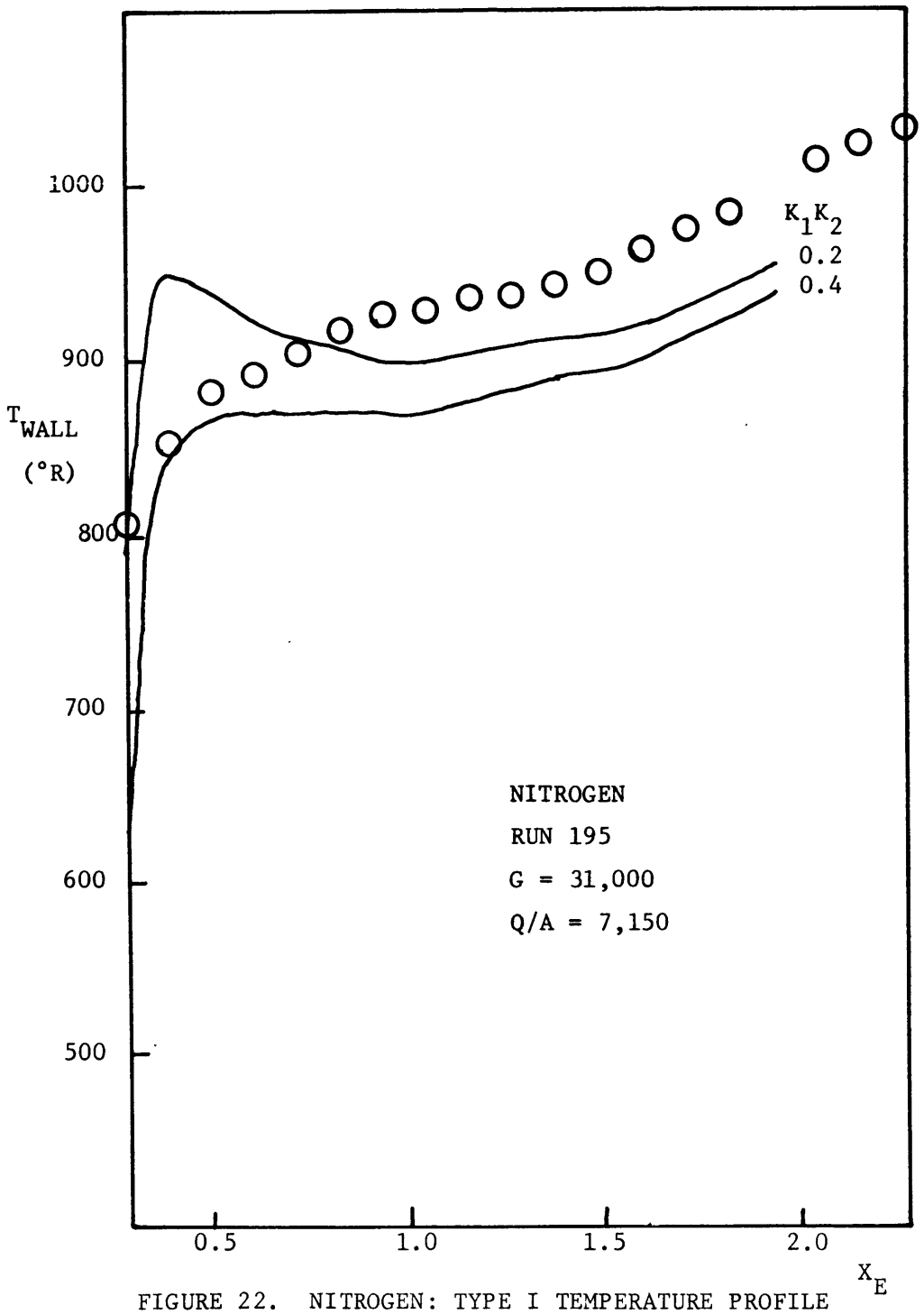

FIGURE 22. NITROGEN: TYPE I TEMPERATURE PROFILE

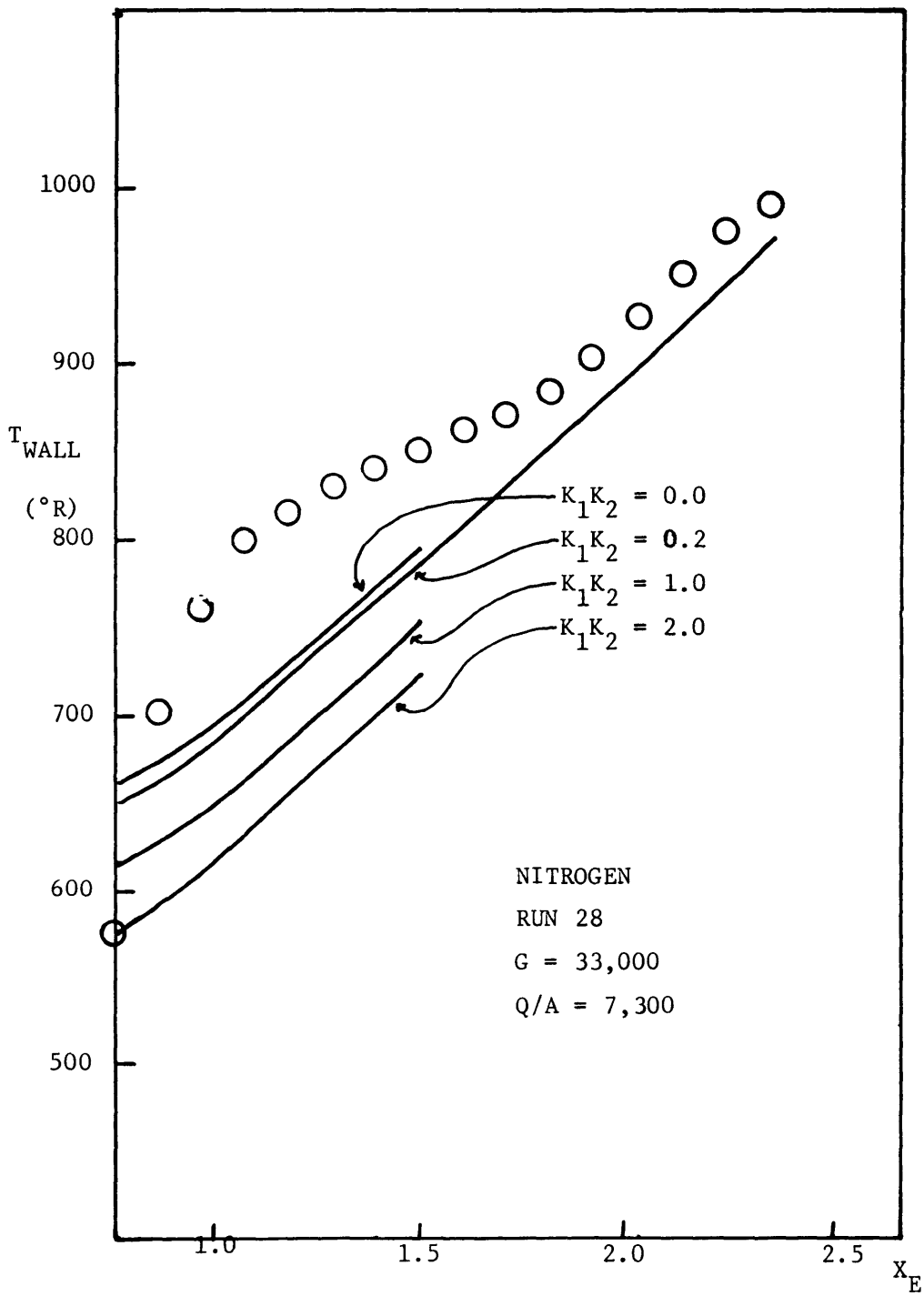

FIGURE 23. NITROGEN: TYPE II TEMPERATURE PROFILE

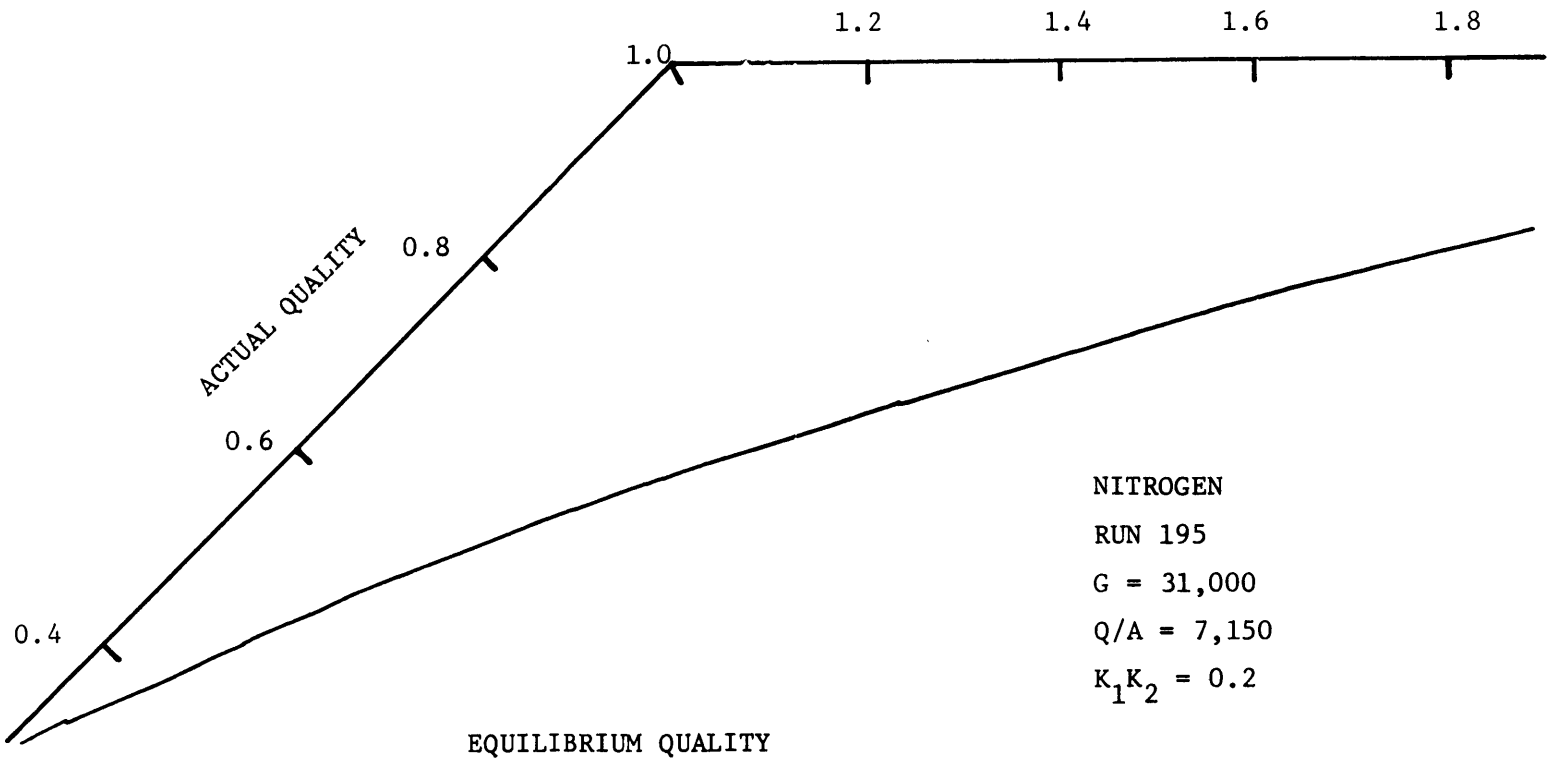

FIGURE 24. TYPE I NITROGEN: ACTUAL QUALITY VS. EQUILIBRIUM QUALITY

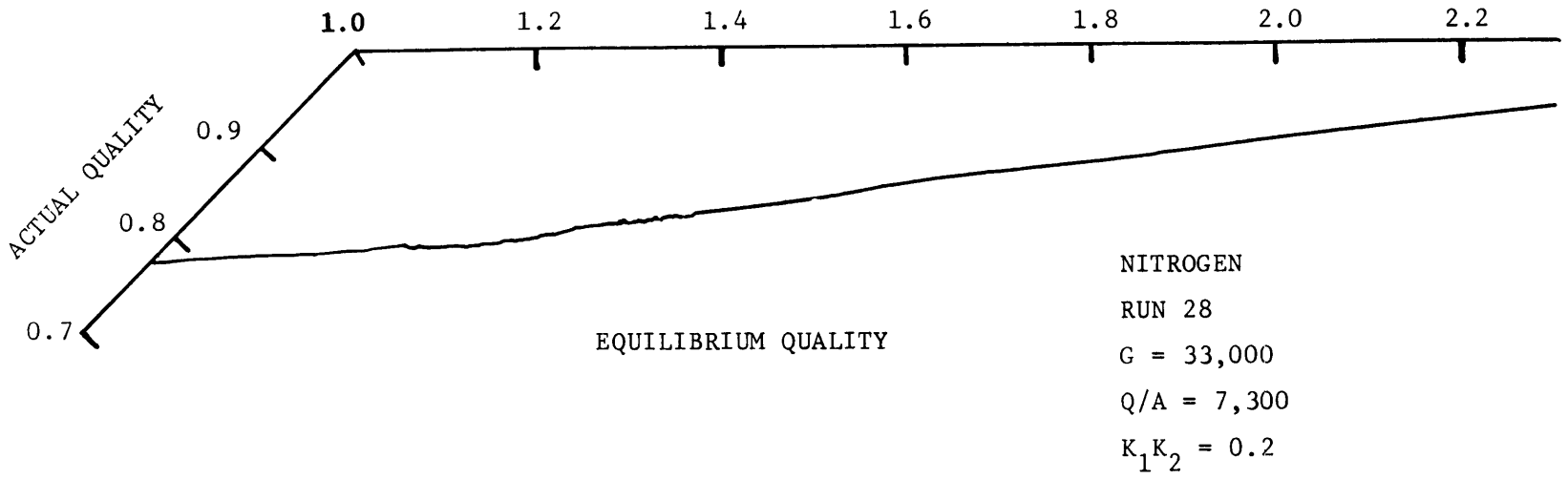

FIGURE 25. TYPE II NITROGEN: ACTUAL QUALITY VS. EQUILIBRIUM QUALITY

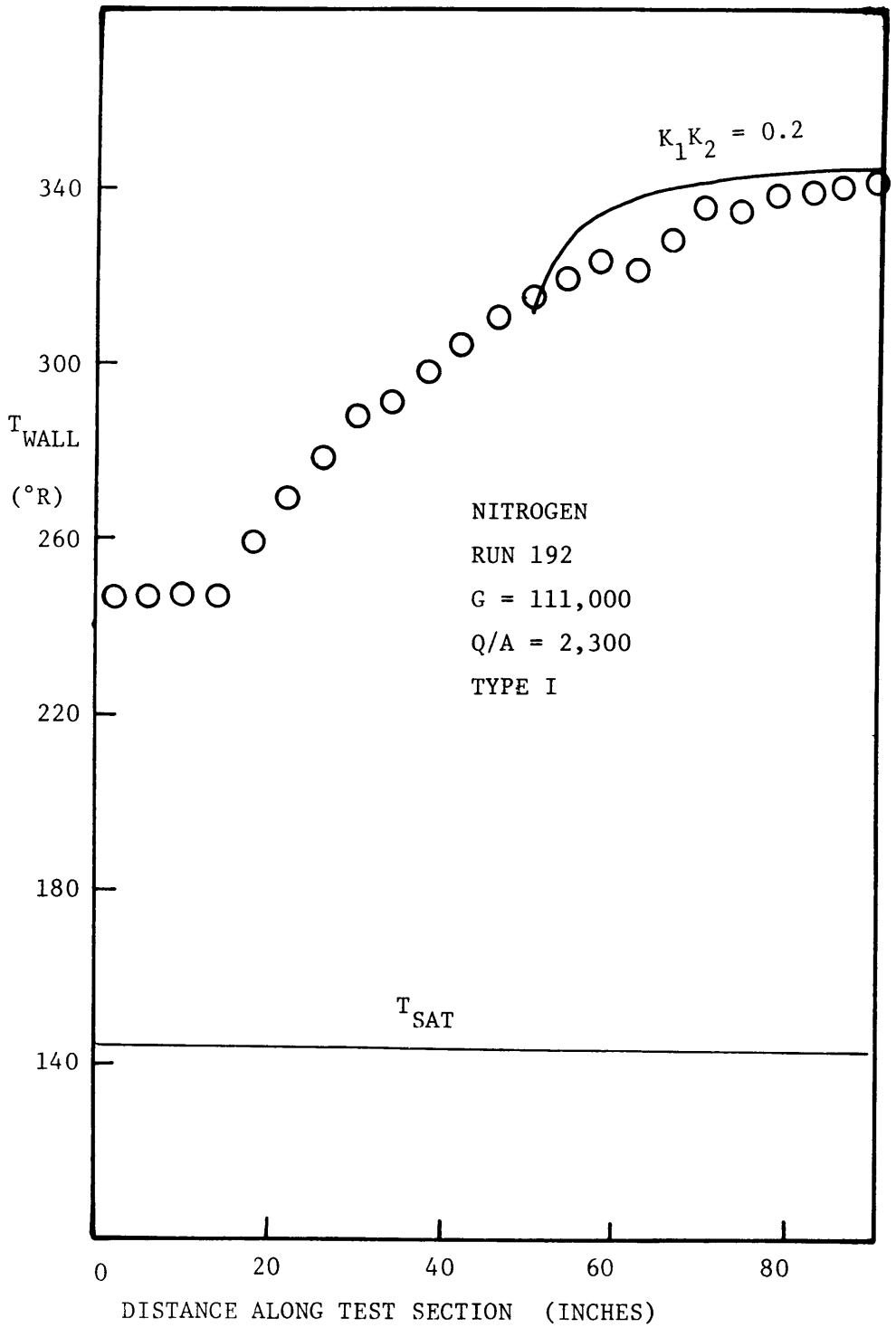

FIGURE 26. TYPE I NITROGEN: TEMPERATURE PROFILE

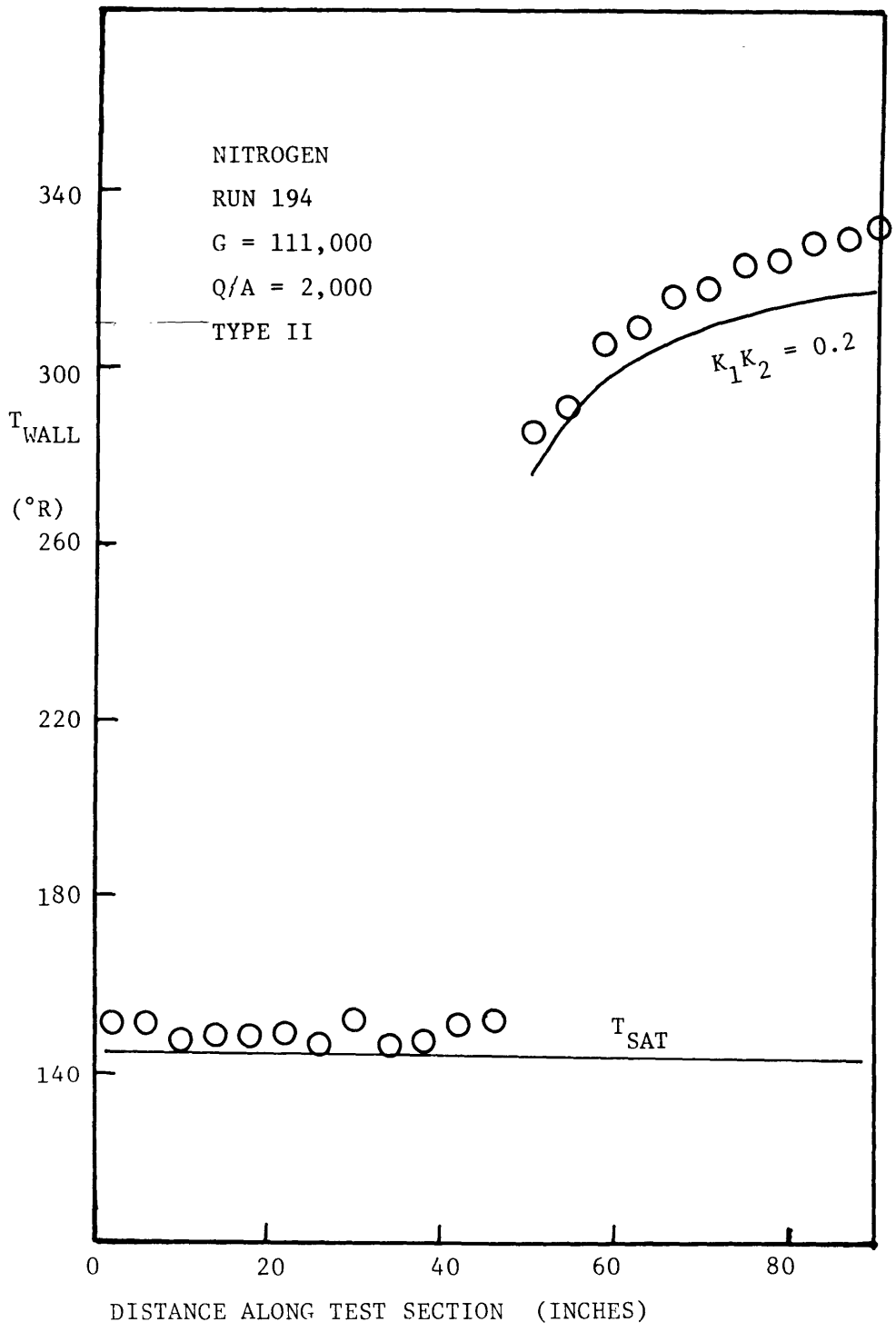

FIGURE 27. TYPE II NITROGEN: TEMPERATURE PROFILE

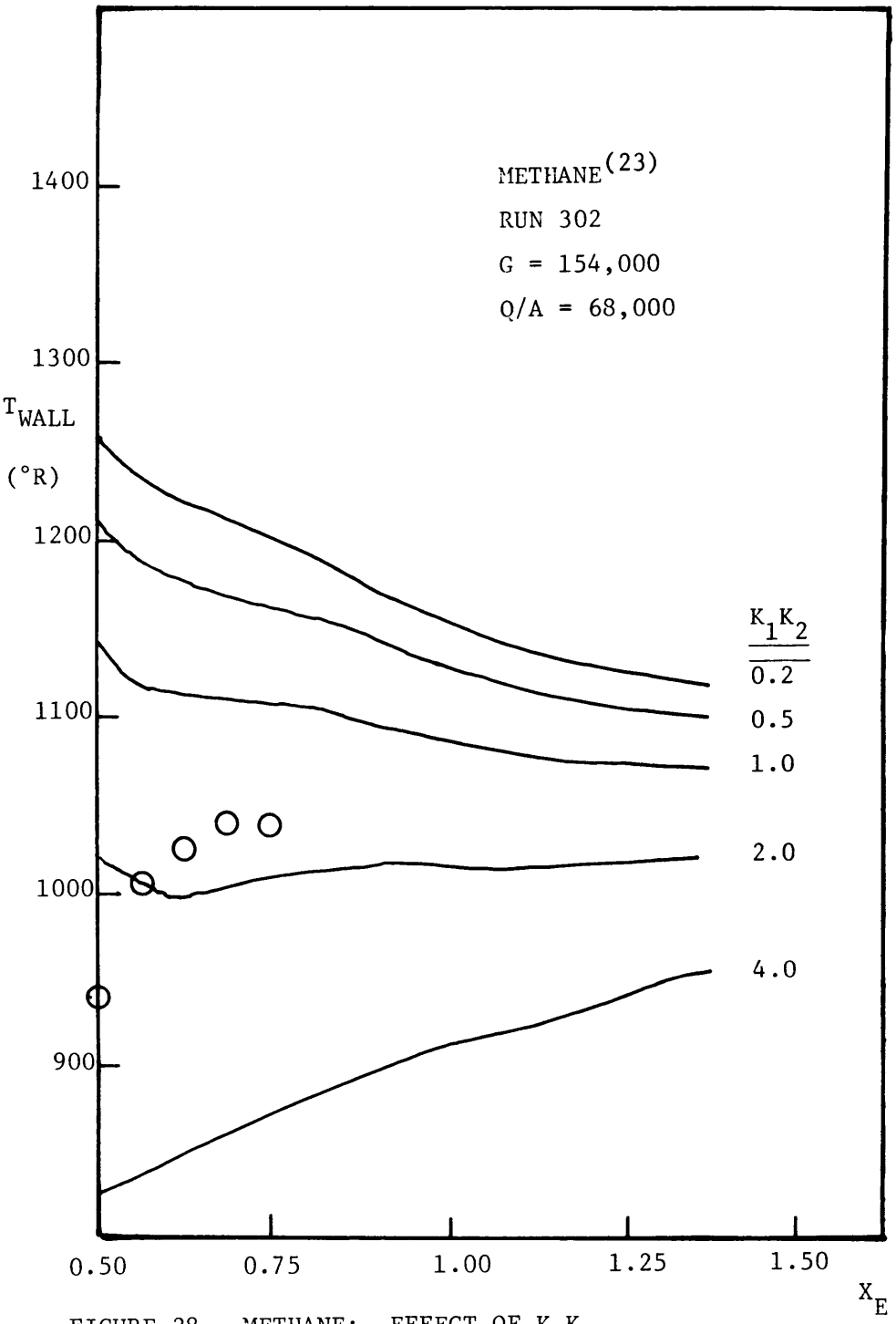

FIGURE 28. METHANE: EFFECT OF K_1K_2

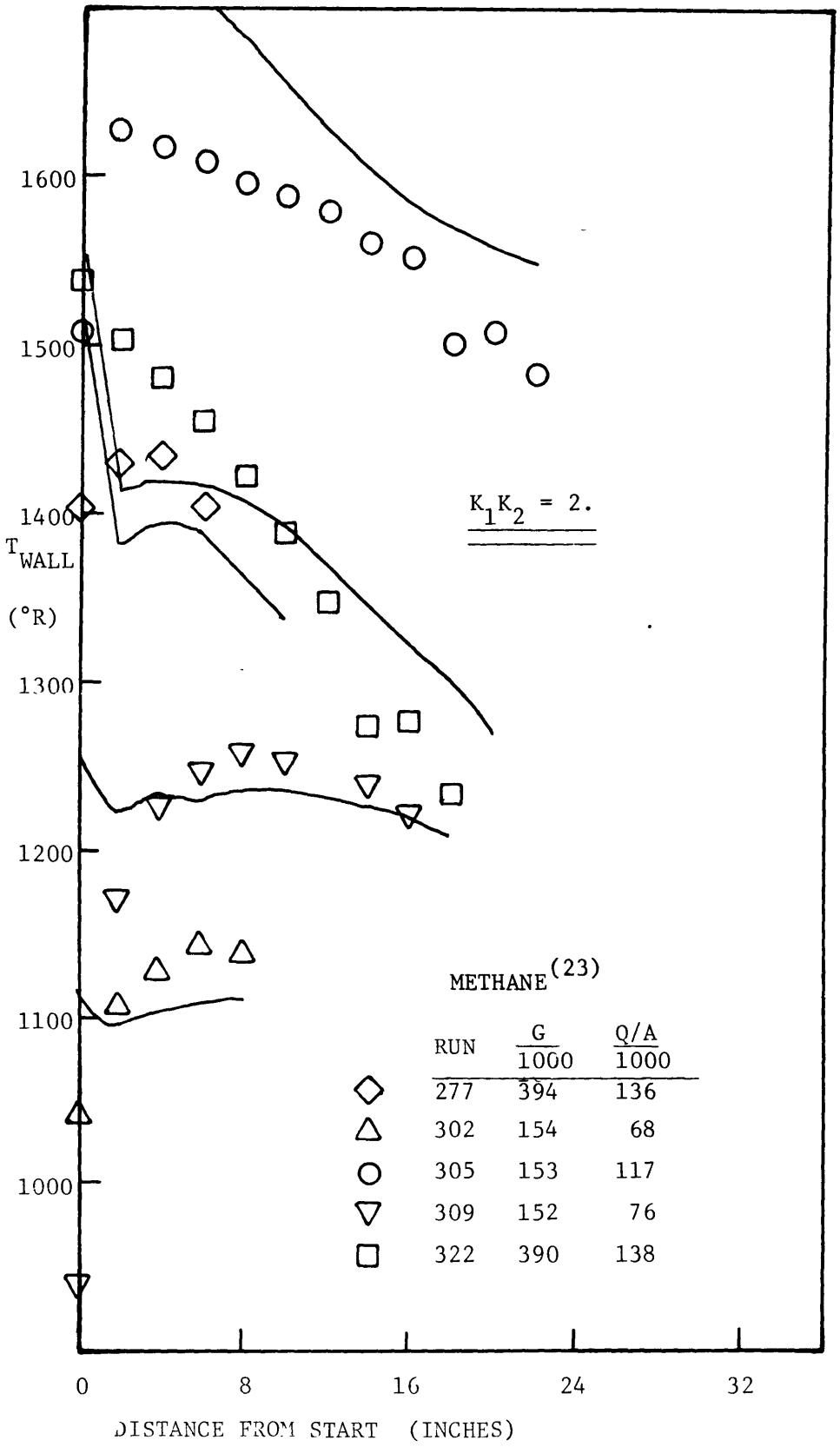

FIGURE 29. METHANE: FOUR OTHER RUNS AT K_1K_2= 2.

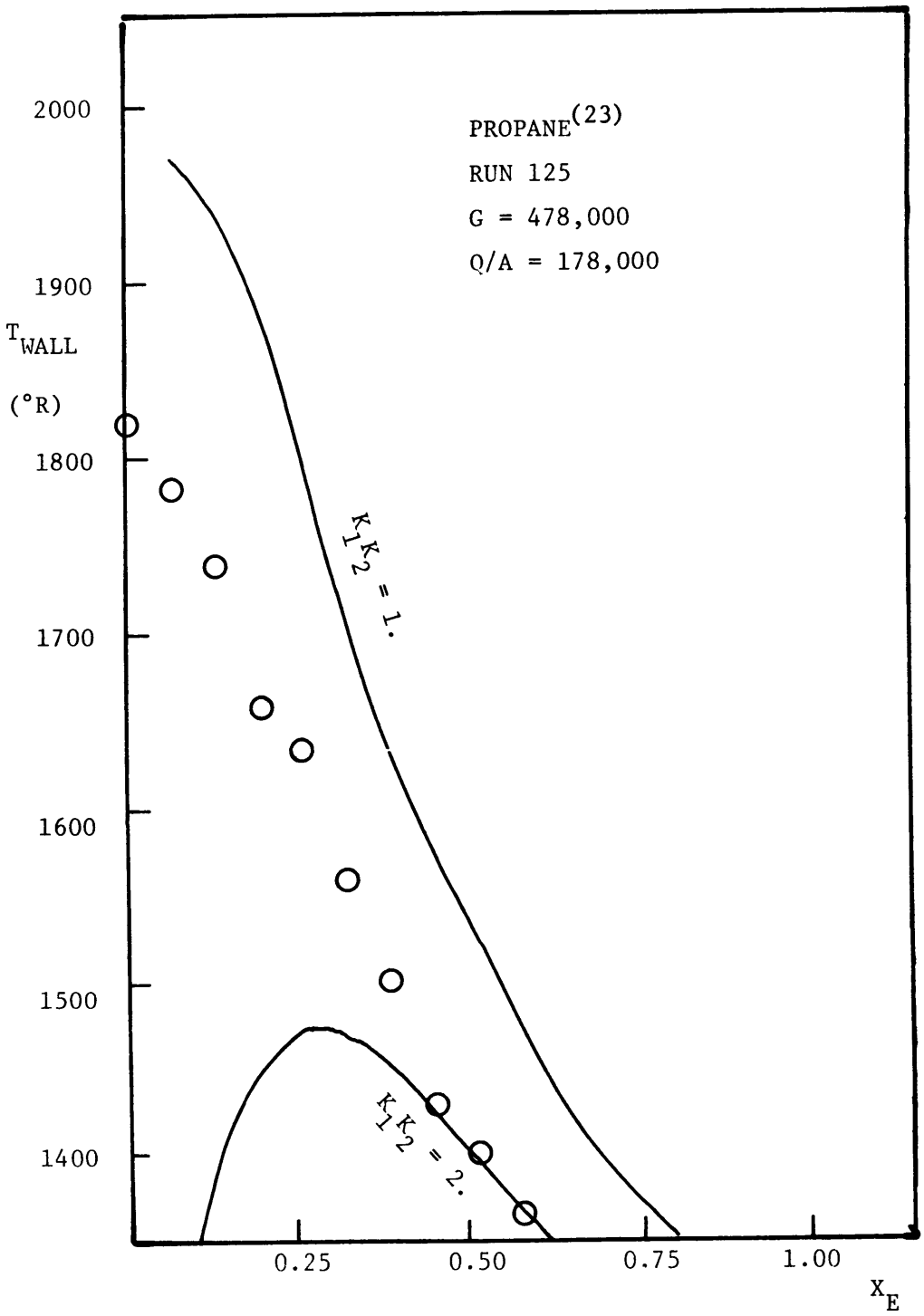

FIGURE 30. PROPANE: TEMPERATURE PROFILE, HIGH MASS FLUX

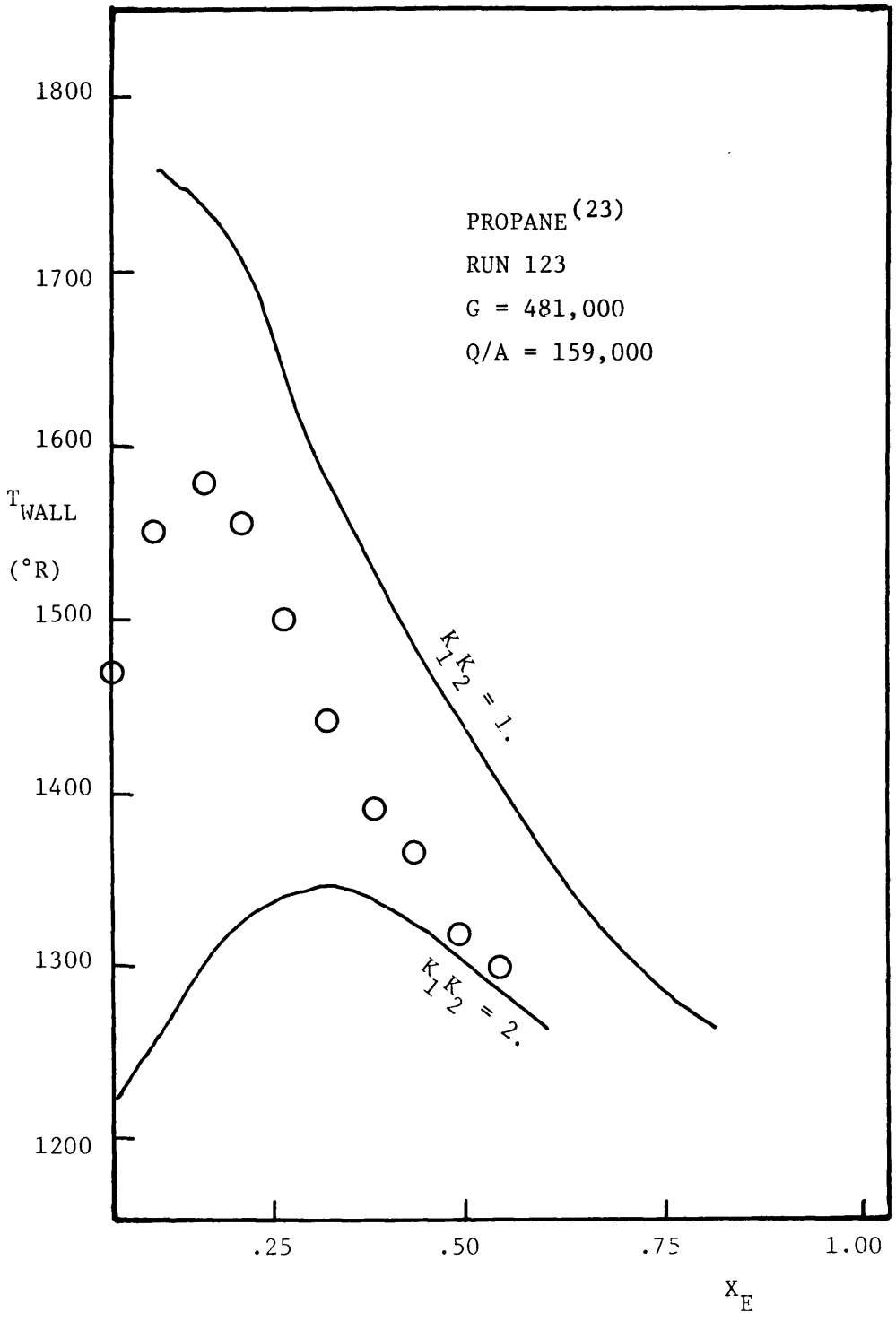

FIGURE 31. PROPANE: TEMPERATURE PROFILE, HIGH MASS FLUX

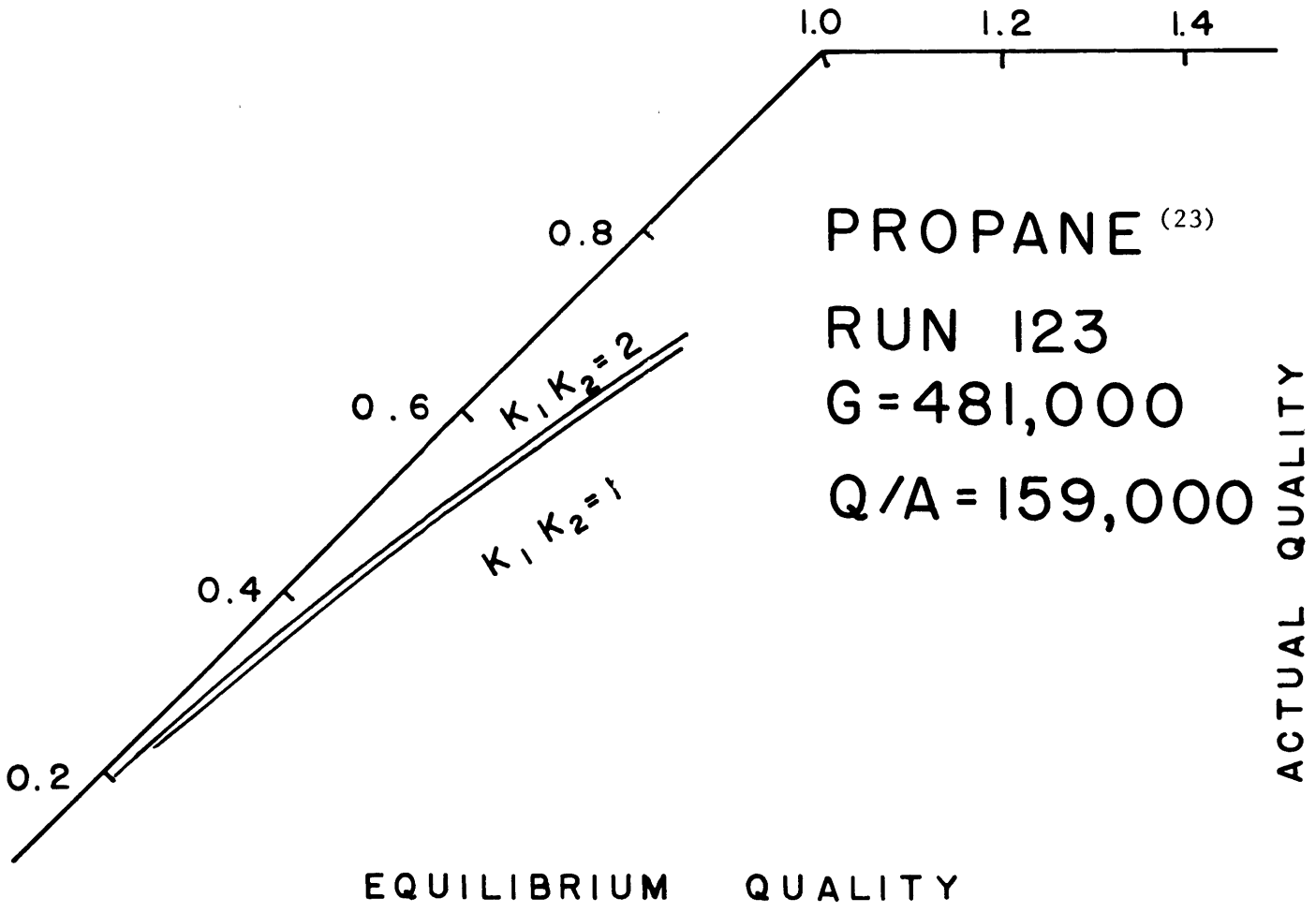

FIGURE 32. ACTUAL QUALITY VS. EQUILIBRIUM QUALITY

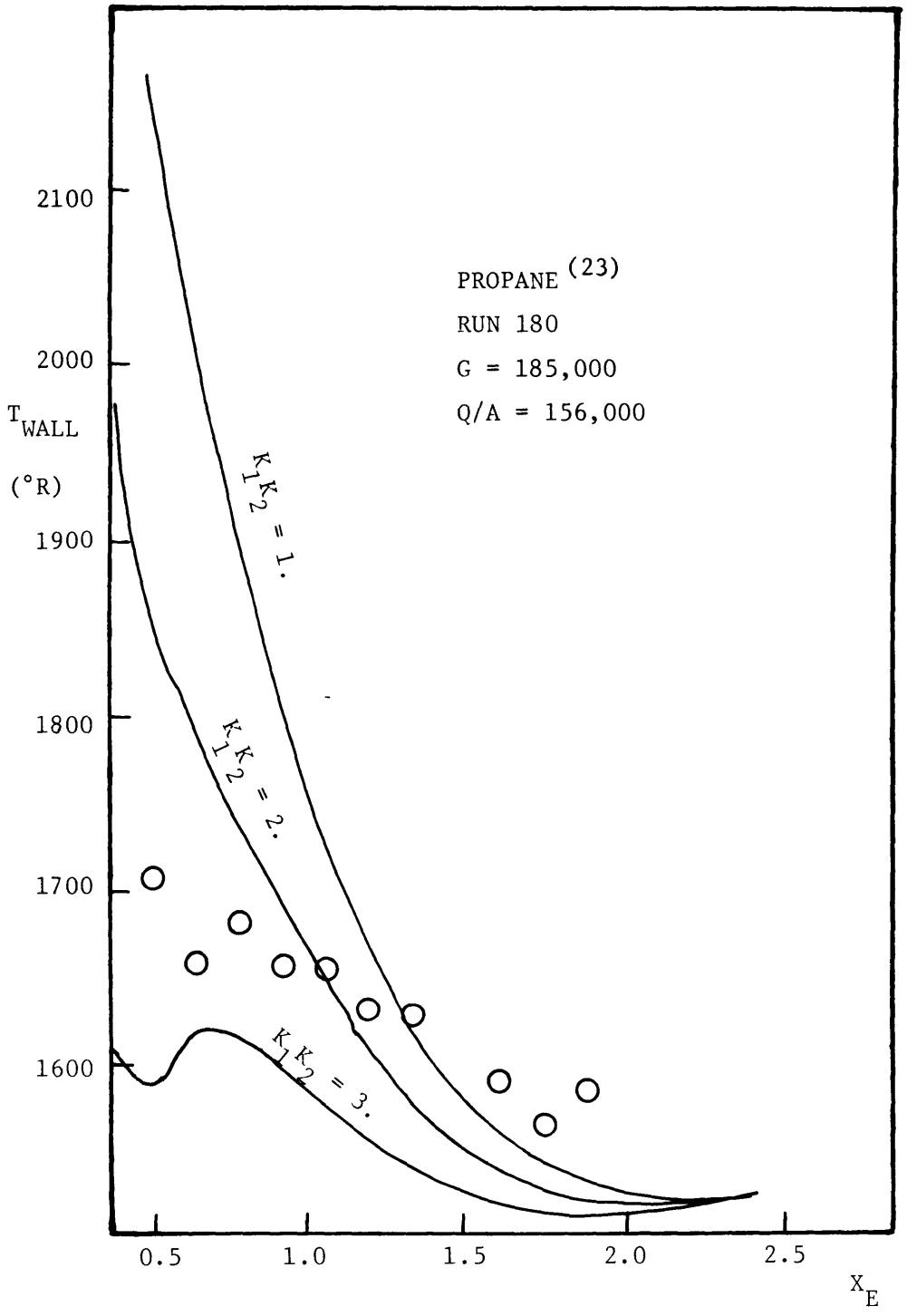

FIGURE 33. PROPANE: TEMPERATURE PROFILE, LOW MASS FLUX

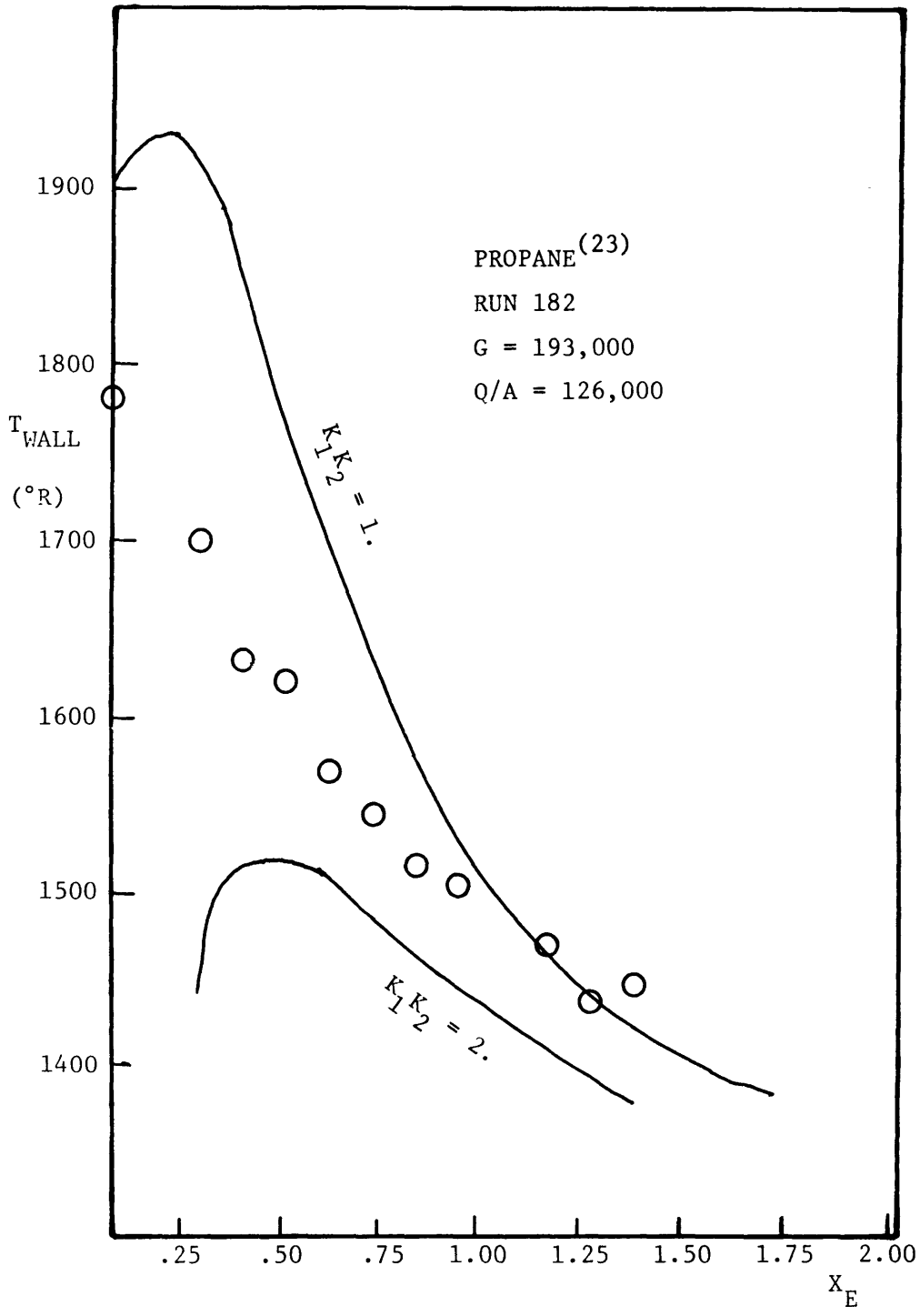

FIGURE 34. PROPANE: TEMPERATURE PROFILE, LOW MASS FLUX

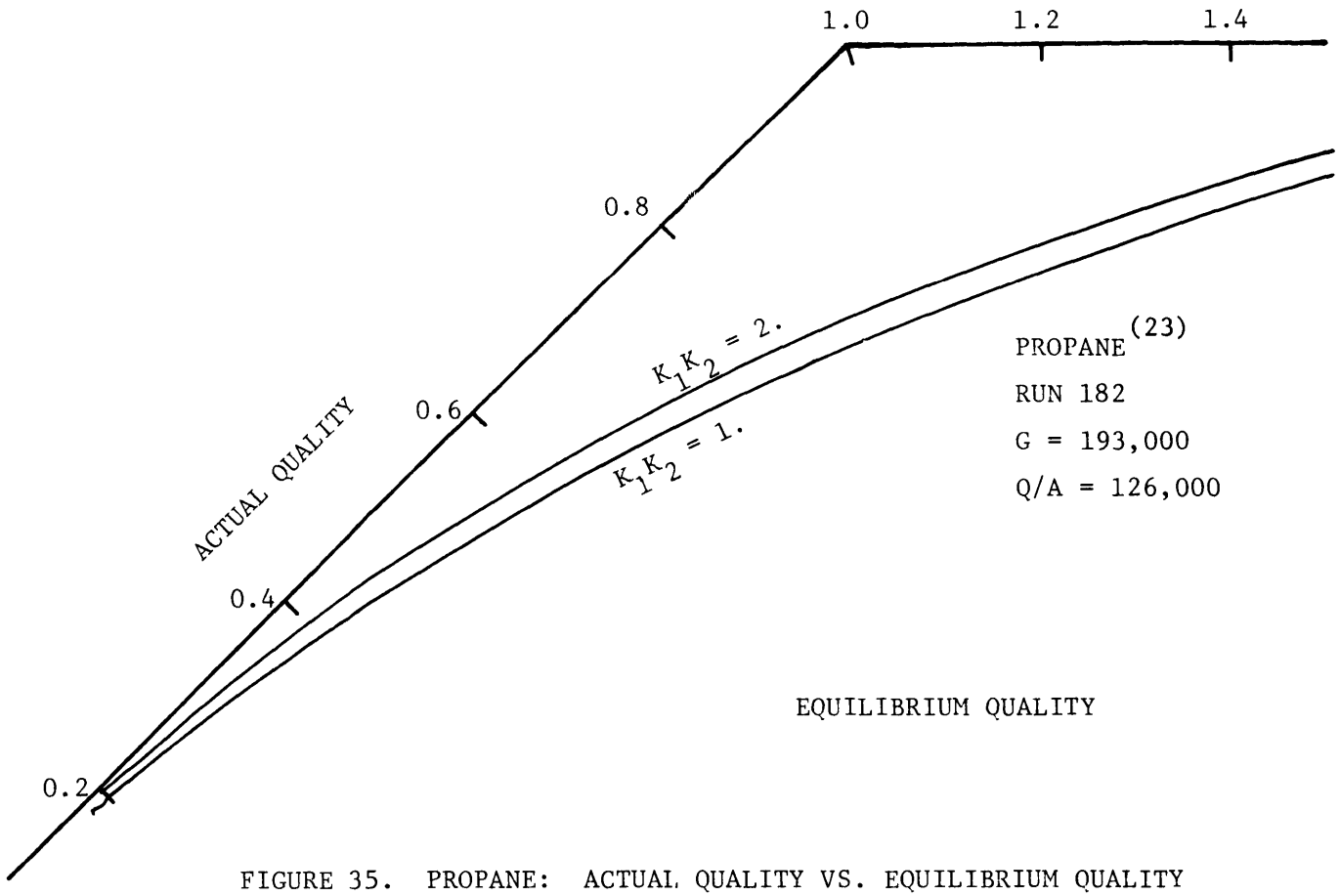

FIGURE 35. PROPANE: ACTUAL QUALITY VS. EQUILIBRIUM QUALITY

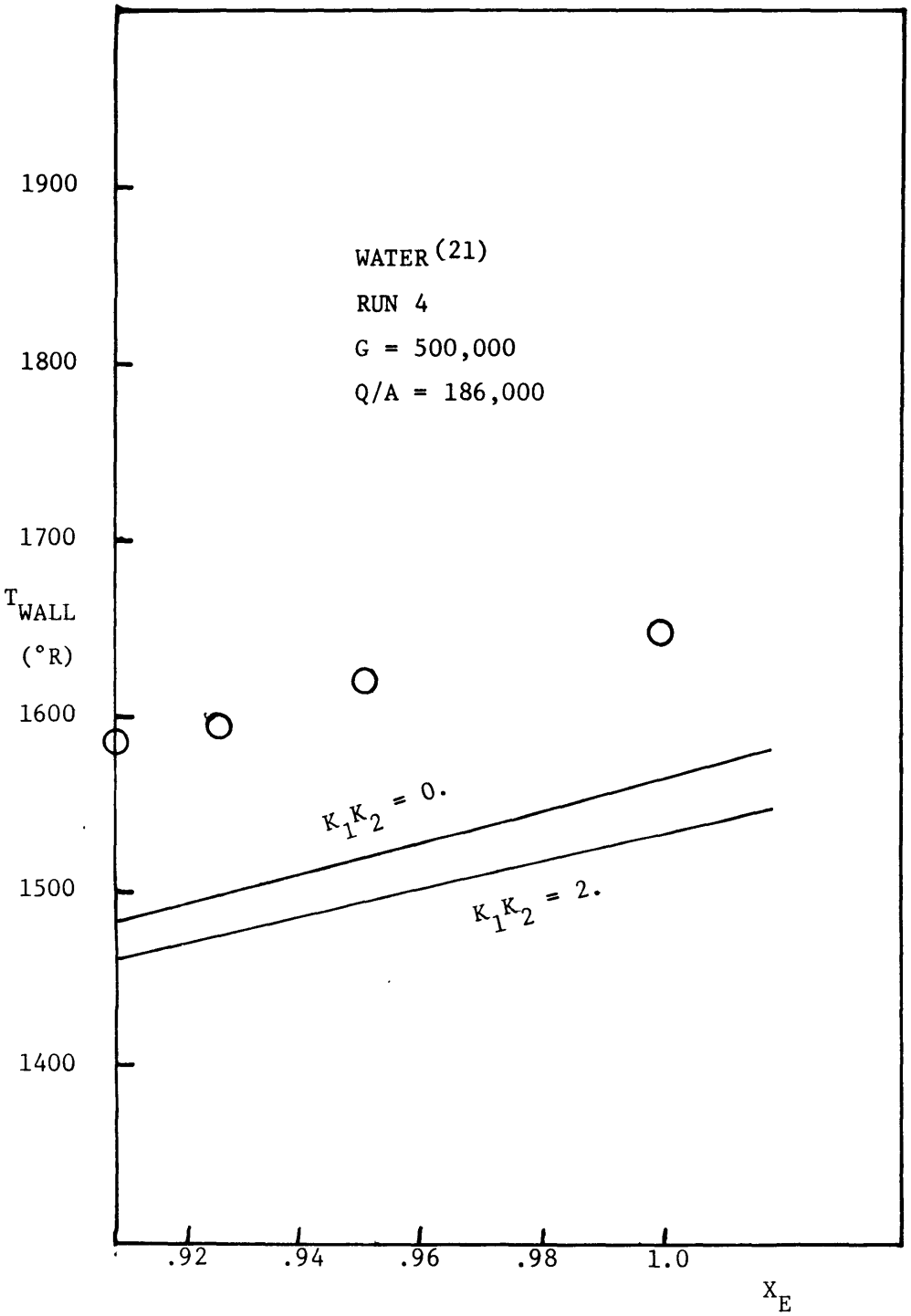

FIGURE 36. WATER: TEMPERATURE PROFILE (G. E. Data)

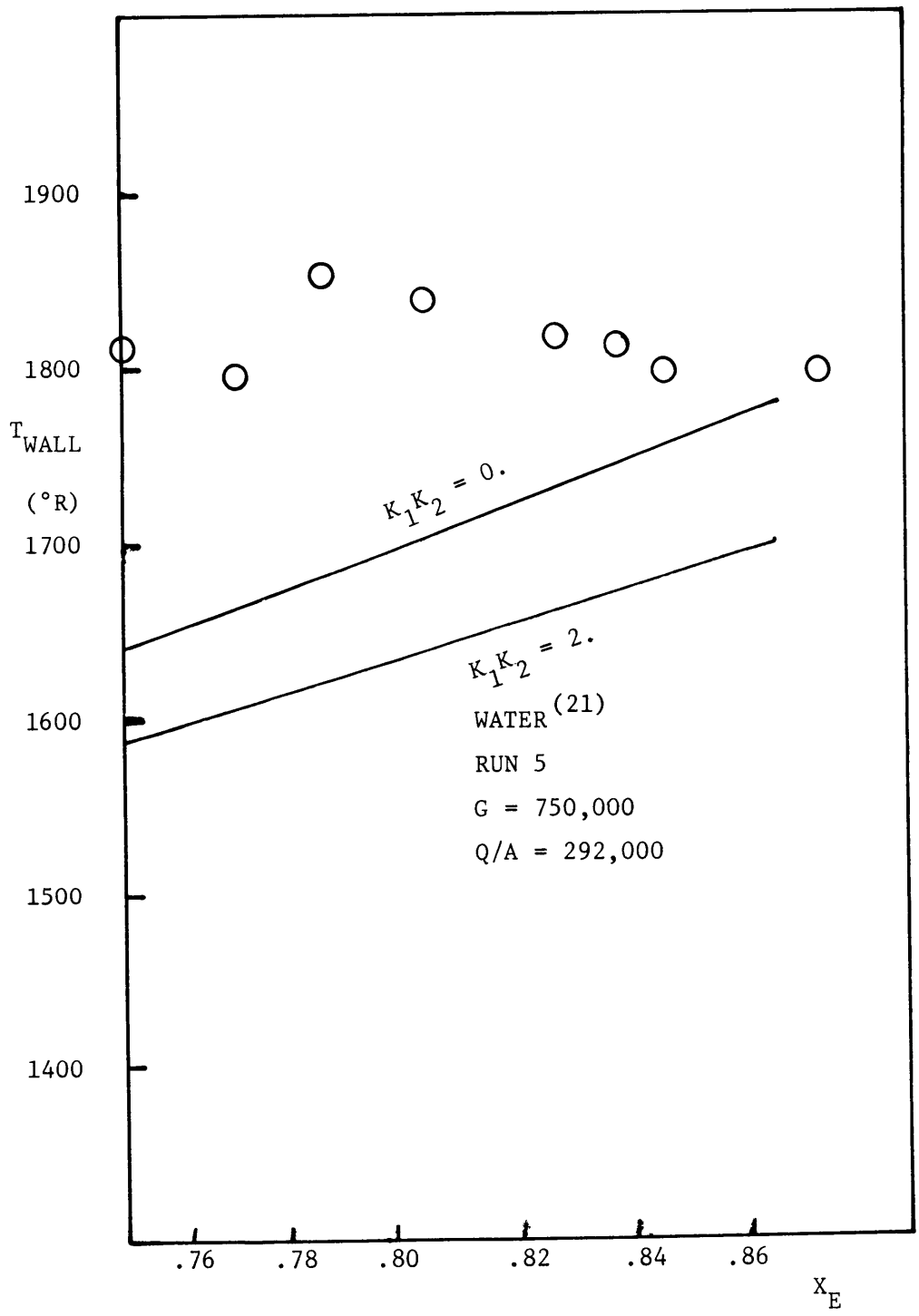

FIGURE 37. WATER: TEMPERATURE PROFILE (G. E. Data)

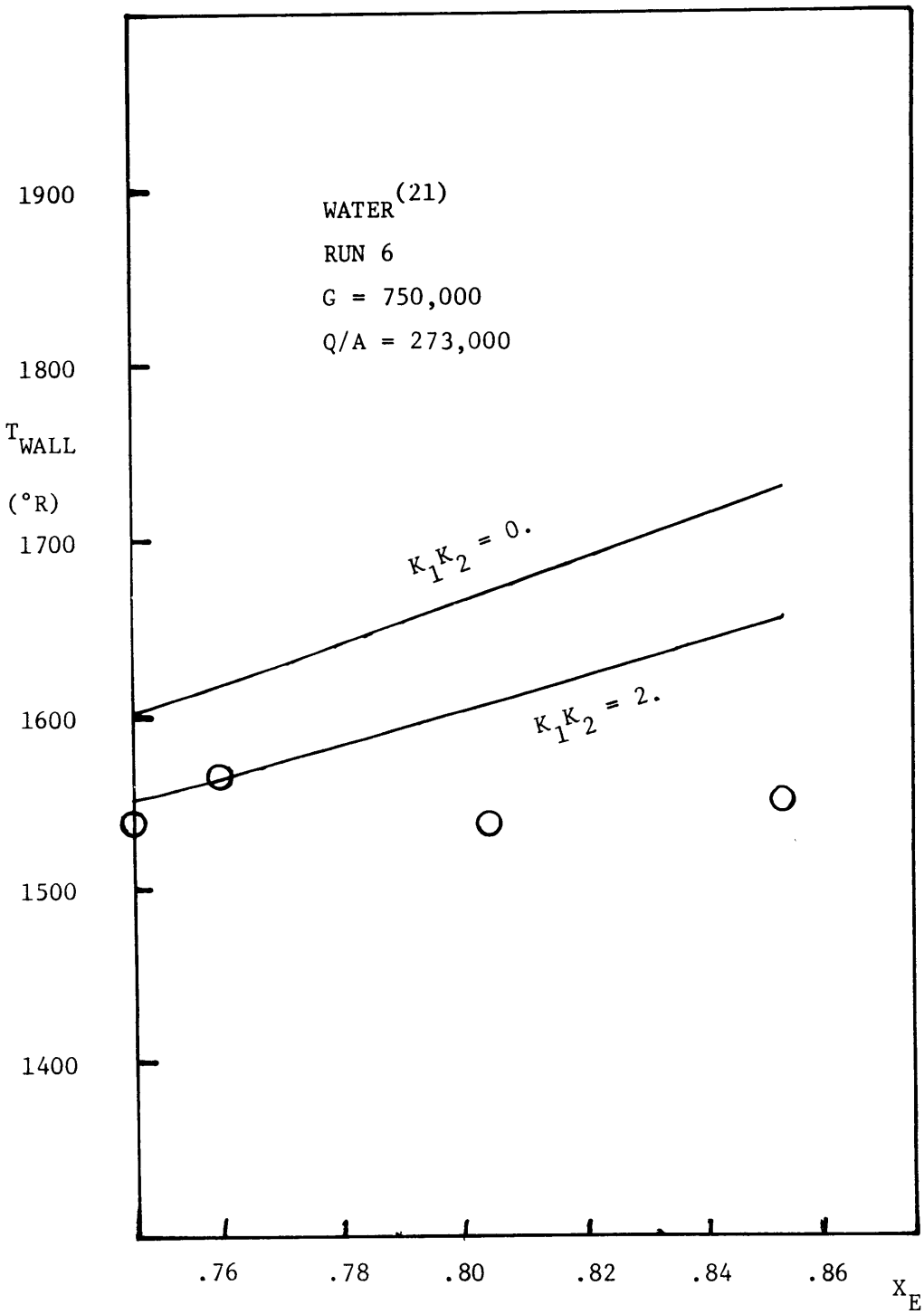

FIGURE 38. WATER: TEMPERATURE PROFILE (G. E. Data)

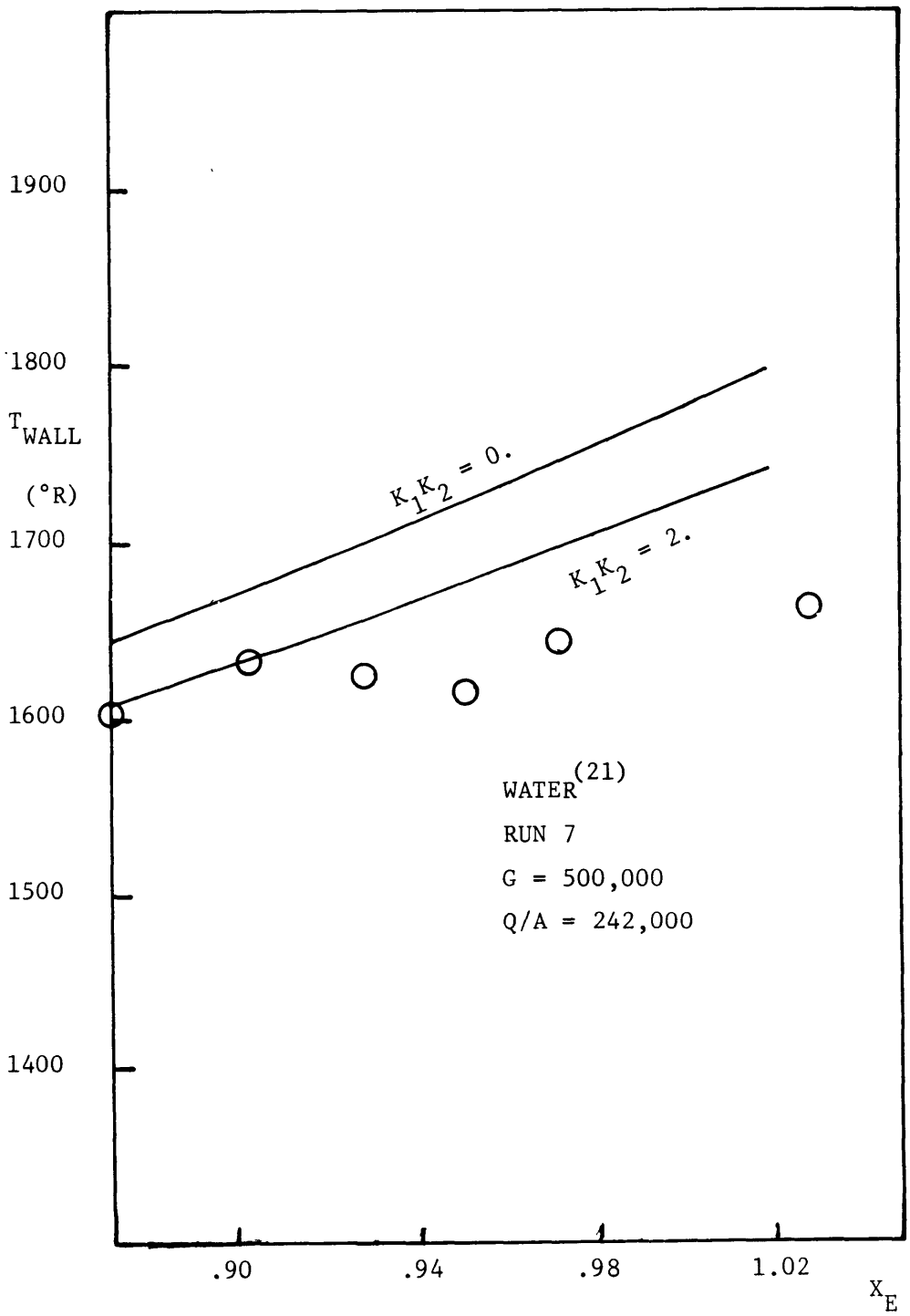

FIGURE 39. WATER: TEMPERATURE PROFILE (G. E. Data)

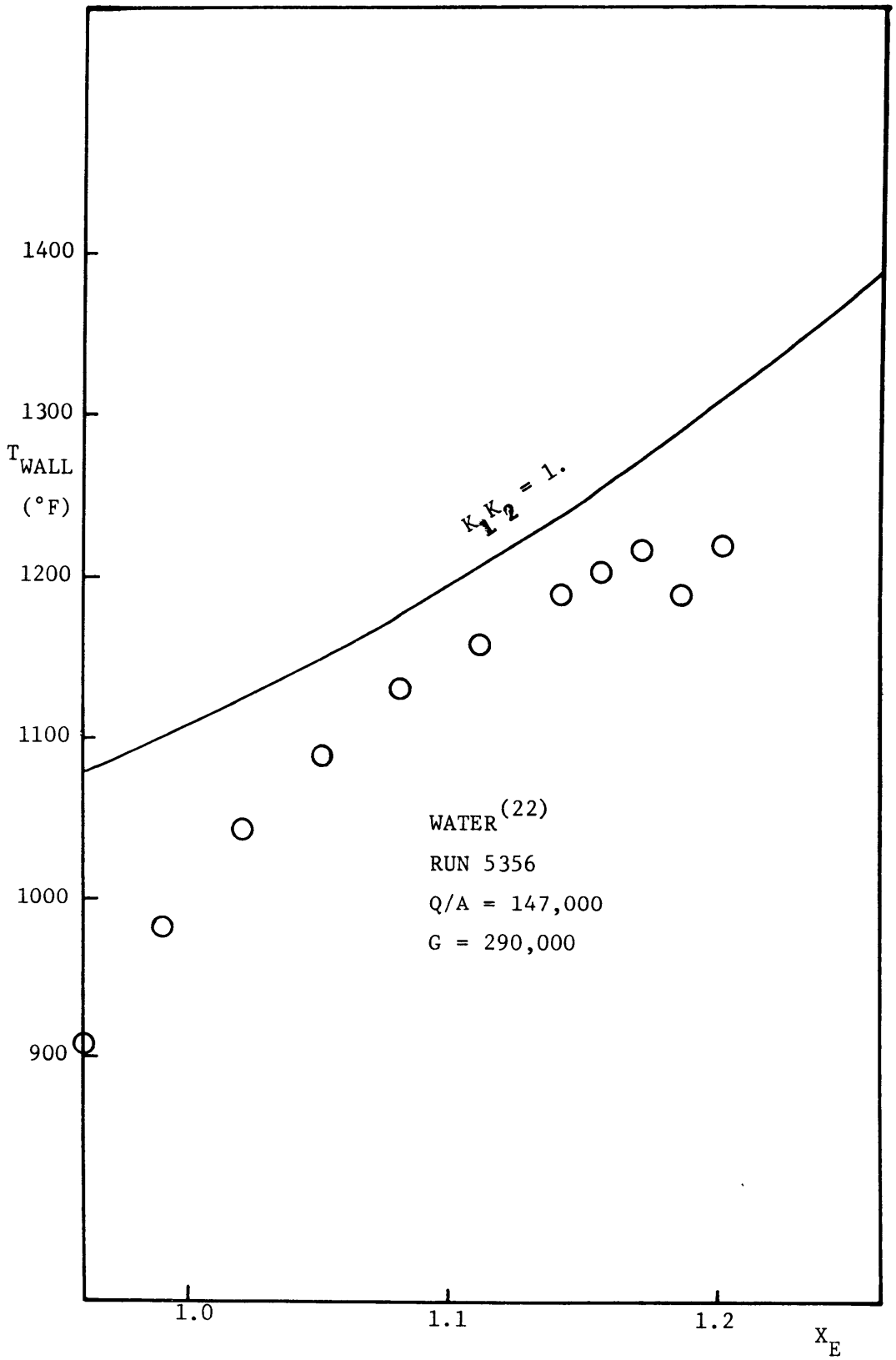

FIGURE 40. WATER: TEMPERATURE PROFILE (Harwell Data)

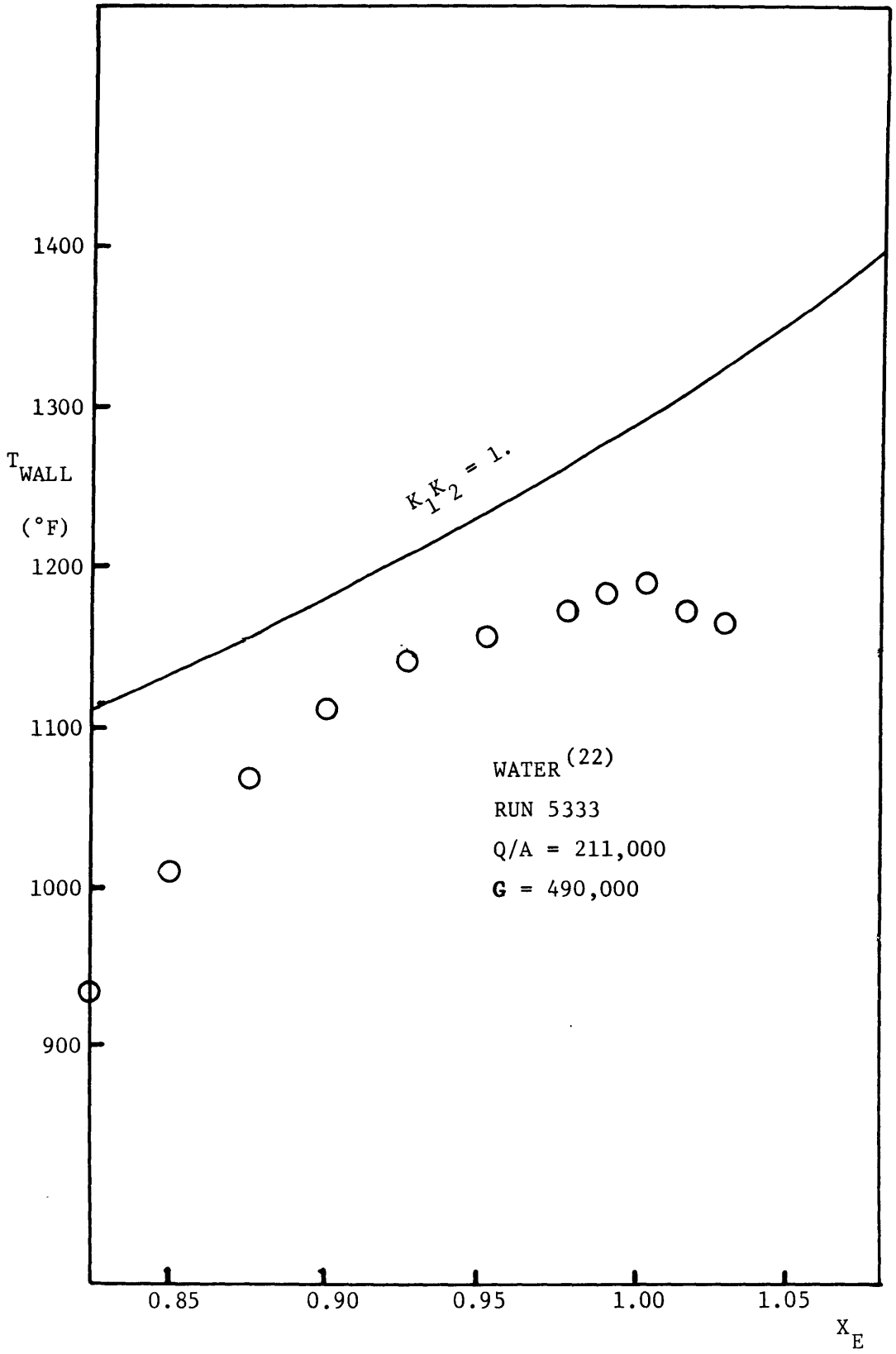

FIGURE 41. WATER: TEMPERATURE PROFILE (Harwell Data)

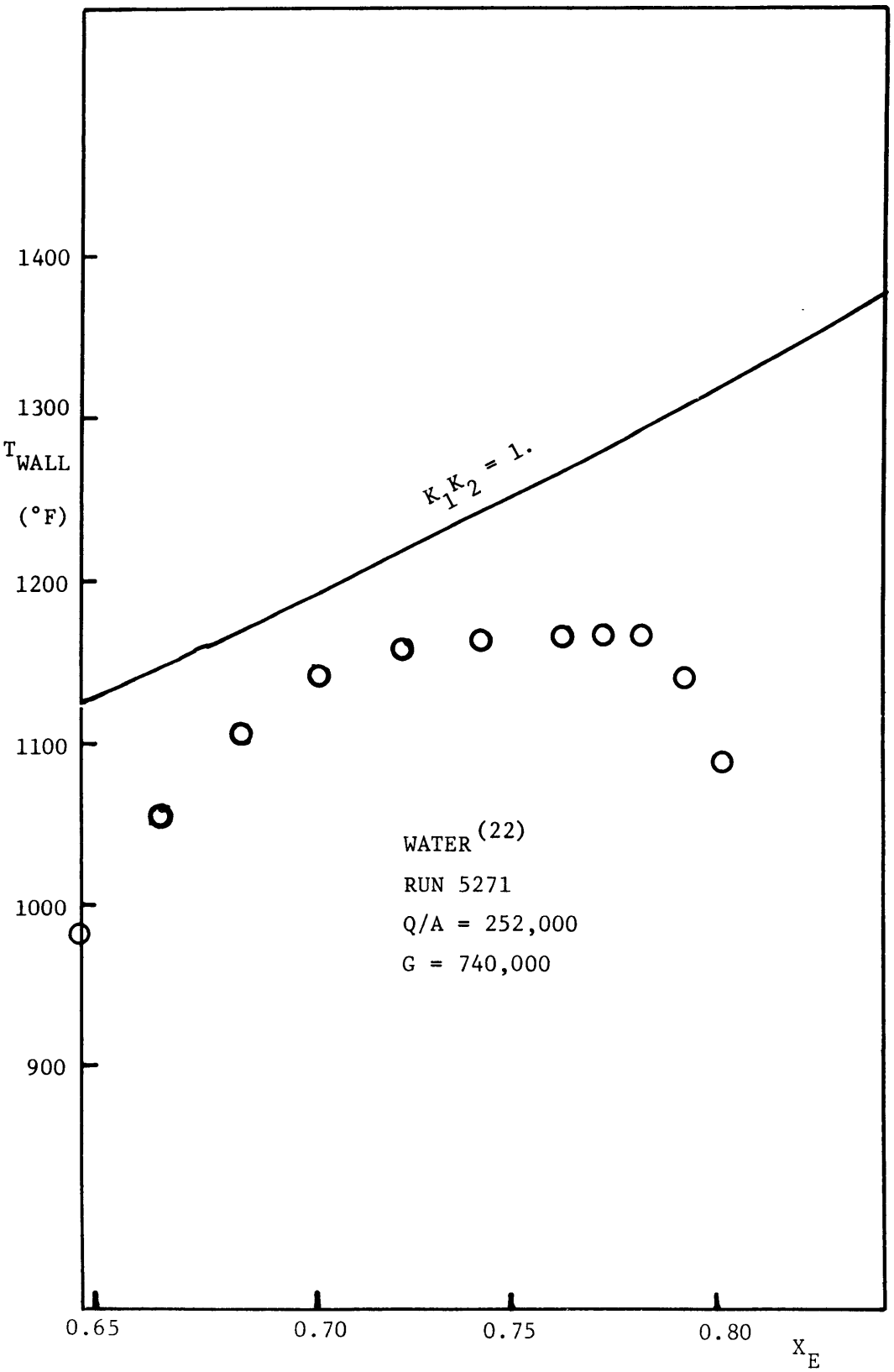

FIGURE 42. WATER: TEMPERATURE PROFILE (Harwell Data)

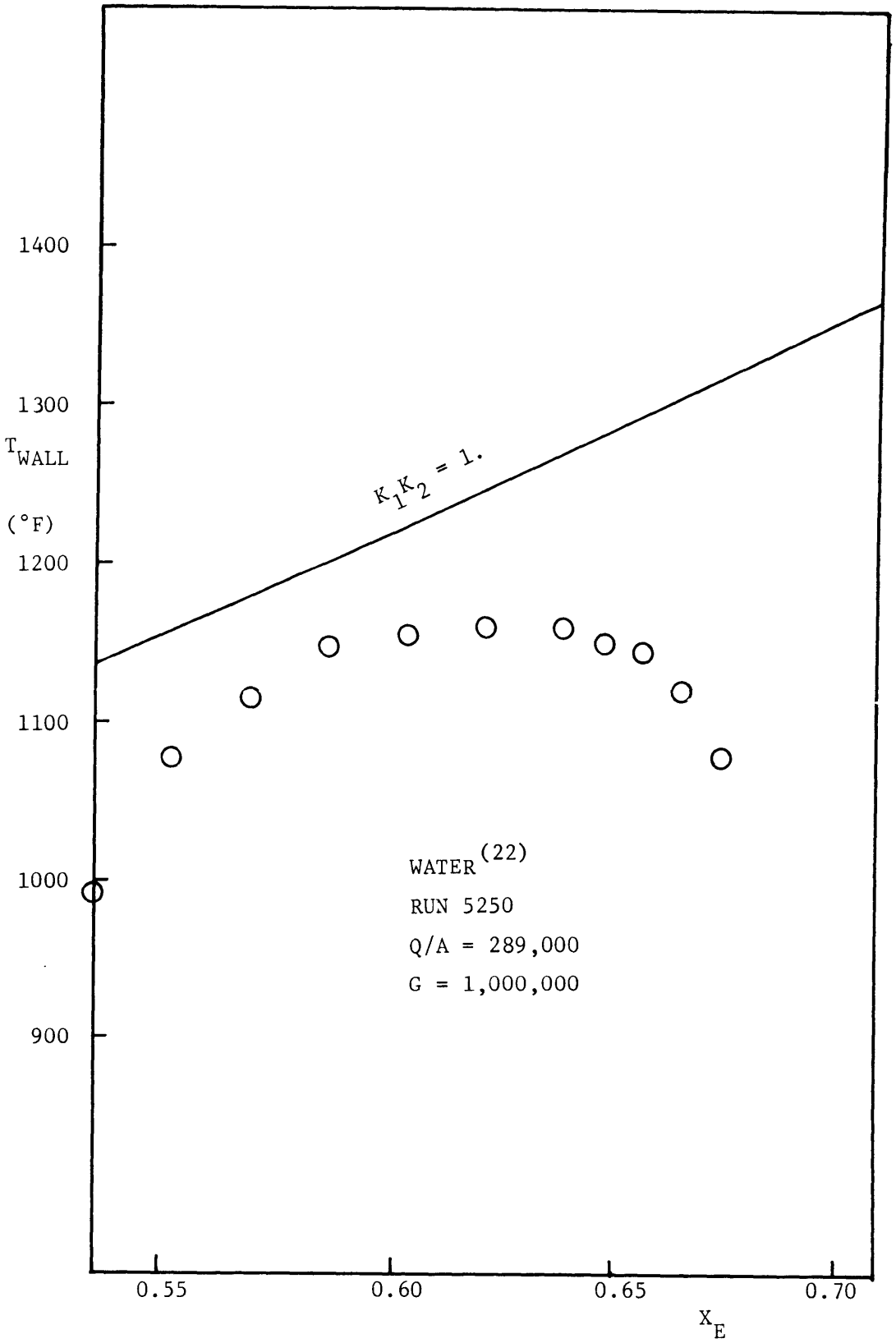

FIGURE 43. WATER: TEMPERATURE PROFILE (Harwell Data)

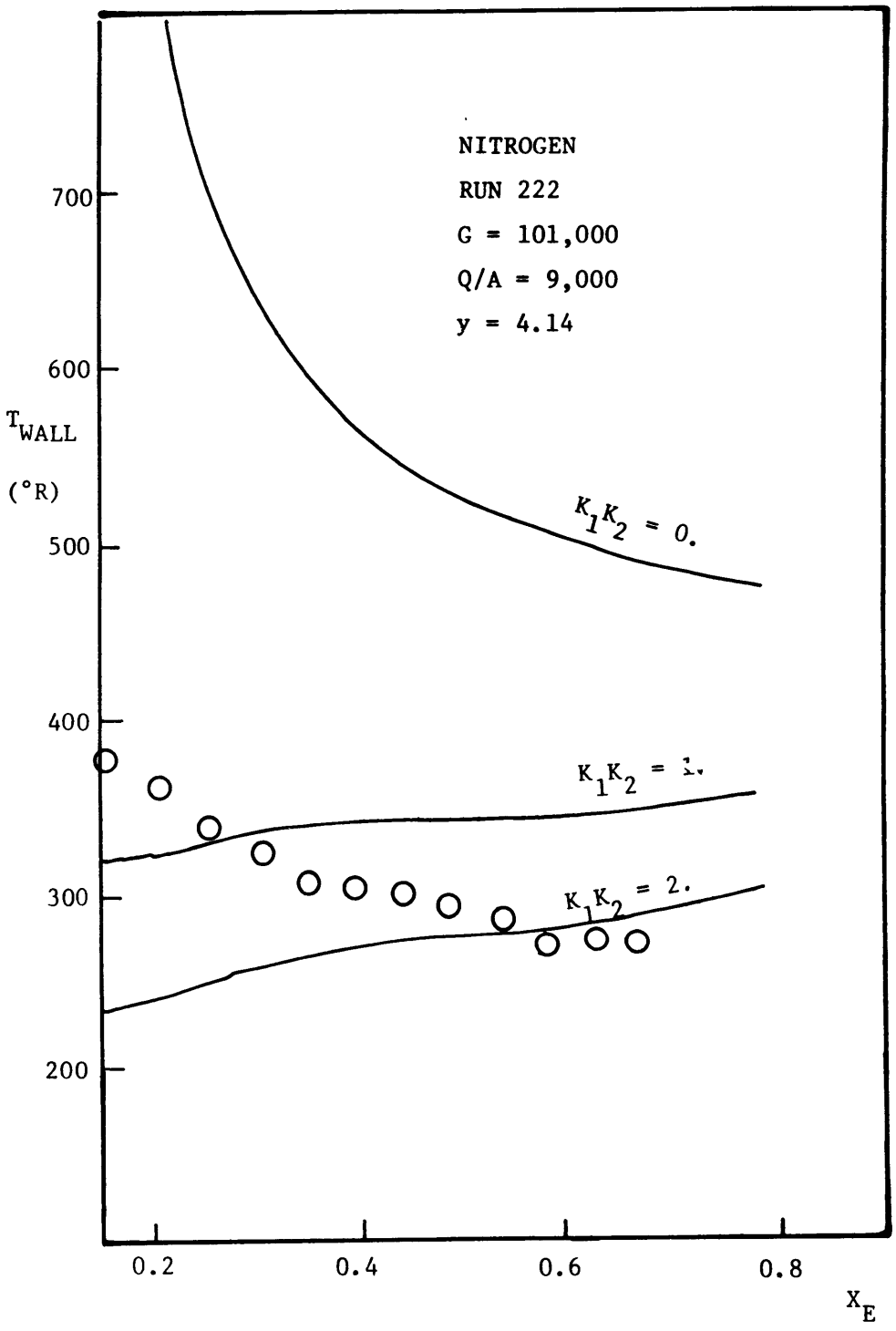

FIGURE 44. NITROGEN: TYPE I WITH TWISTED TAPE

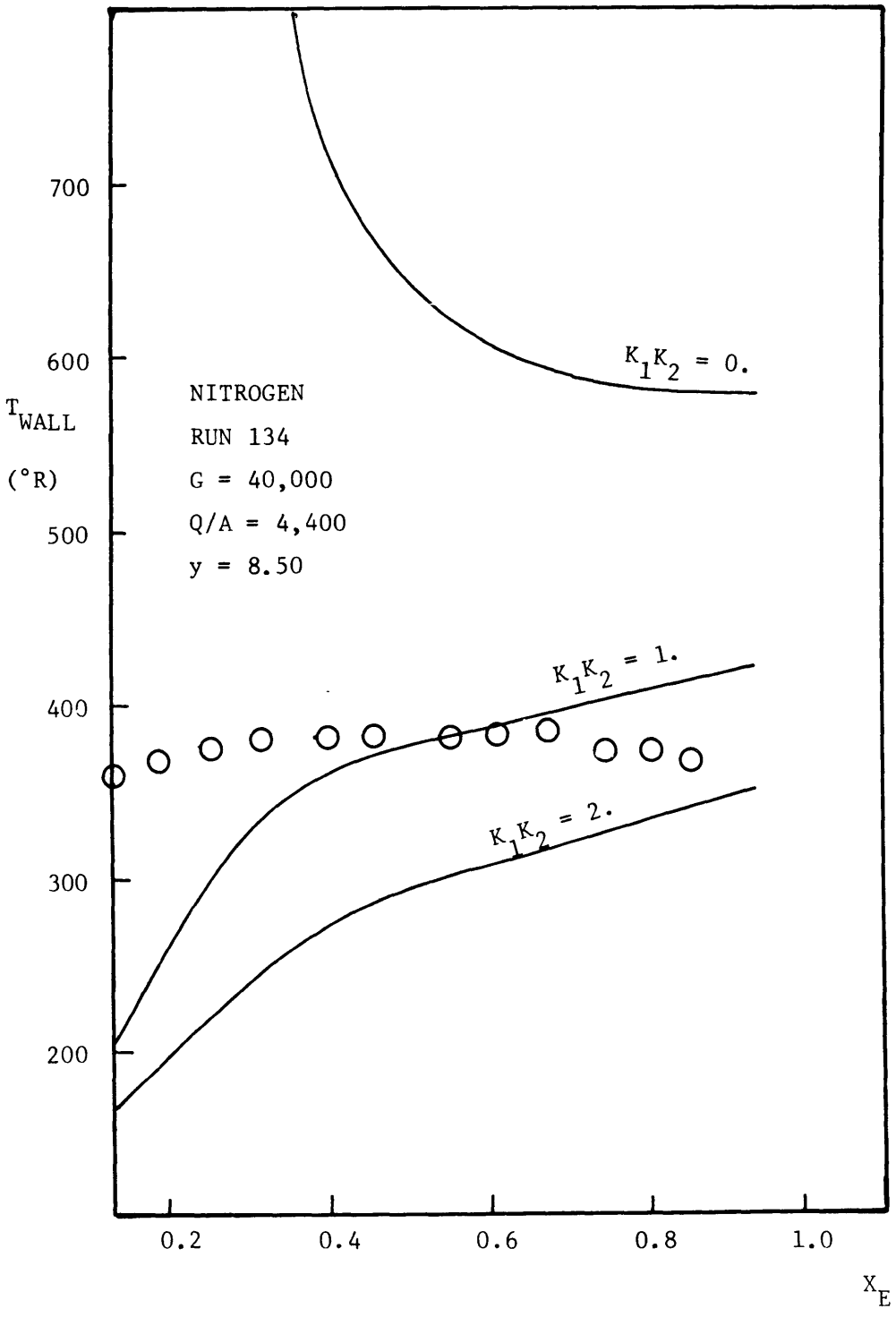

FIGURE 45. NITROGEN: TYPE I WITH TWISTED TAPE

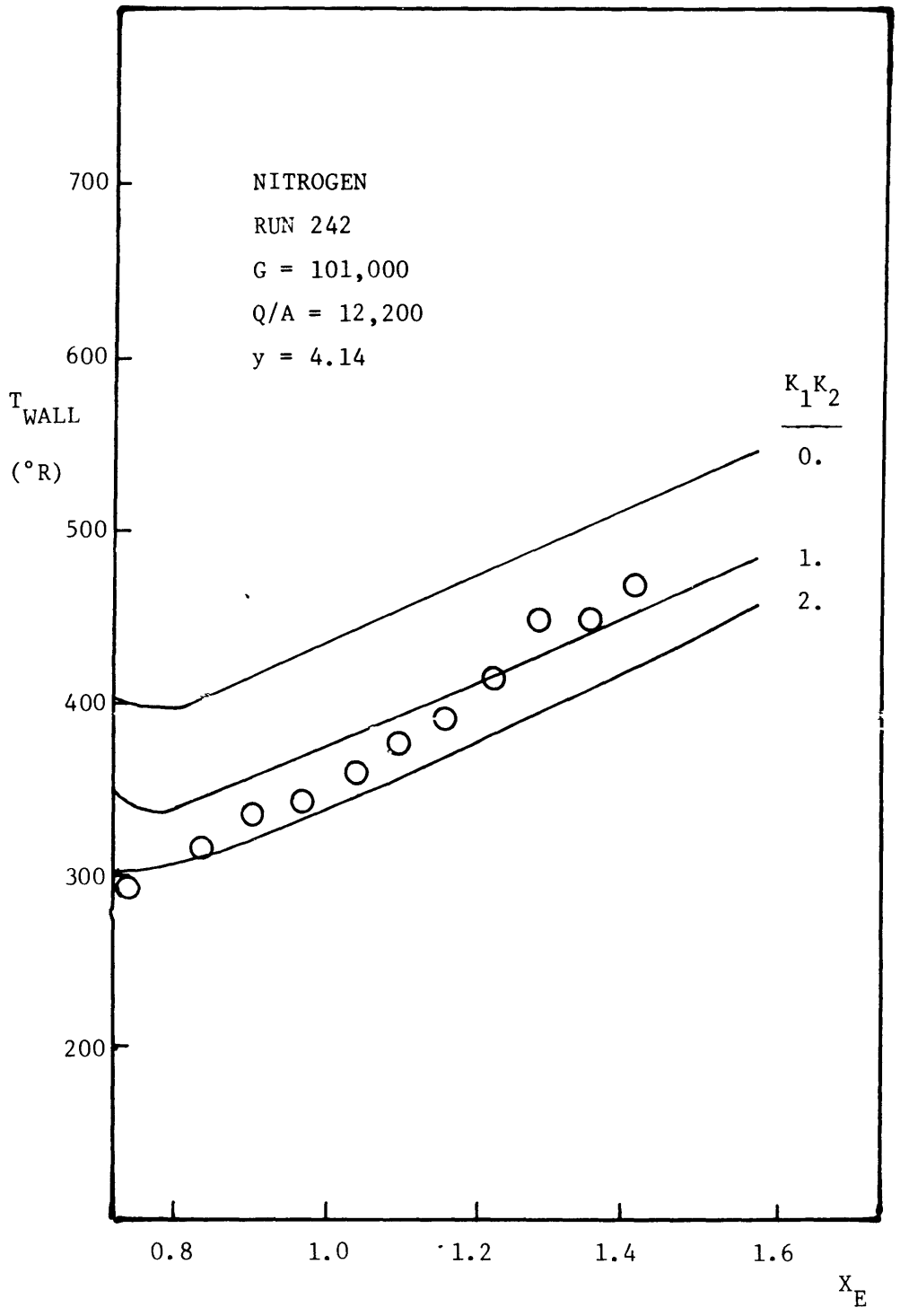

FIGURE 46. NITROGEN: TYPE II WITH TWISTED TAPE

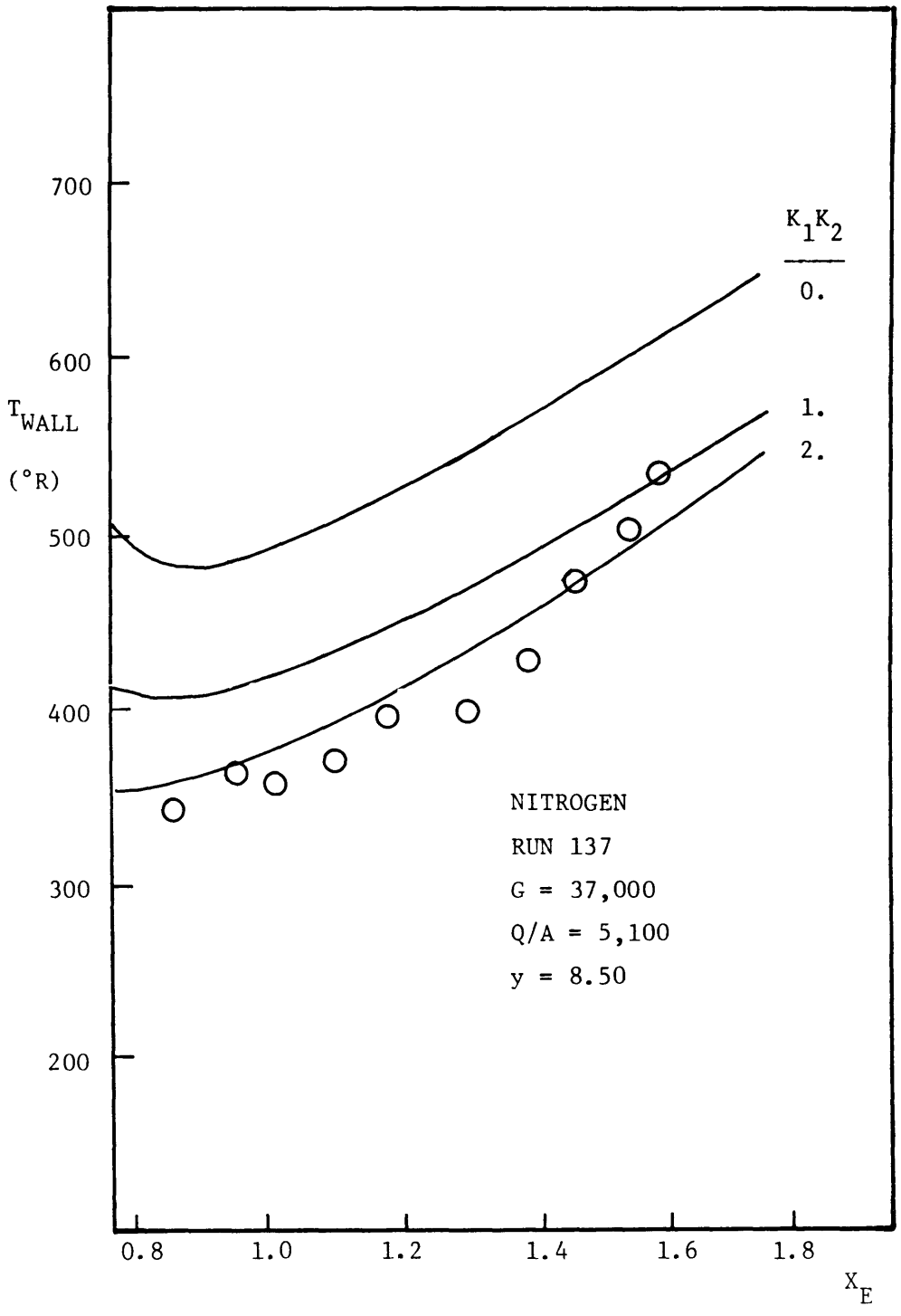

FIGURE 47. NITROGEN: TYPE II WITH TWISTED TAPE

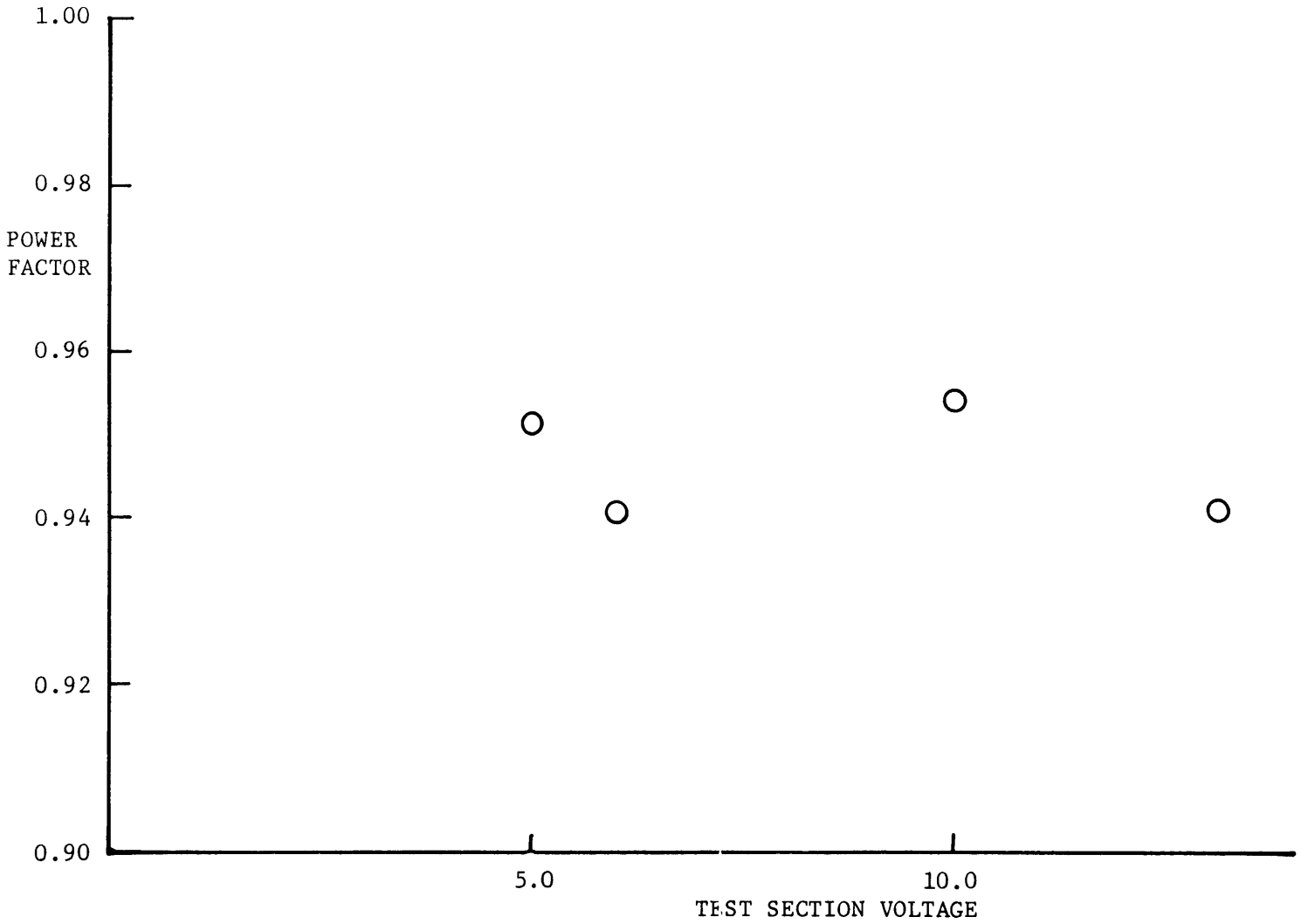
1.00
0.98
POWER
FACTOR
0.96
0.94
0.92
0.90
5.0
10.0
TEST SECTION VOLTAGE

FIGURE 48.

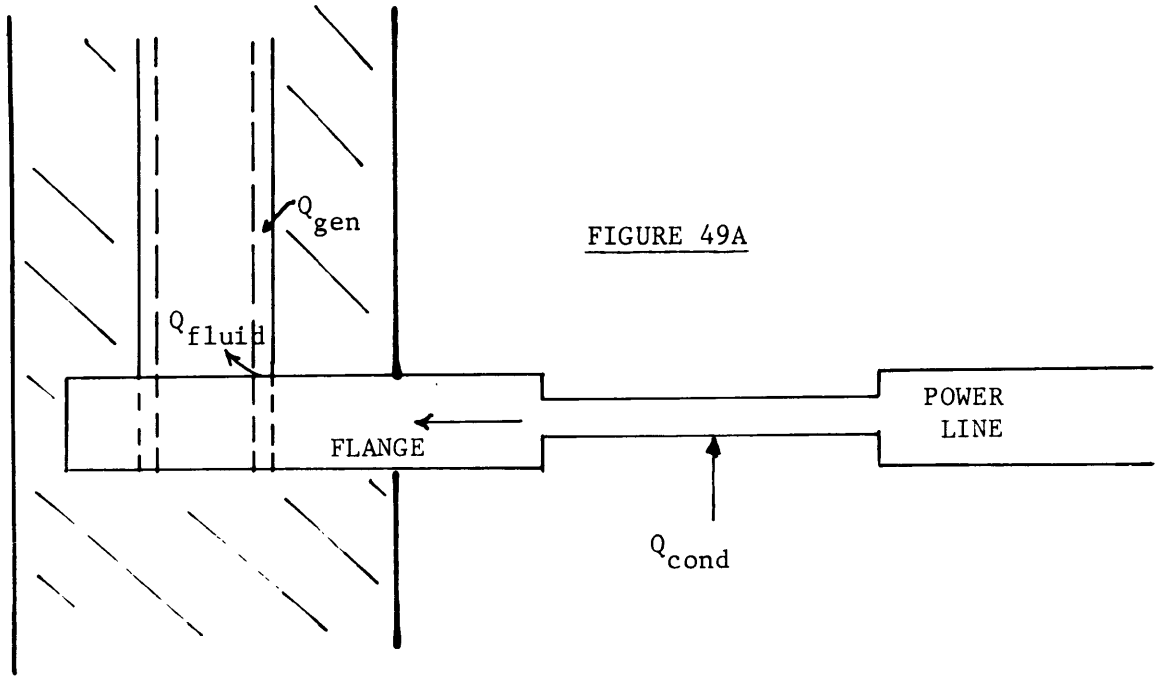

FIGURE 49A

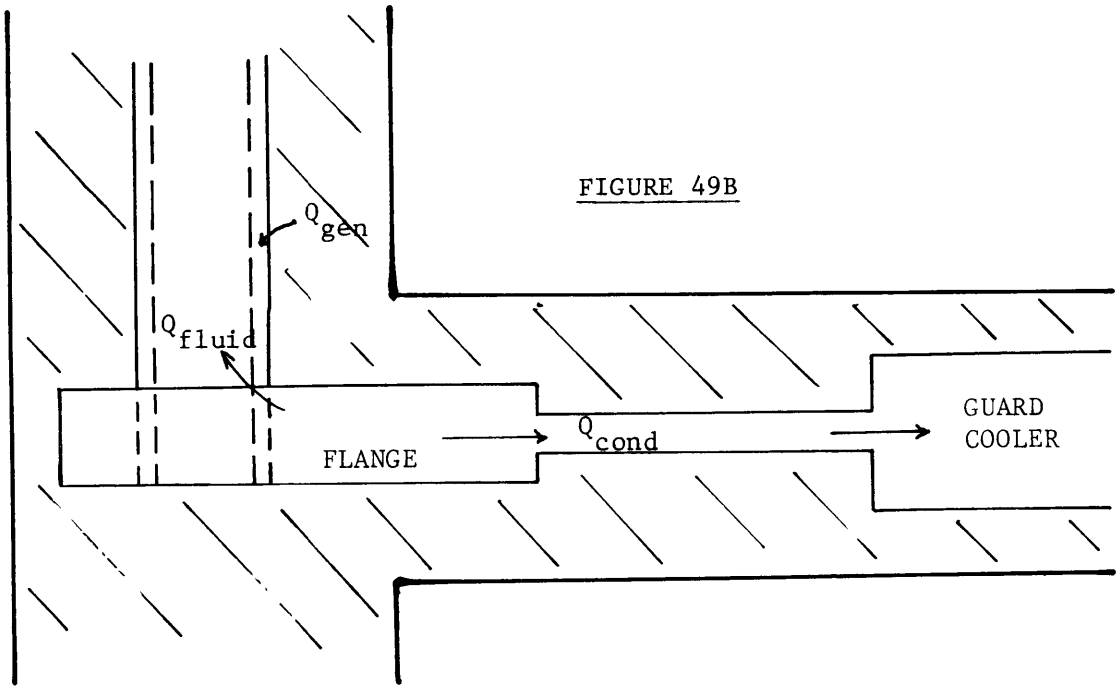

FIGURE 49B

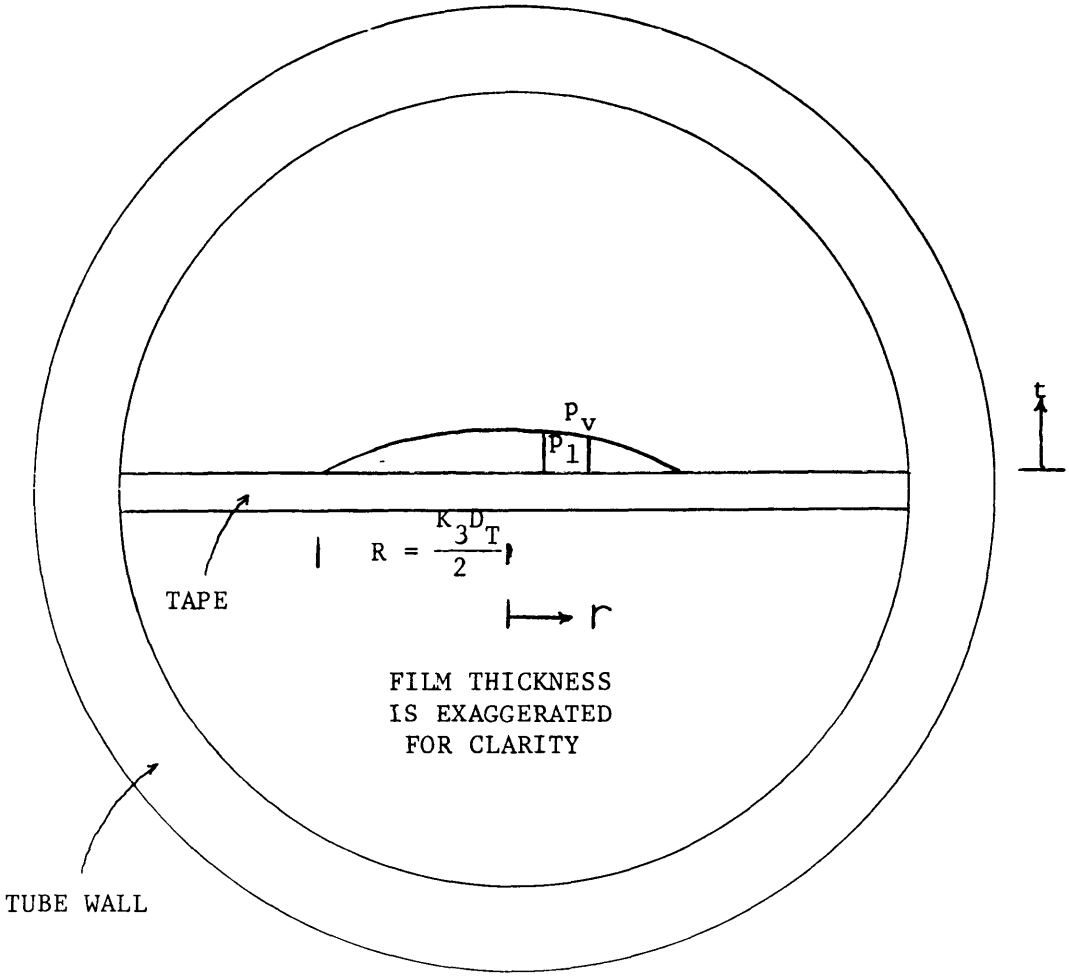

FIGURE 50. PROFILE OF LIQUID STREAMER

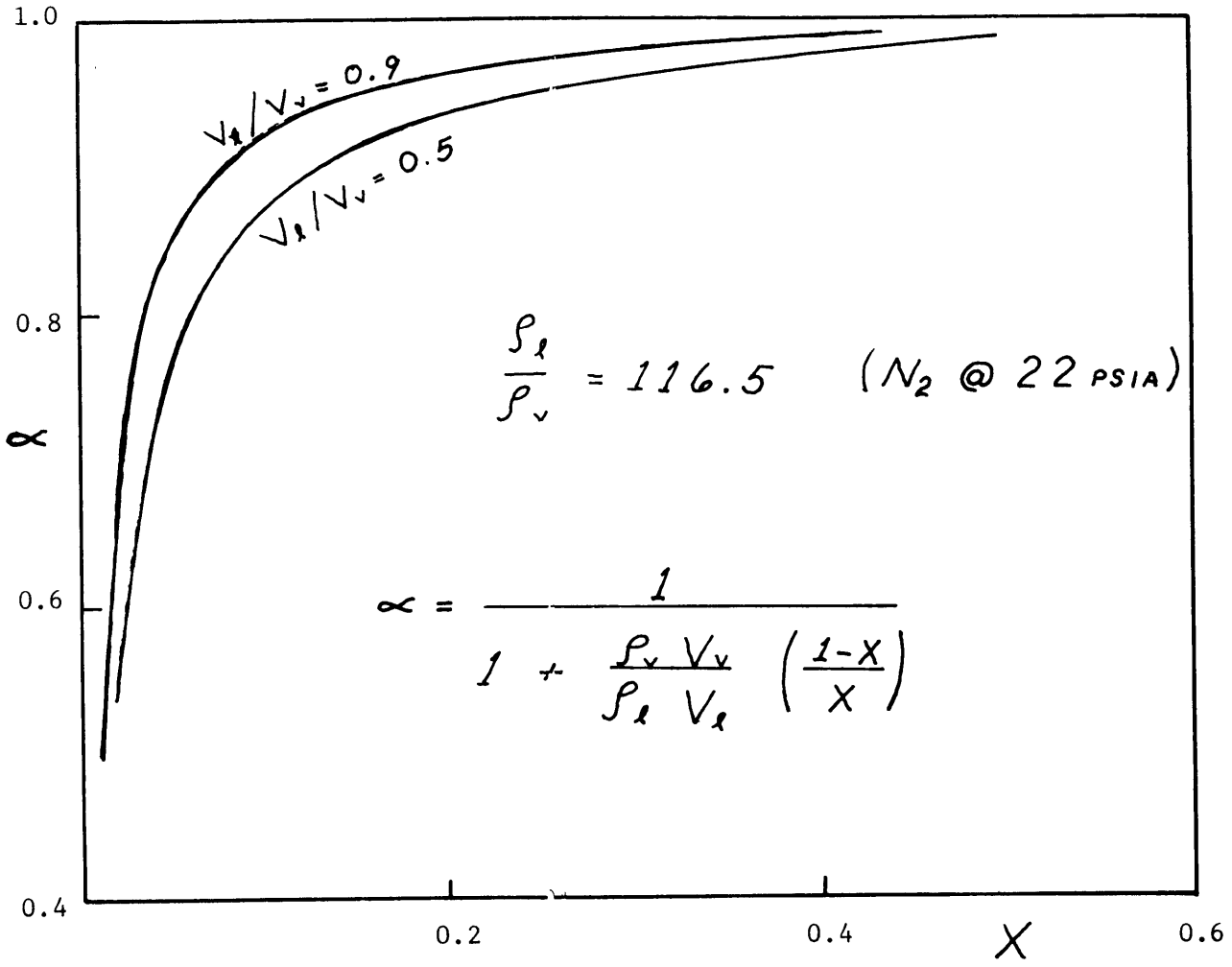

FIGURE 51. VOID FRACTION VS. QUALITY

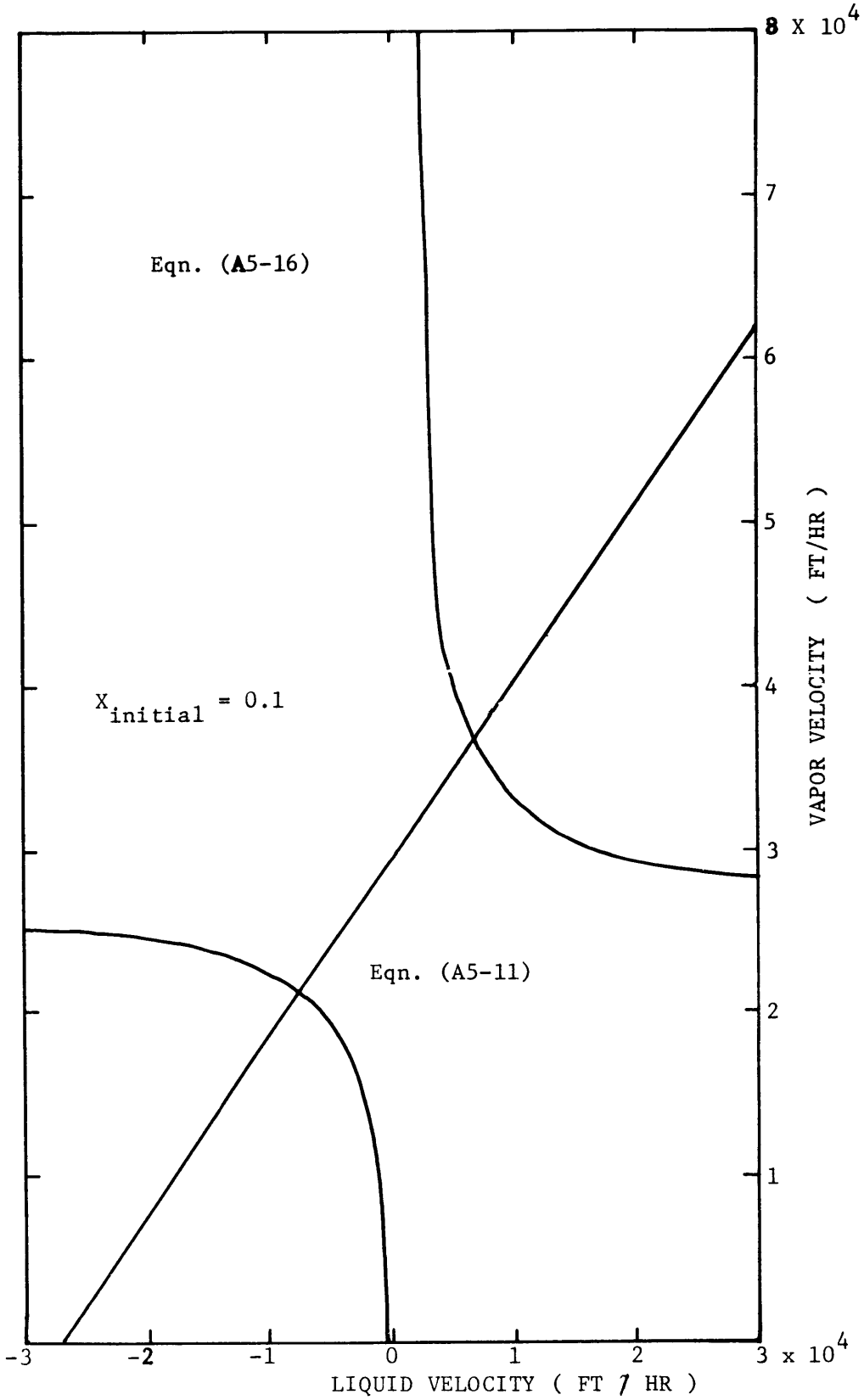

FIGURE 52. VELOCITY ITERATION

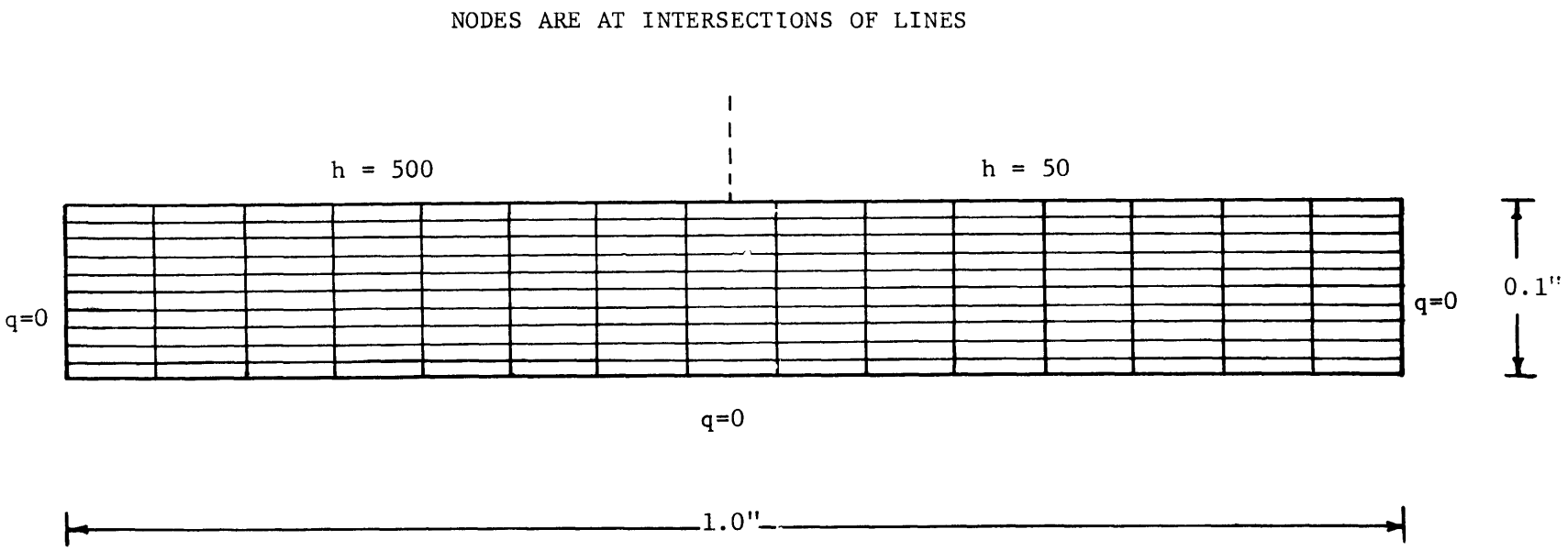

FIGURE 53. BOUNDARY CONDITIONS FOR THE AXIAL CONDUCTION PROBLEM

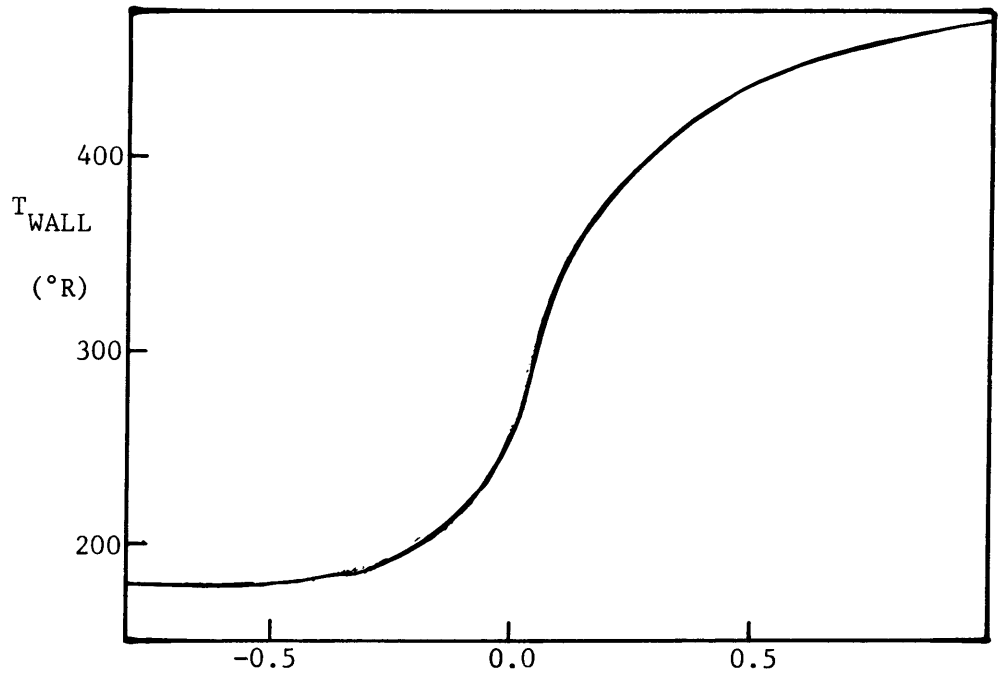

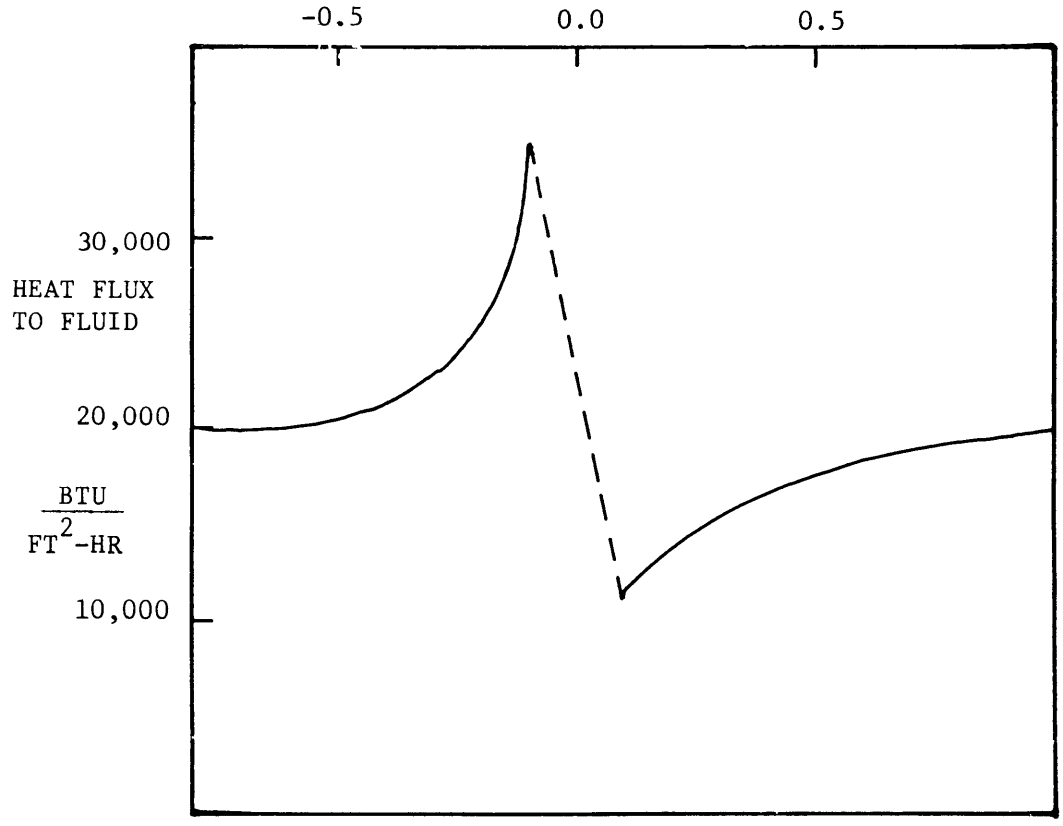

FIGURE 54. EFFECTS OF AXIAL CONDUCTION AT BURNOUT POINT